Using Light to Regulate the Activity of RET Kinase

Design, Synthesis and Evaluation of Photoswitchable DFG-out RET Kinase Inhibitors

YONGJIN XU

UNIVERSITY OF GOTHENBURG

Department of Chemistry and Molecular Biology
University of Gothenburg
2021

DOCTORAL THESIS

Submitted for fulfilment of the requirements for the degree of
Doctor of Philosophy in Chemistry

Using Light to Regulate the Activity of RET Kinase

Design, Synthesis and Evaluation of Photoswitchable DFG-out RET Kinase Inhibitors

YONGJIN XU

ISBN: 978-91-8009-444-3 (PRINT)
ISBN: 978-91-8009-445-0 (PDF)

Medicinal Chemistry Group
Department of Chemistry and Molecular Biology
University of Gothenburg
SE-412 96
Sweden

Printed by Stema Specialtryck AB
Borås, Sweden, 2021

To my parents

Abstract

Protein kinases are essential for signal transduction and regulate most cellular processes, such as metabolism, membrane transport, motility, and cell cycle. Although they play a critical role in cells and have a strong association with diseases, details of their physiologic and pathologic mechanisms remain at least partially unclear, especially the spatiotemporal dynamics of the signalling. Reversible photo-regulation of kinase inhibitors could be an approach to gain spatiotemporal control, thereby resolving the above-mentioned issues.

This thesis comprises the synthesis and characterisation of novel azoheteroarenes photoswitches and their use in the development of photoswitchable kinase inhibitors. REarranged during Transfection (RET) is a kinase belonging to the receptor tyrosine kinase family. RET was used as a model target in the development of photoswitchable DFG-out kinase inhibitors.

A methodology was initially developed to synthesize aromatic *N*-heterocycle derived azoheteroarenes, using Buchwald-Hartwig coupling and microwave-assisted dehydrogenation as the keys steps. With this methodology as the main strategy, a series of azoheteroarenes was prepared and their photophysical properties were based on UV-vis absorption spectroscopy and ^{1}H-NMR. Among them, quinoline and 7-azaindole based azoheteroarenes showed the efficiency of synthesis and outstanding photophysical properties in all aspects.

By integrating the quinoline-based azoheteroarene into the pharmacophore of a reported DFG-out kinase inhibitor, the first photoswitchable DFG-out RET kinase inhibitor was synthesized and evaluated with respect to the photophysical properties and bioactivity. Four different strategies were explored in order to enlarge the difference of biological activity between the *E*-isomer and light enriched *Z*-isomer, using a quinolone-based azoheteroarene as a model system: (i) installing substituents on the quinoline ring; (ii) introducing the second azo unit; (iii) introducing fluorine atoms on the *ortho*-position of the azoheteroarene phenyl ring; and (iv) changing the heterocyclic moiety. In addition, the corresponding stilbene compounds were prepared as more thermally stable model compounds of the azo-based kinase inhibitors. This provided detailed data on the structure-physical properties relationship, as well as structure activity relationship. As a result, the 7-azaindole-derived azo type inhibitor showed excellent thermal stability and resistance to photo-fatigue. Moreover, it displayed a significant difference of inhibition activity between the *E*-isomer and the light-enriched *Z*-isomer sample in both enzymatic and living cell assays.

Key Words: RET kinase, kinase inhibitor, DFG-out, photoparmacology, azoheteroarene, Buchwald-Hartwig coupling, quinoline, 7-azaindole, bioactivity

List of publications

I. Synthesis and Photophysical Characterization of Azoheteroarenes

Yongjin Xu, Chunxia Gao, Joakim Andréasson, Morten Grøtli

Org. Lett. **2018**, *20*, 4875-4879

II. Design and Development of a Photoswitchable DFG-Out Kinase Inhibitor

Yongjin Xu, Chunxia Gao, Liliana Håversen, Thomas Lundbäck, Joakim Andréasson, Morten Grøtli

Manuscript submitted, 2021

III. Design and Development of Photoswitchable DFG-Out RET Kinase Inhibitor with Quinoline and 7-azaindole Based Azoheteroarenes

Yongjin Xu, Chunxia Gao, Måns Andreasson, Liliana Håversen, Marta Carrasco, Cassandra Fleming, Thomas Lundbäck, Joakim Andréasson, and Morten Grøtli

Manuscript, 2021

Contribution report

Paper I. Performed all the synthesis and photophysical characterization.
Wrote the manuscript draft and supporting information, except for the part of TDDFT calculations.

Paper II. Performed all the work, including molecule design/ modelling, synthesis, photophysical characterization and biological assay.
Wrote the manuscript draft and supporting information.

Paper III. Performed part of the molecule design/modelling, all the synthesis except methyl and ethyl substituted stilbene isomers, all the photophysical characterization and biological assay.
Wrote the manuscript draft and supporting information.

List of Abbreviation and Symbols

ABL	Abelson tyrosine kinase
ADP	Adenosine diphosphate
AGC	Protein A, G, and C kinase family
AKT	Protein kinase B (PKB)
Ala	Alanine
ALK	Anaplastic lymphoma kinase
AML	Acute myeloid leukemia
Asp	Aspartic acid
ATP	Adenosine triphosphate
Boc	tert-Butyloxycarbonyl
BRAF	B-Raf proto-oncogene, serine/threonine kinase
BRET	Bioluminescence resonance energy transfer
BTK	Bruton's tyrosine kinase
CAMK	Ca^{2+}/Calmodulin-dependent kinase family
CDK	Cyclin-dependent kinase
CK1	Casein kinase 1 family
CLL	Chronic lymphocytic leukemia
CMGC	Proline-directed serine/threonine kinases, including CDKs, MAPK, GSKs and CDK-like kinases
CML	Chronic myeloid leukemia
CSF1R	Colony stimulating factor 1 receptor
DCM	Dichloromethane
DFG	Aspartic acid-Phenylalanine-Glycine
DFT	Density functional theory
DMF	*N*,*N*-Dimethylformamide
DMSO	Dimethyl sulfoxide

DNA	Deoxyribonucleic acid
DTT	Dithiothreitol
EGFR	Epidermal growth factor receptor
e.g.	For example
ERK	Extracellular signal-regulated kinases
FDA	U.S. Food and Drug Administration
FGFR	Fibroblast growth factor receptor
GDNF	Glial cell line-derived neurotrophic factor
GIST	Gastrointestinal stromal tumor
Gly	Glycine
Glu	Glutamic acid
GPCR	G Protein-coupled receptors
GSH	Glutathione
GSK3	Glycogen synthase kinase 3
HCC	Hepatocellular carcinoma
HER2	Human epidermal growth factor receptor 2
His	Histidine
IC_{50}	Half-maximal inhibitory concentration
IGF1R	Insulin-like growth factor 1 receptor
JAK	Janus kinase
JNK	c-Jun N-terminal kinase
k_{off}	The first-order rate constant for the dissociation of the protein-ligand complex
k_{on}	The second-order rate constant of the binding reaction
LED	Light-emitting diode
MAPK	Mitogen-activated protein kinase
MCL	Mantle cell lymphoma
MEK	Mitogen-activated protein kinase kinase

MEN2	Multiple endocrine neoplasia type 2
MTC	Medullary thyroid cancer
mTOR	Mammalian target of rapamycin
MW	Microwave
NBS	*N*-Bromosuccinimide
NCBI	National Center for Biotechnology Information
NHL	Non-Hodgkin lymphoma
NIS	*N*-Iodosuccinimide
NSCLC	Non-small cell lung cancer
OXONE	Potassium peroxymonosulfate
PBS	Phosphate buffered saline
PDB	Protein data bank
PDGFR	Platelet-derived growth factor receptor
Ph+ ALL	Philadelphia-positive acute lymphoblastic leukemia
Phe	Phenylalanine
PI3K	Phosphoinositide 3-kinase
PKL	Protein kinase-like family
PLC	Preparative layer chromatography
PSD	Photostationary distribution
PTC	Papillary thyroid carcinoma
PYK	Pyruvate kinase
RAF	RAF proto-oncogene serine/threonine-protein kinase family
RAS	Small GTPase protein family
RCC	Renal cell carcinoma
RET	Rearrangement during transfection
RGC	Receptor guanylate cyclase family
ROCK	Rho-associated protein kinase

rt	Room temperature
RTK	Receptor tyrosine kinase
Ser	Serine
SMKIs	Small molecule kinase inhibitors
SLL	Small lymphocytic lymphoma
STAT	Signal transducer and activator of transcription
STE	Serine/Threonine kinase family
$t_{1/2}$	Half-life
TFA	Trifluoroacetic acid
TFAA	Trifluoroacetic anhydride
THF	Tetrahydrofuran
THP	Tetrahydropyran
TK	Tyrosine kinase
TKL	Tyrosine kinase-like family
TLC	Thin layer chromatography
Tos	*p*-Toluenesulfonyl
TRK	Tropomyosin receptor kinase
UV	Ultraviolet
Val	Valine
VEGFR	Vascular endothelial growth factor
λ	Wavelength

Table of content

1 Aim of the thesis

The overall aim of the work presented in this thesis is to design and develop photoswitchable DFG-out RET kinase inhibitors. Aromatic *N*-heterocycles are ubiquitous in the chemical structure of kinase inhibitors and play key roles for their bioactivity, which together with their unique electrostatic properties make the aromatic *N*-heterocycle derived azoheteroarenes interesting starting points for developing photoswitchable kinase inhibitors.

The specific objectives of the thesis were:

- Investigate a methodology to synthesize the *N*-heterocycle derived azoheteroarenes and characterize their photophysical properties, and select the optimal azoheteroarenes for the following work;

- Design, synthesis and evaluation of the optimal azoheteroarene based photoswitchable DFG-out RET kinase inhibitors;

- Optimize the above developed kinase inhibitors by adjusting the photophysical properties, as well as modifying the geometry of the heterocyclic “head”.

2 Background

2.1 Protein Kinase

2.1.1 Concept, classification and function of protein kinase

Kinases constitute a large family of enzymes widely existing in eukaryotic and prokaryotic cells. They mediate most of the signal transductions in cells by catalysing the transfer of phosphate groups from high-energy, phosphate-donating molecules (e.g. ATP) to specific substrates.[1]

Ever since the report of the first kinase about 70 years ago, there has been intense interest in the discovery of new kinases. With the assistance of DNA cloning and sequencing in the mid-1970s, it rapidly became clear that the human genome sequence allows for the identification of 518 kinases which constitute approximately 1.7% of all human genes.[2]

Kinases can be classified into broad groups by the substrate they act upon: protein kinases, lipid kinases, and carbohydrate kinases. In this thesis, I only focus on the protein kinases. Protein kinases can be divided into five categories according to the amino acid residues that are phosphorylated: Serine/threonine protein kinases, tyrosine-specific protein kinases, histidine-specific protein kinases, tryptophan protein kinases, and aspartyl/glutamyl protein kinases. Based on sequence comparisons of their catalytic domains, aided by knowledge of sequence similarity and the structure outside the catalytic domains, known biological functions, and a similar classification of the yeast, worm, and fly kinomes, human protein kinases also can be classified into 11 families: Protein A, G, and C kinase family (AGC), Ca^{2+}/calmodulin-dependent kinase family (CAMK), proline-directed serine/threonine kinases (CMGC), receptor guanylate cyclase family (RGC), tyrosine kinase family (TK), tyrosine kinase-like family (TKL), Sterile 20 serine/threonine kinase family (STE), casein kinase 1 family (CK1), protein kinase-like family (PKL), and atypical kinase family. Among all of them, TK is the largest group, consisting of 90 members.[2]

By phosphorylating certain residues, protein kinases can modify the function of a substrate protein in numerous ways (Figure 1). For example, phosphorylation can increase or decrease a protein's activity, stabilize it or mark it for destruction, localize it within a specific cellular compartment, and initiate or disrupt its interaction with other proteins.[3] Therefore, protein kinases are critical for metabolism, cell signalling, protein regulation, cellular transport, secretory processes and many other cellular pathways, which makes them very important to human physiology.

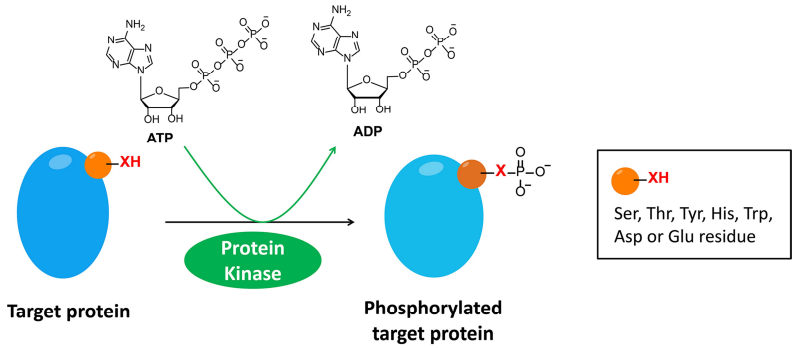

Figure 1. Kinases mediate protein phosphorylation.

2.1.2 Structure of protein kinases

Although protein kinases are classified into different families based on their amino acid sequence, their three-dimensional structures share some common features.[4] The conserved catalytic domain consists of two lobes: an *N*-terminal lobe (N-lobe), containing five beta-stranded sheets and one conserved alpha helix (αC-helix), and a C-terminal lobe (C-lobe) comprising six alpha helixes, and an activation loop (A-loop) which is located next to the αC-helix of the N-lobe. The two lobes are connected by a flexible hinge region (Figure 2),[5] while the ATP-Mg^{2+} complex is situated in a deep cleft located between the lobes.

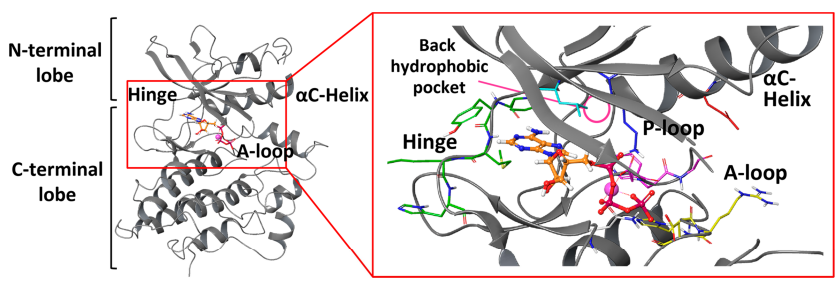

Figure 2. Kinase structure with conserved motifs (3DKC) in complex with ATP and Mg^{2+}; ATP (extra bold molecule in orange and red); Hinge (green); Gatekeeper (cyan); DFG motif (magenta); HRD motif (yellow); Roof lysine (blue); αC-helix Glutamic acid (red); Back hydrophobic pocket (pink circle).

Several conserved motifs in the area between the lobes are the main features of kinases and contribute to the catalysis of the ATP involved phosphorylation.[6] The hinge consists of approximately five amino acids, and usually forms two hydrogen-bonds with the adenine ring of ATP, which contribute to a significant part of the ATP binding affinity. The "gatekeeper" residue (cyan in Figure 2) is located adjacent to a hinge region on one of the β-sheets of the N-lobe. The

gatekeeper separates the adenine binding site from an adjacent back hydrophobic pocket (pink circle in Figure 2) and controls access to this hydrophobic pocket. This position is prone to mutation, and if it was replaced by a larger size amino acid, the increased steric hindrance of the "gatekeeper" may obstruct the inhibitor's binding to the hinge or back hydrophobic pocket, which could result in drug resistance.[7,8] Additionally, a notably conserved amino acid sequence located in the activation loop is Asp-Phe-Gly (DFG). The Asp residue, together with an extra Asn residue (white in Figure 2) and β, γ-phosphoryl groups of ATP, chelate Mg^{2+} to activate the γ-phosphoryl group of ATP. The active kinase conformation is termed as "DFG-in" (Figure 3A). However, this motif can adopt another conformation by flipping, which results in Asp and Phe residues swapping their positions. The flipped DFG motif moves the aspartate away from the ATP binding site, leading to a catalytically incompetent state termed the "DFG-out" state. Importantly, the "DFG-out" state opens a new allosteric pocket directly adjacent to the ATP binding pocket (Figure 3B).[9]

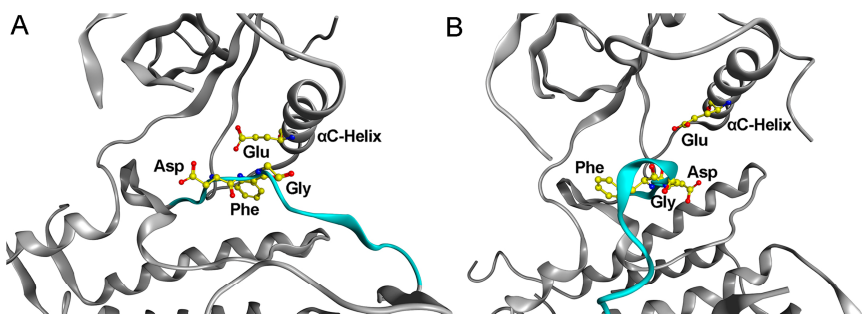

Figure 3. The relative position of the DFG motif, αC-helix Glu residue and part of the flipping activation loop (cyan) in different conformers: (A) DFG-in conformer of RET kinase (PDB ID 6NEC); (B) DFG-out conformer of KDR kinase (PDB ID 3WZE).

Another well conserved motif is the His-Arg-Asp (HRD) triad that precedes the activation loop, and which plays a major role in catalysis. This motif can deprotonate the residue of the substrate to be phosphorylated which then attacks the activated γ-phosphoryl groups of ATP. The "DFG" and "HRD" motifs constitute the key structures and function of the activation loop.[10,11]

Two additional important motifs for kinase activity include the "roof-lysine" and αC-helix. This lysine is located on the β3 sheet of the N-lobe and stretches the side chain down to the cleft. When the αC-helix adopts an inward conformation (αC-in conformation) the conserved glutamic acid residue in the helix forms a salt bridge with the "roof lysine". Then, the lysine side chain

establishes hydrogen bonds with oxygen atoms of α and β phosphates of ATP that together with Mg^{2+} ions allow the phosphate transfer. While the αC-helix turns to a αC-out conformation, the salt bridge disrupts which breaks the coordination of the phosphate groups, resulting in loss of catalytic function. [12,13]

The P-loop joins two anti-parallel beta-strands that are a part of the N-lobe beta-sheet structure of the kinase domain. This loop has considerable conformational flexibility. In the inactive conformation, the P-loop may be largely disordered. In the active kinase conformation, the P-loop may resemble something more akin to a classic beta-turn and can interact with the triphosphate group of bound ATP.[14]

2.1.3 Tyrosine kinases and the mechanisms of dysregulation

Tyrosine kinases (TKs) can be sub-classified as receptor and non-receptor proteins. Receptor TKs (RTKs) transduce extracellular signals to the cytoplasm, whereas non-receptor TKs are intracellular proteins that relay intracellular signals. RTKs contain a ligand-binding extracellular domain, an intracellular catalytic domain, a transmembrane (TM) domain and juxtamembrane (JM) domain. The TM domain may contain a disulphide bond that connects the extracellular and intracellular regions of the receptor.[15] The highly conserved catalytic domain is responsible for TK activity and several regulatory functions.

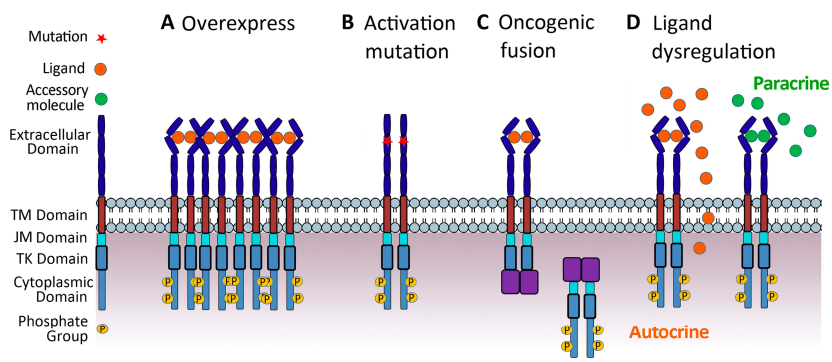

Figure 4. Mechanisms of RTK hyperactivation and dysregulation.[16] (A) Overexpression due to gene amplification or altered transcription; (B) Activating mutations in the extracellular or kinase domains resulting in ligand-independent constitutive activation of the receptor; (C) Oncogenic fusions may cause oligomerization (left) or alter subcellular localization (right); (D) Ligand dysregulation: either autocrine or paracrine resulting in receptor activation and various cellular responses. Redraw based on the reference.

RTKs can be abnormally activated via mechanisms, such as overexpression, mutation/translocation and atypical ligand induction,[16,17] as shown in Figure 4.

Overexpression of RTKs is the mechanism that most commonly leads to cancer. For example, FGFR1 amplifications can result in breast cancer (19% of ER-positive breast cancer), prostate cancer (16%), bladder cancer (9%), lung cancer (6%) and 17% of squamous cell carcinoma.[18] Overexpression is mainly caused by focal duplications of RTK-containing genomic regions or polysomy but also results from altered transcription and epigenetic aberrations (Figure 4A).

Non-synonymous mutation can lead to changes in protein structure and function, and then result in pathogenic activation of RTKs in different manners (Figure 4B).[19] Mutations may also weaken autoinhibitory interactions which are important for maintaining the inactive state of RTKs, thus causing aberrant kinase activation. When the mutations interfere with the external downregulation of RTKs, it can also result in abnormal kinase activity.

Another oncogenic mechanism is RTK fusion generated by chromosomal rearrangements (Figure 4C). Usually, the RTK kinase domain is fused to different partner proteins. They can drive oligomerisation or alter the subcellular localisation, expression and/or stability of associated RTKs, and then result in ligand-independent kinase activity.[20,21]

Except the aspect of RTK, dysregulation of RTK ligands (usually overexpression of growth factors) can also contribute to tumorigenesis. Ligand dysregulation can be drive by autocrine or paracrine mechanisms.[22,23] The former is expressed by the cell where the RTK is located, while the latter depends on the tumour cell microenvironment (Figure 4D).

2.1.4 Dysfunction of protein kinase and disease

Kinases transiently phosphorylate specific amino acids on ~30% of all human proteins, including molecules that govern complex cellular processes, such as growth, differentiation, proliferation and apoptosis.[24] Given the importance of these cellular activities, it is unsurprising that abnormal phosphorylation should transpire to be a cause or consequence of human disease, particularly developmental and metabolic disorders and cancers.[25]

A survey showed that approximately half of these disease-associated kinases were TKs.[19] Among the 915 curated disease-associated mutations, over 80% of mutations directly affected or encompassed the catalytic domain of the respective kinase gene. Cancer is the most common disease resulting from the mutation of TK.[26-28] Some representative TK mutation-associated diseases are listed in Table 1.

Table 1. Diseases caused by mutations in specific protein kinases.

Tyrosine kinase	Diseases
RET	Lung, ovarian, bladder, large intestinal carcinomas; pheochromocytoma; thyroid tumours and glioblastomas; Hirschsprung's disease
BTK	X-linked agammaglobulinaemia; lung carcinoma
MET	Papillary renal cancer; sporadic renal cell carcinoma; childhood hepatocellular carcinoma
ALK	Non-Hodgkins lymphoma; ovary, breast and lung cancers; neuroblastomas; glioblastomas
ROS2	Renal cell and colorectal carcinoma
ABL	Chronic myelogenous leukaemia
JAK3	X-linked SCID; acute megakaryoblastic leukaemia; gastric adenocarcinoma
KIT	Testicular and ovarian tumours
FGFR1	Stem cell leukaemia lymphoma (FGFR1–ZNF198 chimerism); pancreatic adenocarcinomas; glioblastoma; breast carcinomas; lung cancers
FGFR2	Glioblastoma, breast, gastric, lung, ovarian, cervical and endometrial cancers
FGFR3	Prostrate and cervical cancer, lung, bladder, upper digestive tract and intestinal carcinomas and plasma cell myeloma
FLT4	Increase in metastasis in adenocarcinoma and lymph node cancer, glioblastoma, kidney and ovary carcinomas and melanoma
PDGFRα	Gastrointestinal stromal tumours
TRKC	Breast, colon, lung and pancreatic tumours
VEGFR2	Capillary infantile hemangioma; colon cancers

Except for mutation, abnormal expression is another frequent kinase associated pathogenic factor. For example, overexpression of PDGFRβ is usually observed in metastatic medulloblastoma,[29] and increased expression of PYK2 may lead to renal cell carcinoma and breast cancer.[30,31]

In addition to the TK family, the dysregulation of other kinases may be responsible for some human malignant diseases. Hyperactive GSK3β may lead to Alzheimer's disease.[32] GSK3 generally opposes the action of insulin and GSK3 hyperactivity may contribute to insulin resistant (type II) diabetes.[33]

2.2 Kinase inhibitors

2.2.1 FDA approved kinase inhibitors

Considering the prevalent role of kinases in pathological conditions and their potential commercial value, the development of kinase-targeted drugs has attracted tremendous attention from both large and small pharmaceutical companies over the past 30 years. Kinase is currently one of the most important drug targets (groups) in the drug industry and academia.[34,35] By the end of June 2021, there were 72 small molecule kinase inhibitors (SMKIs) approved by the FDA (Table 2). It should be noted that 35 of them target the RTKs. Some other SMKIs have been approved for use in other countries or regions. For example, fasudil was approved as a ROCK1/2 inhibitor for cerebral vasospasm and pulmonary arterial hypertension in China and Japan in 1995. Filgotinib (JAK1 inhibitor) was rejected by the FDA due to toxicity concerns, e.g. testicular toxicity in males, but approved for rheumatoid arthritis in both the European Union and Japan in September 2020.

Table 2. FDA-approved small molecule kinase inhibitors, and their kinase targets, and therapeutic indications.

Year	Generic name	Presumed target(s)	Originally approved indications
1999	Sirolimus	mTOR	kidney transplantation
2001	Imatinib	Bcr-Abl, c-KIT, PDGFR	CML
2003	Gefitinib	EGFR	NSCLC
2004	Erlotinib	EGFR	NSCLC
2005	Sorafenib	VEGFR, PDGFR, BRAF, FTL3, RET, c-KIT	HCC, RCC
2006	Dasatinib	Bcr-ABL, SRC, KIT, EPHA2, PDGFRβ	Ph+ CML, Ph+ ALL
	Sunitinib	VEGFR, PDGFR, FLT3R, c-KIT, RET	RCC, Imatinib resistant GIST
2007	Temsirolimus	mTOR	RCC
	Lapatinib	EGFR, HER2	HER+ breast cancer
	Nilotinib	BCR-ABL	Ph+ CML
2009	Everolimus	mTOR	RCC
	Pazopanib	VEGFR2, PDGFR, c-KIT	RCC
2011	Ruxolitinib	JAK1/2	Myelofibrosis
	Crizotinib	ALK, ROS1	ALK or ROS1-postive NSCLC
	Vemurafenib	BRAF	$BRAF^{V600E}$ melanomas
	Vandetanib	EGFR, VEFGR, RET	Medullary thyroid cancers
2012	Ponatinib	BCR-ABL, SRC	Ph+ CML, Ph+ ALL
	Cabozantinib	RET, VEGFR2, PDGFR, c-KIT	Medullary thyroid cancer
	Tofacitinib	JAK3	Rheumatoid arthritis
	Regorafenib	VEGFR2, TIE2	Colorectal cancer, GIST, HCC

	Bosutinib	Bcr-Abl	CML
	Axitinib	VEGFR, PDGFR, c-KIT	Ph+ CML
2013	Dabrafenib	BRAF	$BRAF^{V600E}$ melanomas
	Trametinib	MEK1/2	$BRAF^{V600E}$ melanomas
	Ibrutinib	BTK	MCL, CLL/SLL
	Afatinib	EGFR, HER2	NSCLC with EGFR mutation
2014	Nindetanib	VEGFR, PDGFR, FGFR	Idiopathic pulmonary fibrosis
	Idelalisib	PI3Kδ	CLL, follicular B-cell NHL, SLL
	Ceritinib	ALK	NSCLC with ALK translocation
2015	Alectinib	ALK, RET	NSCLC with ALK translocation
	Palbociclib	CDK4/6	HER2 positive breast cancer
	Lenvatinib	VEGFR, RET,	Differentiated thyroid cancers
	Osimertinib	EGFR	NSCLC with EGFR mutation
	Cobimetinib	MEK1/2	$BRAF^{V600E}$ melanomas
2017	Ribociclib	CDK4/6	HER2 negetive breast cancer
	Brigatinib	ALK, EGFR	ALK positive NSCLC
	Midostaurin	FLT3, c-KIT	AML, mastocytosis
	Nerotinib	EGFR, HER2, ErbB2	HER2 overexpressed breast cancer
	Baricitinib	JAK1/2	Rheumatoid arthritis
	Abemaciclib	CDK4/6	HER2 negtive breast cancer
	Copanlisib	PI3Kα/δ	Follicular B-cell NHL
	Netarsudil	ROCK	Glaucoma
	Acalabrutinib	BTK	MCL, CLL
2018	Encorafenib	BRAF	$BRAF^{V600E}$ melanomas
	Binimetinib	MEK1/2	$BRAF^{V600E}$ melanomas
	Duvelisib	PI3Kγ/δ	CLL, SLL
	Dacomitinib	EGFR	NSCLC with EGFR mutation
	Gilteritinib	FLT3, AXL	AML with FLT3 mutation
	Larotrectinib	Trk	Solid tumors with NTRK fusion
	Lorlatinib	ALK, ROS	ALK-positive NSCLC
	Fostamatinib	Syk	Chronic immune thrombocytopenia
2019	Erdafitinib	FGFR	Urothelial cancer
	Alpelisib	PI3Kα	Breast cancer
	Pexidartinib	CSF1R, c-KIT	Tenosynovial giant cell tumor
	Entrectinib	Trk, ROS, ALK	ALK-positive NSCLC
	Upadacitinib	JAK	Rheumatoid arthritis
	Fedratinib	JAK2	Myeloproliferative diseases
	Umbralisib	PI3Kδ	Marginal zone lymphoma
	Zanubrutinib	BTK	MCL
2020	Avapritinib	PDGFRα	GIST
	Tucatinib	HER2	HER2-positive breast cancer
	Pemigatinib	FGFR2	Cholangiocarcinoma with FGFR2 fusion
	Tabrecta	MET	NSCLC with ex14 mutation
	Selpercatinib	RET	NSCLC, MTC
	Selumetinib	MEK1/2	Neurofibromatosis type I
	Ripretinib	KIT	GIST, Mastocytosis
	Pasalisib	PI3K	Glioblastoma
	Pralsetinib	RET	RET fusion-positive NSCLC
2021	Tivozanib	VEGFR	RCC
	Tepotinib	c-MET	NSCLC
	Trilaciclib	CDK4/6	SCLC
	Infigratinib	FGFR1/2/3	Cholangiocarcinoma

Furthermore, 63 of the approved kinase targeting drugs are active against more than one type of cancer, and only a few have been approved for non-oncological indications. For example, the JAK3 inhibitor tofacitinib is used for rheumatoid arthritis, the mTOR inhibitor sirolimus was applied to decrease the risk of rejection after organ transplantation; and the PDGFR/VEGFR/FGFR inhibitor nintedanib was approved for idiopathic pulmonary fibrosis.

2.2.2 The outlook and challenge of developing kinase inhibitors

The majority of clinical trials target only 43 protein kinases and approximately 50% of these inhibitors target kinases for which there are already existing approved drugs.[36] The full potential of the human kinome as a source of new drugs has not been fully explored since more than 100 kinases have unknown functions and 50% of all kinases are largely uncharacterized. Thus, attempts to identify the functions of those kinases, develop modulators to control their activities and improve human health are ongoing.[37]

Although kinase inhibitors have successful applications in oncology and inflammatory disease and other areas, there remain some challenges in kinase-related medicinal chemistry. Clinic acquired resistance is a major barrier to successful long-term cancer therapy. The development of resistance-mutant specific inhibitors can prolong patient survival, however, sequential resistance inevitably occurs.[38,39] For example, the third-generation EGFR T790M inhibitor, osimertinib, is rendered ineffective by an EGFR C797S mutation.[40] Additionally, achieving selectivity over homologous proteins remains one of the most significant challenges in early-stage kinase inhibitor projects, which is essential for understanding the target biology and avoiding off-target toxicity.[41,42] Medicinal chemistry researchers have attempted to resolve this by developing small molecules with novel mechanisms of action, such as induced degradation,[43] reversible covalent inhibition[44,45] and targeting remote cysteine.[46] Additional approaches have been explored to address the selectivity issue, such as utilising type III binding modes, obligate-covalent targeting and targeting P-loop conformations.[47] Moreover, modern techniques for profiling kinase inhibitors have been developed and wide range kinome profiling of compound libraries has been employed as an efficient approach for the discovery and optimization of lead compounds.[48-50]

2.2.3 Classification of kinase inhibitors

Based upon the binding mode of the molecules over their kinase targets, the small molecule protein kinase inhibitors are divided into seven main groups, including reversible (Groups I, I½, II, III, IV and V) and irreversible inhibitors

(VI), as described in Table 3.[51] It should be noted that the classification of one inhibitor can be different when it binds to a different target kinase. For example, crizotinib is a type I kinase inhibitor when it targets ROS1 (PDB ID: 3ZBF), whereas the binding models fit the feature of type I½B kinase inhibitor when it binds to ALK (PDB ID: 2XP2). Another example is bosutinib, which is either a type I or type IIB inhibitor when bound to different targets (Table 3).

Table 3. Classification of small molecule protein kinase inhibitors.[51]

Inhibitor type	Features	Inhibitor-Target	PDB ID
I	Binds in and around the ATP-binding pocket of an active enzyme	Gefitinib-EGFR	2ITY
		Bosutinib-Src	4MXO
		Dasatinib-Abl	2GQG
I½ A/B	Binds in and around the ATP-binding pocket of an inactive DFG-in enzyme	-	-
I½ A	Extends into the back cleft	Dasatinib-Lyn	2ZVA
		Lapatinib-EGFR	1XKK
I½ B	Does not extend into the back cleft	Crizotinib-Met	2WGJ
		Erlotinib-EGFR	4HJO
II A/B	Binds in and around the ATP-binding site of an inactive DFG-out enzyme	-	-
II A	Extends into the new hydrophobic pocket resulted from activation loop flipping	Axitinib-VEGFR	4AG8
		Ponatinib-Abl	3OXZ
II B	Does not extend into the new hydrophobic pocket	Bosutinib-Abl	3UE4
		Sunitinib-Kit	3G0E
III	The allosteric inhibitor bound next to the ATP-binding site	Trametinib-MEK1	7JUR
IV	The allosteric inhibitor bound away from the ATP-binding site	GNF-2-Abl	3K5V
V	Bivalent inhibitor spanning two kinase domain regions	-	-
VI	Covalent inhibitor	Ibrutinib-BTK	5P9J

Protein kinase type I inhibitors have been shown to bind to the active form of their protein kinase targets. Type I½ inhibitors reversibly bind within the ATP-binding pocket of an inactive DFG-Asp-in conformation of their target protein kinases. Most of these inhibitors have the αC-helix out-conformation with a distorted R-spine (Table 3). The type I½A subgroup occupies the front cleft and gate area and extends into the back cleft of the protein kinase, whereas type

I½B inhibitors occur in the front cleft and gate area but do not extend into the back cleft of protein kinases.[52]

Type II inhibitors bind to the DFG-Asp-out conformation protein kinase and type IIB drugs are restricted to the front cleft and gate area, while type IIA drugs occupy the front cleft and gate area and extend into the back cleft.[53]

Type III inhibitors occupy a site next to the ATP-binding pocket so that both ATP and the allosteric inhibitor can bind simultaneously to the protein. These compounds are steady-state non-competitive or uncompetitive inhibitors with respect to ATP as ATP cannot prevent their interaction with the enzyme.[54]

Type IV allosteric inhibitors bind to sites distant from the substrate binding sites. One example of a type IV inhibitor is GNF-2, an antagonist of BCR-ABL, which binds to the myristoyl binding site and stabilises the inactive enzyme form.[55]

Type V inhibitors are bivalent inhibitors that span two kinase domain regions; usually, one of the regions is the ATP binding cleft.[56] This type of kinase inhibitor tends to have higher selectivity compared to single-site inhibitors since they generate more interactions with target enzymes; however, they have lower efficacy *in vivo* due to low bioavailability with the large structure.[57] The research and development of type V kinase inhibitors are currently at the preclinical stage.

Type VI inhibitors are those drugs that bind covalently to their protein kinase target. Ibrutinib is the first FDA-approved drug that forms a covalent bond with its target, a 'blockbuster drug' in hematologic tumour therapy.[58]

2.3 RET kinase and inhibitors

2.3.1 Structure and physiology of RET kinase

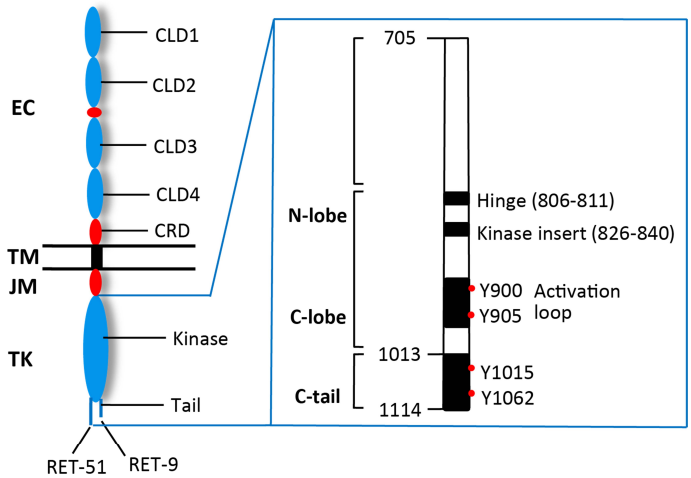

Figure 5. Schematic representation of structure of the RET protein.[59] Left: The simplified structural modules of RET kinase; Right: Structural details of the RET kinase domain (RET-51 isoform). Redraw based on the reference.

RET is the abbreviation of 'rearranged during transfection', a proto-oncogene discovered in 1985 when Takahashi et al. exogenously transfected a DNA sequence of human lymphoma cells into mouse-derived NIH3T3 cells and found that the gene had rearranged. This gene encoded the RET kinase, which is an RTK.[60] RET kinase consists of 1114 amino acids and has four domains (Figure 5): the extracellular domain, a single-pass TM domain, a JM domain and an intracellular TK domain. The intracellular TK domain regulates cell differentiation and proliferation through extracellular signalling. Depending on the number of amino acids contained in the C-terminal tails at the TK domain, three protein subtypes (RET9, RET51 and RET43) may be identified: RET9 and RET51 are ubiquitous, while RET43 is present only in primates and some lower species.[61] The RET extracellular domain consists of four cadherins (Ca^{2+}-dependent adhesion molecules) repeats (CLD1-4), one Ca^{2+} binding site and one cysteine-rich domain (CRD) (Figure 5). The ligands for RET protein kinase are soluble dimeric growth factors of the glial cell line-derived neurotrophic growth factor (GDNF) family (GFL), including GDNF, neurturin, persephin and artemin.[62] GFLs bind to glycosylphosphatidylinositol-linked co-receptors, named GFRα1-4, thus forming a binary complex which aggregates the other RET proteins in the extracellular domain. Such aggregation results in the *trans*-

autophosphorylation of specific tyrosine residues (Y900, Y905, Y1062, Y1096) within the TK domain of each RET receptor. The downstream signalling pathways are activated via connexin and signalling proteins, which further regulate cell growth and differentiation (Figure 6).[63]

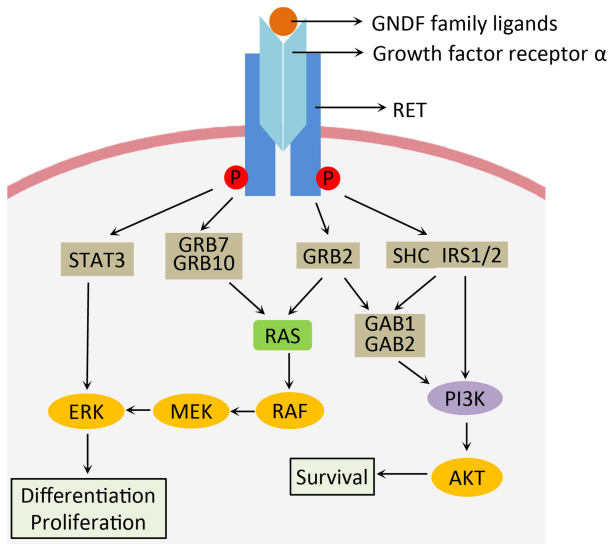

Figure 6. Schematic representation of RET kinase signalling.[63] Redraw based on the reference.

2.3.2 RET kinase associated diseases

The aberrant expression of RET protein kinase has correlations with a variety of diseases, such as non-small-cell lung cancer (NSCLC), multiple endocrine neoplasia type 2 (MEN2) and medullary thyroid carcinoma (MTC).[64] The mechanism of the aberrant expression of RET kinase includes RET gene mutation, fusion and alteration and high levels of RET expression. RET mutations cause the autosomal dominant inheritance of MEN2 syndromes, which are prone to MTC, pheochromocytoma, parathyroid hyperplasia, intestinal ganglioneuromatosis, corneal nerve thickening and marfanoid habitus.[65] More specifically, MEN2 results from RET missense mutations that typically target cysteines of the RET CRD domain (leading to RET dimerization) and methionine 918 (M918T) immediately downstream the activation loop (increasing the affinity of ATP).[66] In addition to MEN2, mutations are also found in more than 50% of sporadic MTC cases.[65] RET fusions are found in approximately 2% of NSCLC[67] and 7% of sporadic papillary thyroid carcinomas (PTC),[68] more commonly in radiation-associated

(approximately 60%)[69] and young PTC patients (approximately 30%).[70] The fusion is usually connected with chromosomal rearrangements which cause fusion of the RET intracellular domain and lead to aberrant expression and ligand-independent activation. Additionally, the structural RET gene alterations are also associated with multiple cancer types, for example, RET M918T alteration is normally observed in paraganglioma and atypical lung carcinoid, while RET V804M alteration is common in colorectal adenocarcinoma, meningioma, gastrointestinal stromal tumour and hepatocellular carcinoma.[71] Moreover, RET overexpression (in the absence of structural alterations) have been reported in breast carcinoma and pancreatic adenocarcinoma.[72,73]

2.3.3 RET kinase inhibitors

Due to its key role in previously mentioned diseases, RET kinase has been an attractive therapeutic target, particularly for various cancers. Numerous efforts have been made to develop small-molecule RET kinase inhibitors.[74] It should be noted that two specific RET kinase inhibitors, selpercatinib and pralsetinib, were approved for thyroid cancer and/or lung cancer in 2020 (Figure 7). Multi-kinase inhibitors with potent activity over RET have been approved by FDA for the treatment of thyroid and other types of cancer.[71,75] These include vandetanib (for MTC),[76] cabozantinib (for MTC and renal cell carcinoma),[77] lenvatinib (for differentiated thyroid carcinoma and renal cell carcinoma),[78] ponatinib (for chronic myeloid leukaemia and Philadelphia chromosome-positive acute lymphoblastic leukaemia),[79] sunitinib (for renal cell carcinoma and imatinib-resistant gastrointestinal stromal tumour),[80] regorafenib (for colorectal cancer and gastrointestinal stromal tumour)[81] and sorafenib (for differentiated thyroid carcinoma, renal cell carcinoma and hepatocellular carcinoma).[82] These FDA-approved kinase inhibitors can be divided into two classes: type I, which includes selpercatinib, pralsetinib, lenvatinib and vandetanib; and type II, which includes cabozantinib, ponatinib, sorafenib, regorafenib and sunitinib. All type II inhibitors are multi-targeted and able to inhibit VEGFR2 and KIT (except for RET), and sometimes target other RTKs of the split kinase domain family (FGFR1, MET, PDGFR, VEGFR1/3), other TK/TKL families or STE kinases. This can confound the contribution of RET inhibition to the antitumour effect of the drug. Moreover, the off-target inhibition can generate adverse events and toxicity through targeting non-RET kinases such as VEGFR2.[83,84] Additionally, although some of them, such as cabozantinib, are specifically approved for MTC, which has a higher proportion of RET oncogenic mutations. However, response rates in RET-driven cancers are not as high as the ones observed in other fully explored therapeutic targets, such as EGFR, ALK or ROS1. To solve these problems, significant efforts have been made to generate

highly potent and selective RET inhibitors and two type I inhibitors, selpercatinib and pralsetinib, have been recently approved. As for type II RET inhibitors, some highly specific lead compounds have been developed as potential clinical candidates, such as Hu1-117,[85] HSN608[86] and GSK3179106[87] (Figure 7). However, as RET is constitutively expressed throughout different organs in both healthy and diseased tissues, it still inevitably affects the non-disease tissue during RET-targeted therapy and results in side effects.[88,89] Therefore, strategies that allow externally controlled activation of drugs at the site of action at a chosen time will be useful and practical, without concerning the target distribution.

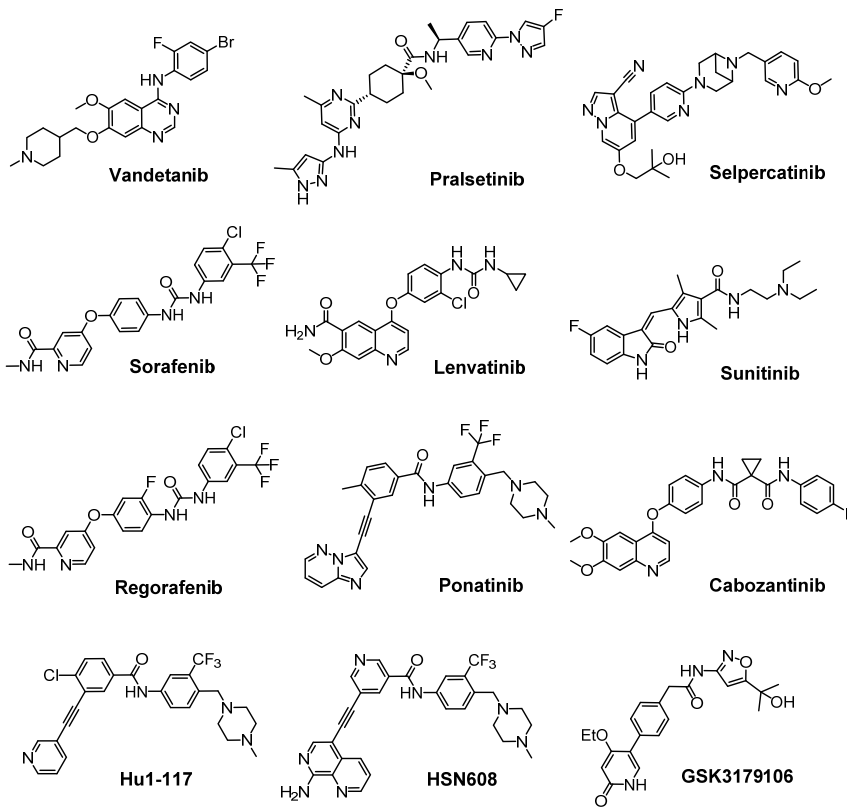

Figure 7. Representative RET kinase inhibitors

2.4 Photopharmacology

2.4.1 The concepts of photopharmacology

Due to the advantages of noninvasive and remote action and the reversibility, speed and facile modulation of the energies involved, light can be an efficient and powerful factor for controlling biological processes.[90] Optogenetics, an experimental method involving the combination of optics and genetics to control well-defined events in cells of living animal tissue, is an example of this.[91] Light can also regulate the biological activity of synthetic molecules by changing their pharmacokinetic or pharmacodynamic properties. Such combinations of photochemistry and pharmacology are known as "photopharmacology".[92,93]

Photopharmacology aims to address the challenges of off-target activity and tissue selectivity by introducing a light-responsive unit to regulate the action of the drug. Such regulation can be conducted qualitatively or quantitatively by adjusting wavelength and intensity, and performed with high spatial and temporal precision, avoiding contamination of the studied object. To achieve this, photopharmacology relies on chemical modification of bioactive molecules in a manner aimed at enabling it with light-controlled function.

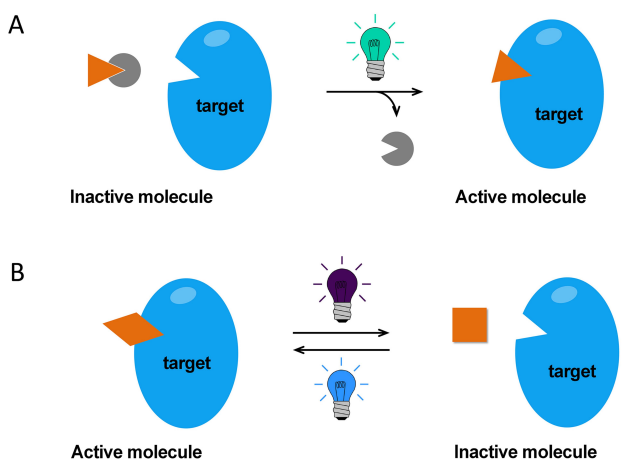

Figure 8. Two approaches in photopharmacology: (A) An irreversible approach with photolabile caging groups; (B) A reversible approach with photoswitches that can interconvert between two isomers by two different wavelength exposures. Orange: bioactive molecule; Grey: caging group.

One of the most widely used approaches is the "photocaging" approach (Figure 8A). A key bioactive molecule is protected with a photolabile protecting group

(termed a "caging" group), which deactivates the molecule until the caging group is removed using light. A large number of such photolabile protecting groups have been developed and used for biological studies.[94,95] However, these molecules undergo irreversible photochemistry whereby the caged molecule becomes the active form once uncaged; this molecule remains active until it is removed in some other biological manner.

Conversely, photoswitchable approaches are reversible (Figure 8B).[96,97] A photoswitch is a type of molecule that can change its structural geometry and chemical properties upon irradiation with light. Usually, many rounds of isomerisation can be performed upon exposing it to different wavelengths of light or thermal processes (Scheme 1).[98,99] To apply such 'photoswitches' to bioactive molecule, there are several criteria that chemical modifications must meet. Firstly, the modified molecule should absorb light effectively and efficiently at a wavelength longer than 340 nm to be compatible with biological systems. Secondly, the modification must make the bioactive molecule able to experience a substantial change in its bioactivity upon irradiation. Thirdly, the new molecule should have favourable pharmacokinetics and should be metabolically stable in a given environment. It cannot be phototoxic, which can occur when intersystem crossing competes with photoswitching.[100] Several photoswitches have been developed and successfully applied in photophamacology (Scheme 1).[101-105] Among them, the azobenzene-based photoswitch is the most widely used class of photoswitch for the photocontrol of the activity of biomolecules. This thesis focuses on this approach.

Scheme 1. Most frequently used photoswitches in photopharmacology.

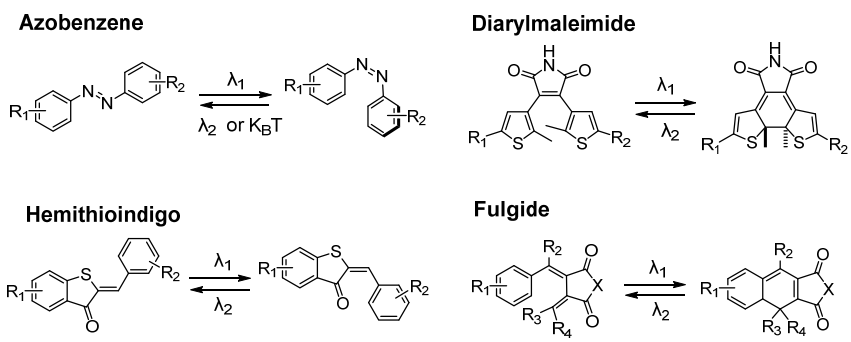

2.4.2 Photoswitchable kinase inhibitors

Currently, photopharmacology has made important breakthroughs in the application to varies of targets, such as ion channels, transporters and pumps,

GPCRs, enzymes or elements of the cytoskeleton. Among them, kinases have gradually become attractive targets.[106] Before this thesis work was begun, only one publication had reported on the development of azobenzene-based photoswitchable kinase inhibitors (Figure 9). The Grøtli group published the first photoswitchable kinase inhibitor targeting RET kinase in 2015.[107] This azo molecule was derived from PP1, a typical RET inhibitor. However, only a 4-fold difference of bioactivity *in vitro* between the two isomers was observed. Further four papers have now been published in this field (Figure 9). In 2019, the Peifer group published their paper on the efforts towards photoswitchable P38/CK1δ kinase inhibitor with vicinal diaryl scaffold. However, the inhibitors were sensitive to reductants such as DTT and GSH.[108] In the same year, the Szymanski group published research on the photoswitchable $BRAF^{V600E}$ kinase inhibitors. They integrated azobenzene into the pharmacophore of vemurafenib, however, the short half-life limited further application.[109] Early this year, the same group published a study on the visible light-regulated photoswitchable CKI kinase inhibitor, derived from longdaysin, a circadian period modulator.[110] Recently, the Trauner group published a photoswitchable covalent JNK3 kinase inhibitor by linking vicinal diaryl scaffold with azobenzene-derived diazocine and an (*E*)-dimethylaminocrotyl amide electrophile.[111]

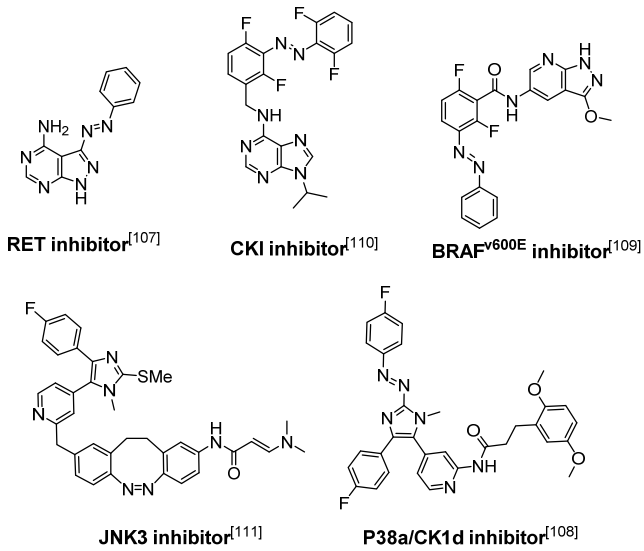

Figure 9. Azobenzene based photoswitchable kinase inhibitors.

3 Methods

3.1 Synthesis of azobenzene derivatives

Azobenzene-derived compounds have been widely used in industry and scientific research in the past hundred years, as dyes,[112] food additives, chemical indicators, radical reaction initiators, and medical agents.[113] Recently, azo compounds have been applied for optical storage materials[114] and photoswitches.[115] The strategies to synthesize azobenzene derivatives have been widely explored (Scheme 2).[116] A classical way to prepare azobenzene based photoswitchable bioactive molecules is via the Mills reaction where aromatic nitroso derivatives react with anilines in glacial acetic acid or strong base to give the corresponding azobenzenes.[117] The nitroso moieties are usually prepared through the oxidation of aniline with m-CPBA or OXONE.[118] Another classic strategy is to synthesize azo compounds in a diazonium salt coupling reaction.[119] This method starts with diazotization of an aromatic primary amine at low temperatures, the resulted diazonium intermediate reacts with an electron-rich aromatic compound and couples on the aromatic ring. This reaction is usually fast and has a high yield. Normally, the *para* position of the electron donating group on the aromatic ring would be substituted. When this position is occupied, the *ortho* position could be substituted. In recent years, a strategy via dehydrogenation of diarylhydrazines has been frequently used in the synthesis of azobenzene-type compounds, especially heterocycle-based azo compounds. Diarylhydrazines can be prepared using one of two approaches: nucleophilic substitution or metal catalysed coupling.[120,121] In the former approach, a phenylhydrazine reacts with a halogenated (Cl or F) aromatic ring via nucleophilic substitution by heating, ideally with a microwave reactor. Then, dehydrogenation is conducted with an oxidant, such as O_2, $Pb(OAc)_4$ or tetrabutylammonium cerium(IV) nitrate, to give the corresponding azo compounds. Regarding the latter approach, the palladium catalysed coupling reaction, e.g. Buchwald-Hartwig coupling of *N*-Boc arylhydrazines with aryl halides (Br or I), was first described in 2003.[121] The generated diarylhydrazine is submitted to a condition, such as NBS in pyridine or CuI/Cs_2CO_3,[122] to remove the Boc protection followed by dehydrogenation in one pot to form the azo bridge. Additionally, the symmetric azobenzene is occasionally reported to be obtained by oxidation using two portions of aniline or by reductive coupling using two portions of aromatic nitro derivatives.[123,124] One drawback of these methods is that the metallic oxidant or reductant used in stoichiometric amounts and the by-products formed are not environmentally friendly.

Scheme 2. The main synthetic strategies for the preparation of azo compounds.

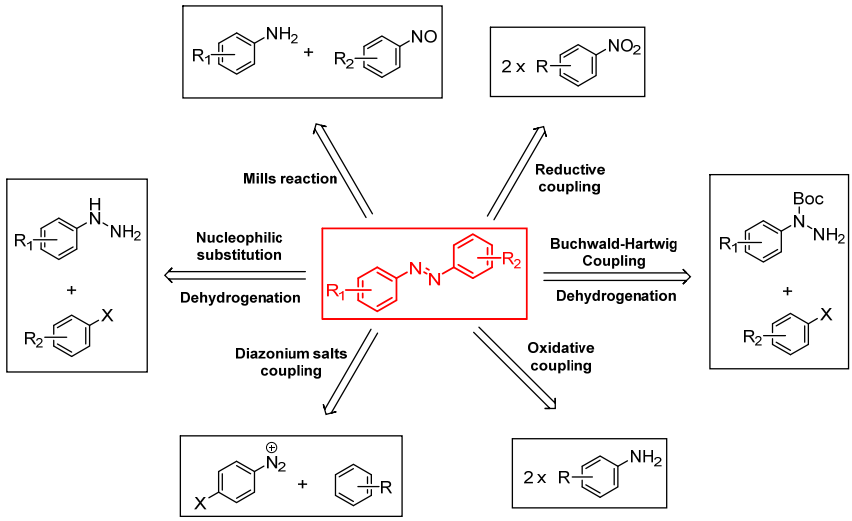

3.2 Photophysical properties of azo compounds

The evaluation of the photophysical properties of azo compounds is mainly based on UV-vis isomerisation absorption spectroscopy, together with other methods, e.g. NMR spectroscopy. Four different photophysical parameters have been the main focus in this thesis: the wavelength of the maximum light absorption, thermal stability of the *Z*-isomer, photostationary distribution (PSD) and reproducibility of photochemical switching.

The light absorption maxima of azo compounds is tunable by various way, e.g. by introducing substituents, which encourages the preparation of molecules that can be isomerised by visible light,[125] which is important for the application of azo compounds *in vivo*.[126,127] This parameter can be read directly from UV-vis absorption spectra.

The thermal stability of the *Z*-isomer is important in biological applications as it is a matter of purity over time. For some azo compounds, *Z*-isomers rapidly convert into their *E*-isomer,[128] which is good for studying rapid biological processes, e.g. calcium signalling. Those azo compounds with stable *Z*-isomers are required for the application in enzymatic inhibition.[129] Additionally, the nature of the solvent that is used during measurement influences the stability of the metastable *Z*-isomer.[130] The lifetime or half-life of *Z*-isomers is usually determined by running thermal switching kinetics in the dark at certain temperatures and then fitting them with an exponential decay function.

The photostationary distribution is the steady-state relative abundance of *E* and *Z*-isomers after the azo compounds have been exposed to a certain wavelength of light. This is also a matter of purity that light irradiation can achieve, the higher the better. The value of PSD (ratio of *E*/*Z*-isomers) is determined by ^{1}H-NMR of the fully irradiated azo compound solution in DMSO-*d6* (5 mM) or by HPLC if the sample was prepared in certain solvents, such as H_2O, MeCN or MeOH.

Finally, azo compounds usually show little sign of fatigue or degradation after repeated switching, likely due to the absence of any side reactions.[131] This experiment was conducted by irradiating the azo compound sample with two different wavelengths alternately to achieve PSD and repeating for 10 or more cycles.

The photoisomerization quantum yield (Ø) is an important parameter for photoswitchable compounds. However, the thermal isomerization (from *Z*-isomer to *E*-isomer) process of azo compounds usually proceeds simultaneously with photo-induced isomerization, which makes it very hard to determine the photoisomerization quantum yield. In this thesis, this parameter has not been evaluated.

3.3 Kinase assays

The vigorous development of kinase inhibitors both in industry and academia demands efficient and accurate assays to evaluate kinase catalytic function. The functional assay can be used to identify inhibitors, estimate affinity, characterize molecular mechanisms of action (MMOAs) and evaluate selectivity. Kinase assays include enzyme assays (cell-free assay) and cellular assays. In this thesis, the ADP-Glo™ RET kinase assay and NanoBRET™ TE intracellular RET kinase assay have been employed to evaluate the enzymatic inhibition activity and intracellular kinase binding affinity, respectively.

3.3.1 ADP-Glo™ kinase assay

The ADP-Glo™ kinase assay is a luminescent ADP detection assay that provides a homogeneous, high-throughput screening method to measure kinase activity by quantifying the amount of ADP produced during a kinase reaction.[132,133] This method is a universal biochemical assay that can be used for any combination of kinase and substrate, regardless of the nature of the substrate such as peptide, protein, sugar, and lipids. The assay is performed in two steps (Figure 10): first, after the kinase reaction, an equal volume of ADP-Glo™ Reagent is added to terminate the kinase reaction and deplete the remaining ATP; Second, the Kinase Detection Reagent is added to

simultaneously convert ADP to ATP and allow the newly synthesized ATP to be measured using a luciferase/luciferin reaction. The light generated is measured using a luminometer. This assay is sensitive enough to detect very low amounts of ADP (20 nM) and can detect generated ADP in a reaction containing up to 1 mM ATP in a linear fashion. The luminescent signal generated is proportional to the ADP concentration produced and is correlated with kinase activity.

In this thesis, the ADP-Glo™ RET kinase assay was run following Promega's protocol with an additional pre-incubation step before ATP and substrate were added to the kinase reaction mixture, 10 µM ATP, 4.0 ng RET kinase, and 0.4 mg/mL substrate (IGF1Rtide) were used. AMUZA LED array system was used to enrich the *Z*-isomer of azo compounds before the assays.

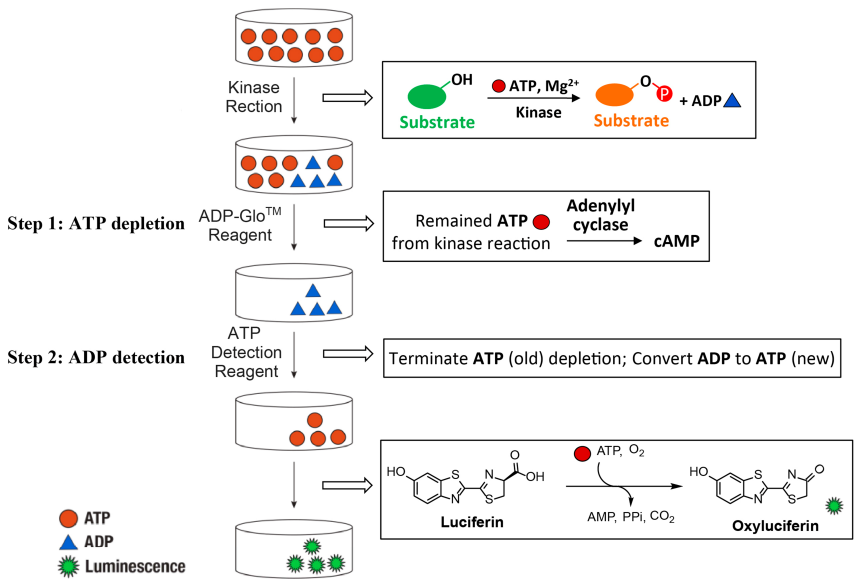

Figure 10. Principle of the ADP-Glo™ Kinase Assay. Redraw based on Promega protocol.

3.3.2 NanoBRET™ target engagement intracellular kinase assay

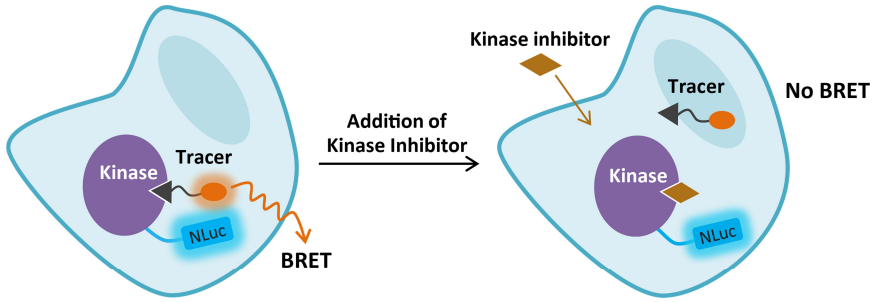

Figure 11. Principle of the NanoBRET™ target engagement intracellular kinase assay.

The NanoBRET™ Target Engagement (TE) Kinase Assay measures compound binding at a selected kinase target which is fused to NanoLuc® luciferase.[134,135] The NanoBRET™ TE Assay allows for the measurement of compound binding in the presence of cellular factors that are known to impact target engagement potency. Specifically, it allows the quantitation of apparent intracellular affinity for a test compound to a diverse set of full-length protein kinases expressed inside living cells. Compound engagement is measured in a competitive format using a cell-permeable fluorescent energy transfer probe, namely the NanoBRET™ tracer. The binding of the test compound results in a loss of a NanoBRET™ signal between the target protein and the tracer inside intact cells (Figure 11). To determine test compound affinity, cells are titrated with varying concentrations of the test compound in the presence of a fixed concentration of tracer. In this thesis, the working concentration of the K-10 tracer was 0.13 µM. AMUZA LED array system was used to enrich the Z-isomer of azo compounds before or during the assays.

4 Azoheteroarenes

4.1 Aromatic *N*-heterocycles in kinase inhibitors

Aromatic heterocycles play an important role in medicinal chemistry. Their skeleton diversity, chemical stability and the possibility to readily decorate them with functional groups, make them highly useful in the development of bioactive molecules.[136,137] Among all type of aryl heterocycles, nitrogen-containing aromatic heterocycles are of great importance to life science, since they are abundant in nature, and especially exist in some natural products subunit, such as the vitamin B family and the nucleobases. The drug molecules that contain aromatic *N*-heterocycles can mimic those natural products to interact with corresponding targets and lead to physiological responses.[138] Due to its natural potential of biological properties, aromatic *N*-heterocycles have always been attractive moieties in drug molecule design or chemical library development for hit compounds screening. An excellent example is their vast applications in the development of type I/II kinase inhibitors. The aromatic *N*-heterocycles mimic the role of adenine of ATP, forming H-bond(s) with the kinase hinge, and this H-bond(s) largely determine the activity of the kinase inhibitors.[139] Almost all the kinase inhibitors contain at least one aromatic *N*-heterocycle except for mTOR inhibitors. Figure 12 lists the most frequently used aromatic *N*-heterocycles in FDA approved kinase inhibitors.

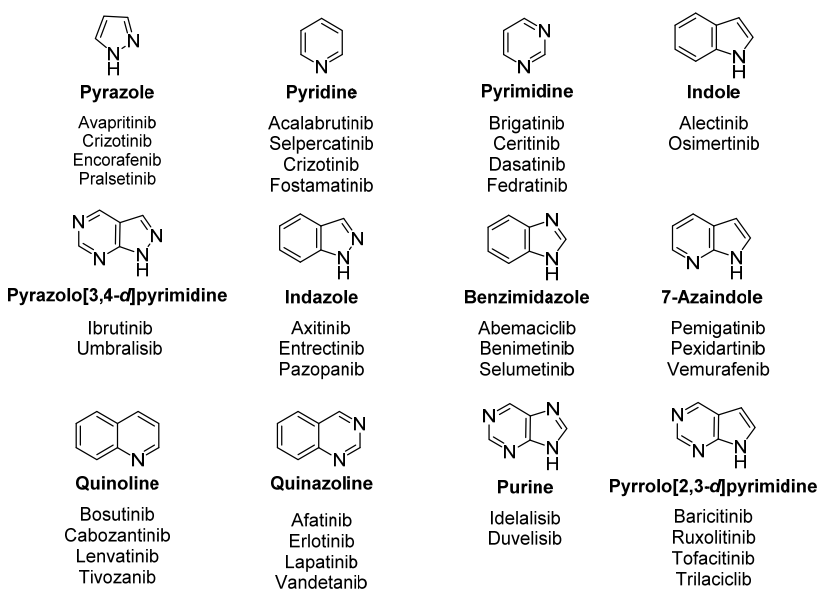

Figure 12. Aromatic *N*-heterocycles in FDA approved kinase inhibitors

4.2 Introduction of azoheteroarenes

Considering the essential role of aromatic *N*-heterocycles for the activity of kinase inhibitors, it is advisable to keep at least one aromatic heterocycle when incorporating azobenzene into the scaffold of kinase inhibitors during the development of photoswitchable kinase inhibitors. This is especially important when it comes to the heterocycles that bind to the hinge. Therefore, the heteroaryl azo unit becomes the photoswitch in the modified kinase inhibitors. If there is only one heteroaromatic ring incorporated, in most cases, such azo switches are called azoheteroarenes. Additionally, previous investigations of azoheteroarenes have shown that the introduction of a nitrogen atom(s) into one of the azobenzene phenyl rings changes the photophysical properties.[140-147] For example, the Fuchter group developed arylazopyrazoles which demonstrated excellent *E/Z*-isomers band separation and, therefore, near 100% PSD in both directions and a long half-life (up to ~1000 days).[145] Due to the impact of different aromatic *N*-heterocycles on the photophysical properties of azo switches, it is important to synthesise a series of aromatic *N*-heterocycle-based azoheteroarenes to study their photophysical properties. This paves the way for developing azoheteroarene-based photoswitchable kinase inhibitors.

4.3 Synthesis of azoheteroarenes

The synthesis of azoheteroarenes usually involves the strategies used for azobenzene, including the Mills reaction[141] and diazonium salt coupling.[140-141] All these strategies form the azo bond by two components of aromatic building blocks in the late/last stage. Some publications also reported a strategy that firstly forms the N-N bridge and then constructs heterocycles.[148] In this project, I attempted to develop a general synthetic strategy to prepare aromatic *N*-heterocycle based azoheteroarenes. The Cho group reported a strategy that initially formed the azo bridge by Buchwald-Hartwig coupling followed by NBS oxidation to provide azobenzene, however, this approach suffered side reactions due to bromination of the phenyl ring(s).[149] The Szymanski group reported a "one pot, two step" strategy that linked the phenylhydrazine on purine-derived aromatic rings by nucleophilic substitution followed by air oxidation to give azoheteroarenes.[143] However, the application of nucleophilic substitution was limited to a certain electron-deficient position with halogenated aromatic heterocycles, e.g. 7-Cl-*9H*-purine. Inspired by these two strategies, we used Buchwald-Hartwig coupling to connect Boc-phenylhydrazine to the aromatic ring, then removed Boc through microwave heating and performed O_2 dehydrogenation in the same pot to provide azoheteroarene, as shown in Scheme 3.

Scheme 3. The synthetic strategy of azoheteroarenes in this project.

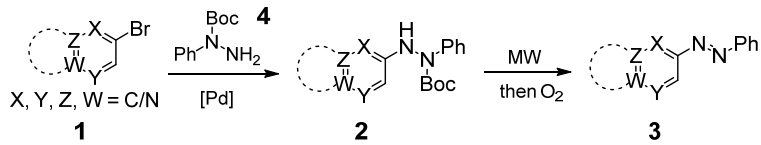

The synthesis and photophysical characterisation of five-membered aromatic *N*-heterocycles (e.g. imidazole, pyrazole or pyrrole)-based azoheteroarenes have been heavily studied.[140,141] Herein, the focus has been six-membered aromatic *N*-heterocycles- and fused aromatic *N*-heterocycles (pyridine and indole derivatives)-based azoheteroarenes; all these heterocycles have been reported as hinge binders of kinase inhibitors.

Bromoheterocycles **1a**−**1d** (entries 1−4; Table 4) were reacted with Boc-protected phenylhydrazine (**4**) under Buchwald-Hartwig conditions ($Pd(OAc)_2$, t-$Bu_3P{\cdot}HBF_4$, Cs_2CO_3, toluene, 110 ^oC, overnight). Good yields of Boc-protected diarylhydrazines **2a**, **2b** and **2d** (more than 65%) were produced. However, **2c** was only obtained in 18% yield. This result was due to a significant reduction of aryl halide (**1c**) by β-H elimination during the coupling reaction.[150] Additionally, some of the target products **1d** were converted to hydrazones by tautomerism, which further reduced the yield.[151]

However, when indole-derived bromoheterocycles were subjected to the conditions described above, no target products were detected. It was assumed that this was because the amine of the heterocycle interfered with the coupling reaction by coordinating the palladium catalyst. In this case, it became necessary to introduce a protecting group to block the amine on the substrates. Initially, Boc was employed to protect the 5-bromoindole to prepare **1e-1**. However, the Boc-group was lost during the Buchwald-Hartwig coupling step. Then, the more thermally stable tosyl group was used to protect the indole ring (**1e-2**). Reacting **1e-2** with **4** under Buchwald-Hartwig conditions gave **2e** in 83% yield. Afterwards, other tosyl protected 5-bromoindole derivatives (**1f**, **1g** and **1h-1**) were treated with the same conditions. Both **1f** and **1g** provided corresponding products **2f** and **2g**, respectively, in high yields (more than 80%). Compound **1h-1** still could not survive under these conditions (with and without **4**) as the tosyl group was lost upon heating. Then, THP, another commonly used protecting group but an electron-donating one for amine, was used to prepare **1h-2**. When this new substrate was submitted to the same conditions as above, half of **1h-2** was consumed, whereas no target product was detected but dehalogenated product. Optimisation of the condition was

Table 4. Synthesis of aromatic *N*-heterocycle-based azoheteroarenes

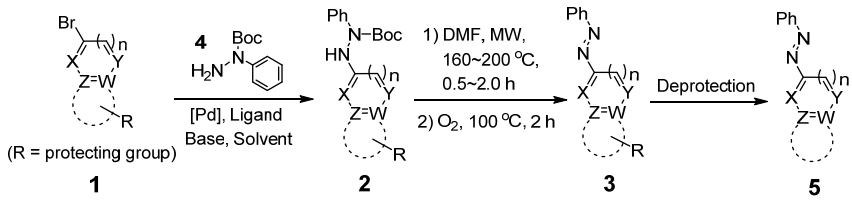

Entry	Substrate	2, yield	3, yield	5, yield
1	**1a** 	**2a**, 75%	**3a**, 85%	-
2	**1b** 	**2b**, 73%	**3b**, 90%	-
3	**1c** 	**2c**, 18%	**3c**, 81%	-
4	**1d** 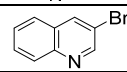	**2d**, 65%	**3d**, 74%	-
5	**1e-0** 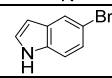	0	-	-
6	**1e-1** 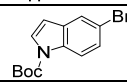	0	-	-
7	**1e-2** 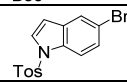	**2e**, 83%	**3e**, 85%	**5e**, 81%
8	**1f** 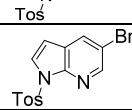	**2f**, 80%	**3f**, 88%	**5f**, 80%
9	**1g** 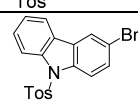	**2g**, 81%	**3g**, 88%	**5g**, 84%
10	**1h-1** 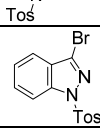	0	-	-
11	**1h-2** 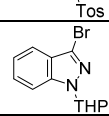	**2h**, 54%	**3h**, 40%	**5h**, 75%
12	**1i** 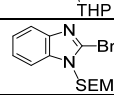	0	-	-
13	**1j** 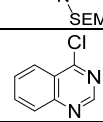	0	-	-

14	**1k**	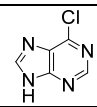	0	-	-
15	**1l-1**		0	-	-
16	**1l-2**		0	-	-

conducted for **1h-2** by changing ligand with XantPhos, rac-BINAP and XPhos. As a result, only the reaction that used XPhos provided the target product **2h** (54% yield) yet the reaction was still not completed even after increasing temperature, extending reaction time and tuning the equivalents of catalyst/ligand and **4**. Regarding 2-bromo-1*H*-benzimidazole, different protecting groups were used to block the secondary amine but all of them failed to couple with **4** under Buchwald-Hartwig coupling conditions, which may have been due to the steric hindrance from the bulky protecting groups. Other aromatic N-heterocyclic halide substrates (**1j**, **1k**, **1l-1**, **1l-2**) were tested under Buchwald-Hartwig coupling conditions with **4** but only dehalogenated products were detected.

With **2a**–**2h** in hand, microwave-assisted O_2 oxidation was performed to obtain azo compounds. To convert intermediate **2** to azo compounds, the Boc group should first be removed since the remained diarylhydrazine is more susceptible to oxidants.[152] For deprotecting of Boc groups, acidic methods are the most widely used, e.g. HCl or TFA. I investigated thermal deprotecting of the Boc group, which has at least two advantages over acidic methods. Firstly, there are no functional groups incompatibility or workup complications.[153] Secondly, the product would exist as free amine after deprotecting and not as salts which may affect the following oxidation activity.[154] Additionally, this method is optimal when run on a small-scale due to the high-temperature requirements and vigorous off-gassing of the reaction. Compound **2a** in DMF under N_2 was initially submitted to a microwave reactor at 200 ^oC and heated for 30 min; all starting materials were consumed. After cooling, the reaction vial was recharged with O_2 and heated at 60 ^oC overnight (the reaction solution colour changed from light brown to dark red) and gave target azo product **3a** in 85% yield. This condition worked well with **2b** and provided **3b** at a yield of 90%. However, when **2c** was submitted to this condition, by-products were detected by LC-MS after microwave heating; the N-N bond of diarylhydrazine was broken and generated two components of aromatic amine. In the second effort towards **2c** oxidation, the deprotecting temperature was decreased to 180 ^oC

and heated for 1 h, however, some **2c** (approximately 15%) remained. The temperature was then increased to 200 °C for 10 min and deprotecting was finished at a little expense of decomposition (approximately 6%). After O_2 oxidation, **3c** was obtained at a yield of 81%. Following this procedure, **2e**, **2f** and **2g** efficiently lead to corresponding azo compounds in yields greater than 85%. However, **2d** suffered from decomposition, **3h** was obtained in a yield of 74% and **2h** was completely decomposed. After maintaining a balance of decomposition and conversion, **2c** was heated at 160 °C for 1 h and then 180 °C for 30 min to provide **3c** at a yield of 40%, while 18% of **2c** remained.

The tosyl group on **3e**, **3f** and **3g** was efficiently removed by Cs_2CO_3 at rt, in yields higher than 80%. The THP group on **3h** was removed by 4 N HCl in 1,4-dioxane to give **5h** at a 75% yield.

Considering the high frequency of purine in ATP competitive kinase inhibitors and quinazoline in TK inhibitors[155-157] and the limited literature on these two aromatic heterocycle-based azo compounds, we synthesised them by other way and evaluated their photophysical properties. Both 6-Cl-purine and 4-Cl-quinazoline are good substrates for aromatic substitution. Therefore, a strategy starting with aromatic substitution to prepare diarylhydrazine was adopted (Scheme 4). Compound **1k** was reacted with phenylhydrazine by microwave heating at 180 °C for 2 h to give the corresponding diarylhydrazine intermediate. Without purification, the reaction vial was recharged with O_2 and heated at 60 °C overnight, which provided target azo compound **6** at a yield of 65%. Compound **1j** was treated under the same conditions. However, no target product (**7**) was detected, although all starting material was consumed. Alternatively, a solution of Boc-protected phenylhydrazine and 4-Cl-quinazoline in n-BuOH was subjected to microwave irradiation at 60 °C for 30 min to complete the substitution and provide intermediate **7** at 95% yield. After deprotection and O_2 oxidation, azo compound **8** was obtained in 24% yield.

Scheme 4. Synthesis of azo compounds **6** and **8**.

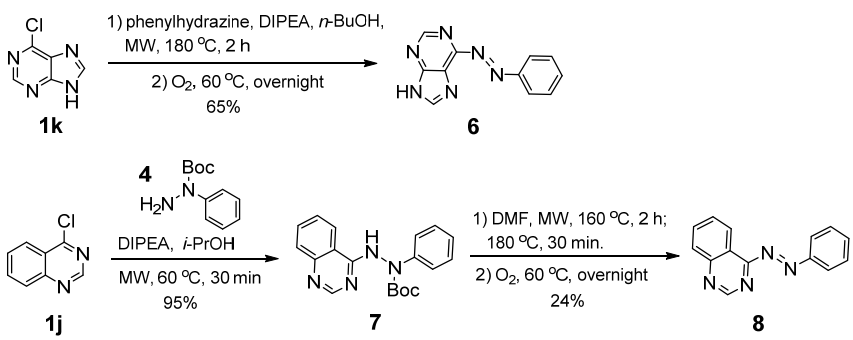

4.4 Photophysical characterization of azoheteroarenes

The characterisation of photophysical properties of these azoheteroarenes was then performed. To evaluate the influence of protecting groups on photophysical properties, **3e-3h** were also evaluated. The basic parameters (solvent, irradiation wavelength, absorption maxima, photoisomerization efficiency) of all the azo compounds were evaluated and summarised in Table 5.

All the UV/vis absorption spectra were obtained in an aqueous solution (30 μM) with certain fractions of DMSO as a co-solvent to assist solvation of the compounds (Table 5). Compound **3g** was the only exception as it was insoluble in water and was thus dissolved in neat DMSO for the photophysical characterisation. The aqueous solution was given priority during characterisation due to the potential application of these azo switches on bioactive molecules for subsequent tests in biological contexts.

Before preparing the solutions for the UV-vis absorption spectra, the stock DMSO solution of these azo compounds (3.0 mM) was thermally adapted by heating at 50 ^{o}C for 72 h to achieve a purity of more than 99% *E*-isomer. The absorption maxima of the $\pi\rightarrow\pi^*$ transition for the respective compounds was observed at a wavelength between 317 and 387 nm, whereas the $n\rightarrow\pi^*$ transitions at longer wavelengths were very weak and barely observed in the absorption spectra. There were several trends exhibited among these azo compounds, as indicated in Table 5. Firstly, the fused aromatic heterocycles-based compounds (**3d**, **5e**–**5h**) showed red-shifted absorption maxima compared to that of monocyclic compounds (**3a**–**3b**). A good example is the tricyclic aromatic heterocycle-based **5g**, which had a $\pi\rightarrow\pi^*$ transition absorption maxima at 387 nm and could be switched between *E*- and *Z*-isomers using visible lights (405 and 523 nm). Based on their absorption maxima, **3a**–**5f** and **6** were switched (to *Z*-isomer) by UV 365 nm. However, no switching was detected for **5h** and **8**, even by ns transient absorption measurement after the excitation pulse at 355 or 410 nm. Afterwards, the UV enriched *Z*-isomers of **3c**–**5f** and **6** were switched back to *E*-isomers by 460 nm light irradiation, while a shorter wavelength light (405 nm) was used to trigger the back switching for monocyclic compounds **3a** and **3b**. Secondly, the photoswitching efficiency was improved with the increase of the size of the heterocycle. The monocyclic azo compounds (**3a**–**3c)** indicated slower switching, with a more than 4-fold longer switching half-life ($t_{1/2}$) compared to the fused aromatic heterocycle-based compounds (**3d**, **5e**–**5h**). Thirdly, the protecting groups affected both the absorption maxima and the photoswitching efficiency. The introduction of electron-withdrawing tosyl group on **5e**–**5g** leads to a red shift of their absorption maxima, e.g. the change from **5g** to **3g**, and also lowered their

switching efficiency upon irradiation. It should be noted that all photoswitching proceeded with isosbestic points, which implies clean conversion between the two implicated isomers.

Table 5. Photoisomerization properties based on UV-vis absorption spectra

Azo compounds	**DMSO (% in H_2O)**	λ_{max} *E* (nm) **$\pi\rightarrow\pi^*$**	λ_{irr} (nm) **(*E*→*Z*, *Z*→*E*)**	**λ_{max} $n\rightarrow\pi^*$after UV**	τ (s) **(*E*→*Z*, *Z*→*E*)**
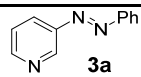 **3a**	1	318	365, 405	426	107, 44
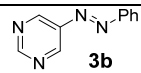 **3b**	1	317	365, 405	426	169, 47
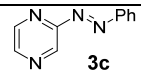 **3c**	1	328	365, 460	433	105, 54
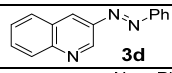 **3d**	10	336	365, 460	432	58, 36
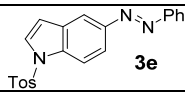 **3e**	50	338	365, 460	431	37, 35
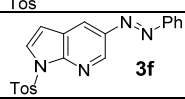 **3f**	50	335	365, 460	430	46, 39
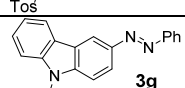 **3g**	100	351	365, 460	435	25, 32
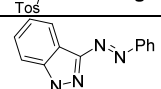 **3h**	20	363	365, 460	442	15, 26
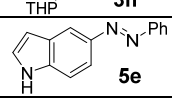 **5e**	5	355	365, 460	433	24, 21
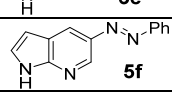 **5f**	7.5	349	365, 460	430	18, 26
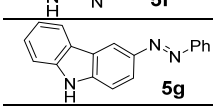 **5g**	33.3	387	405, 523	435	15, 50
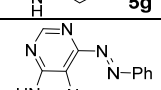 **6**	1	349	365, 460	428	39, 29
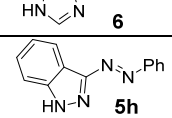 **5h**	5	362	No isomerization was detected		
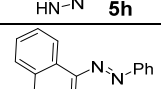 **8**	1	325			

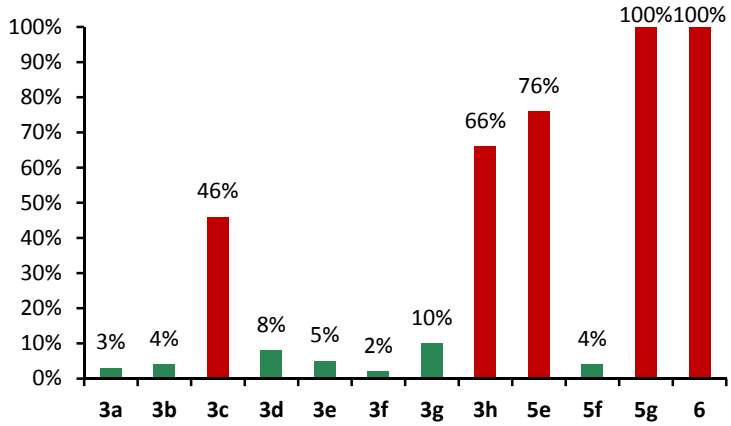

Figure 13. The thermal stability of the *Z*-isomer of azo compounds represented by the ratio that switch back to *E*-isomer after leaving the light enriched *Z*-isomer in the dark at rt for 24 h.

The thermal stability of the *Z*-isomer was briefly evaluated by determining the ratio of the switch back to an *E*-isomer after leaving the light-enriched *Z*-isomer sample in the dark at rt for 24 h (Figure 13). Regarding the fast back-switching cases, including **3c**, **3h**, **5e** and **6**, thermal switching kinetics were recorded to determine the half-life (Appendix 3). It should be noted that the *Z*-isomer of **5g** could quickly switch back to an *E*-isomer (in approximately 1 h). However, significant decomposition was also detected after leaving **5g** in the dark for 2 h, according to the UV-vis spectrum, which was ascribed to hydrolysis of the azo bond. Additionally, compounds **3c**, **3h** and **5e** had the lowest activation energies for thermal $Z \rightarrow E$ isomerization, as estimated by DFT calculations, assuming thermal isomerization through inversion (Appendix 4).[145] The fast back-switching of **6** ($t_{1/2}$ = 1.8 min) can be explained by a different isomerization mechanism, which is rotation instead of inversion. This is because **6** in the *Z*-form showed the largest twisting angles between the plane of the heterocycle and the N-N double bond (Appendix 5).[145] Furthermore, the electron-withdrawing tosyl-protected azo compounds displayed improved thermal stability when comparing **3e**–**3g** with **5e**–**5g**.

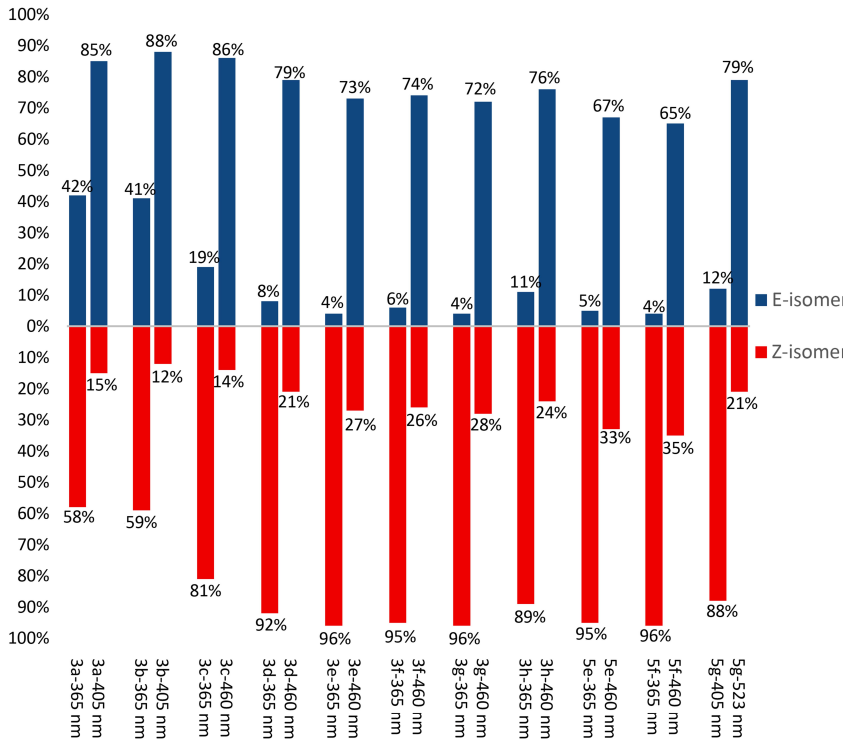

Figure 14. Photostationary distribution of **3a**–**5g** after exposure to two different wavelengths of light.

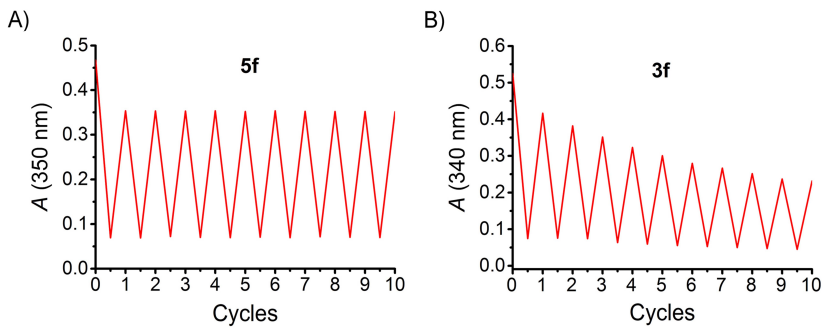

Figure 15. Photoisomerization fatigue resistance of **5f** (A) and **3f** (B), evaluated by 10 cycles of alternate 365 nm/460 nm irradiation, displaying the absorption intensity at certain wavelengths after each irradiation. No significant degradation was observed for **5f** but obvious degradation was observed for **3f**.

The UV-enriched *Z*-isomer purity of **3a**–**5f** ranged from ca. 60% to 96%, while **5g** was irradiated by visible light 405 nm and generated 88% *Z*-isomer (Figure 14). However, the photoinduced *Z*→*E* isomerisations were performed by visible light irradiating of the samples that were enriched in the *Z*-isomer, providing PSD containing between 65% and 88% of the *E*-isomer. The PSD of **6** could not be measured due to its fast thermal isomerisation, which requires special equipment. When comparing photoinduced *E*→*Z* isomerisations between **3g** and **5g** and *Z*→*E* isomerisations of **3e**, **3f**, **5e** and **5f**, it can be observed that the introduction of tosyl group somehow enlarged the PSD for both directions, which may be due to the subsequent separation of n→π* and π→π* absorption bands.

To determine whether these azo switches can withstand repeated photoisomerization in an aqueous solution without degradation, their fatigue resistance was evaluated by exposing the aqueous solution (DMSO solution for **3g**) to 10 cycles of alternate irradiation of two corresponding wavelengths used to achieve PSD. Fortunately, all these azo compounds showed high fatigue resistance after 10 cycles of *E*↔*Z* photoisomerization, except for **3f** (Figure 15).

4.5 Summary

We developed an efficient strategy to synthesise aromatic *N*-heterocycle-based azoheteroarenes, using Buchwald-Hartwig coupling and microwave-assisted O_2 oxidation as the key steps. Using this strategy, we synthesised eight azoheteroarenes (disregarding the azo compounds that have protecting groups). Another two heterocycles containing azoheteroarenes that are frequently used in kinase inhibitors were prepared by another (similar) strategy in this work to investigate more comprehensive profiles of azoheteroarenes in terms of photophysical properties. Furthermore, the absorption maxima, photostationary distribution, isomerisation fatigue resistance, thermal stability of *Z*-isomer and photoinduced isomerisation kinetics of these azo compounds were evaluated based on UV/vis absorption spectra. Among them, **3d** and **5f** displayed ease of synthesis and outstanding photophysical properties in all parameters, which will be applied as the photoswitch in the following development of photoswitchable RET kinase inhibitors.

5 Photoswitchable DFG-out RET kinase inhibitors

5.1 Design of photoswitchable DFG-out RET kinase inhibitors

As discussed in the introduction, the molecular structure and binding mode of DFG-out kinase inhibitors (or type II inhibitors) share some common features. A representative example is ponatinib (Figure 16). When it binds to FGFR4 kinase (PDB ID: 4UXQ),[158] the imidazo[1,2-*b*]pyridazine "head" (green) forms an H-bond with Ala553 of the hinge. The ethynylbenzene "linker" (cyan) bridges the space beside the kinase gatekeeper and stretches to the edge of the ATP binding pocket. This interaction places the amide in the proper position to bind to Glu520 of the αC-Helix and Asp630 of the DFG (out) motif. A hydrophobic "tail" (orange) is located in the allosteric pocket near the catalytic site created by the flip of the DFG motif, the 1-methylpiperazine moiety on the "tail" increases the aqueous solubility. On the other hand, ponatinib shows potent RET kinase inhibition activity with IC_{50} values in the single digit nM level.[79] Therefore, using ponatinib as the template, we designed the general photoswitchable RET kinase inhibitor model by integrating an azoheteroarene into the molecular structure of ponatinib (Figure 16). In this case, the heterocycle replaced the role of imidazo[1,2-*b*]pyridazine as the "head" to bind to the hinge, and the phenylazo moiety replaced the ethynylbenzene as the "linker".

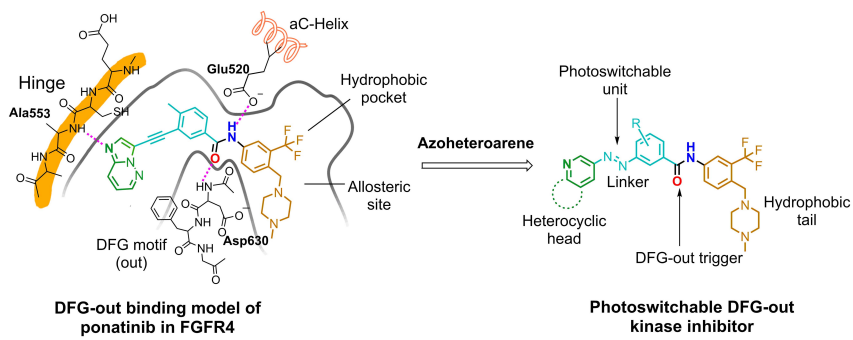

Figure 16. Schematic representation of the design of photoswitchable DFG-out RET kinase inhibitors.

5.2 Development of quinoline "head" based photoswitchable DFG-out RET kinase inhibitor

5.2.1 Development of the azo type DFG-out RET kinase inhibitor with a quinoline ring as the hinge binder

The study of azoheteroarens in the last chapter showed that quinoline based azoheteroarene **3d** is outstanding in the aspects of synthesis and photophysical properties. In addition, the quinoline head is a good hinge binder in RET kinase inhibitors or other RTK inhibitors, such as cabozantinib.[159,160] In this case, we decided to initially develop the quinoline "head"-based photoswitchable RET kinase inhibitor.

Scheme 5. Synthesis of photoswitchable RET kinase inhibitor 15.[a]

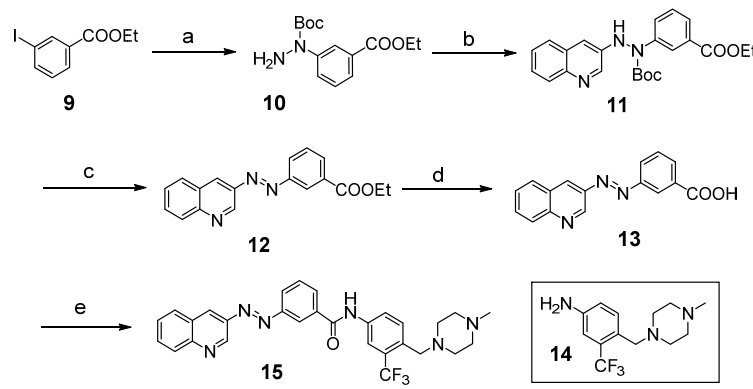

[a]Reagents and conditions: (a) *N*-Boc hydrazine, Cs_2CO_3, CuI, DMSO, 80 °C, 4 h, 85%; (b) 3-bromoquinoline, $Pd(OAc)_2$, t-$Bu_3P{\cdot}HBF_4$, Cs_2CO_3, toluene, 110 °C, 18 h, 50%; (c) DMF, MW, 180 °C, 45 min; then O_2, 100 °C, 2 h, 50%; (d) LiOH, THF/H_2O/MeOH, 50 °C, 3 h, 74%; (e) **14**, EDCI, HOBt, Et_3N, DCM, rt, 36 h, 62%.

Scheme 8 shows the synthetic route to target compound **15**. Compound **10** was prepared from **9** by an Ullmann type coupling. A subsequent Buchwald-Hartwig coupling with 3-bromoquinoline provided **11**. Next, **11** was used in a "one-pot, two steps" dehydrogenation reaction: heating with microwave irradiation (MW) at high temperature to remove the Boc protection, and then heating with O_2 to form the azo bond of **12**. After hydrolysis by LiOH, the resulting acid was coupled with previously reported "tail" moiety **14** to give the target product **15** (Scheme 5).[161] The salt form **15·HCl** was prepared by mixing **15** with 4 N HCl in 1,4-dioxane and then removing the solvent.

After **15** and its salt were produced, their photophysical properties were characterized based on their UV-vis absorption spectra (Figure 17, Table 7).

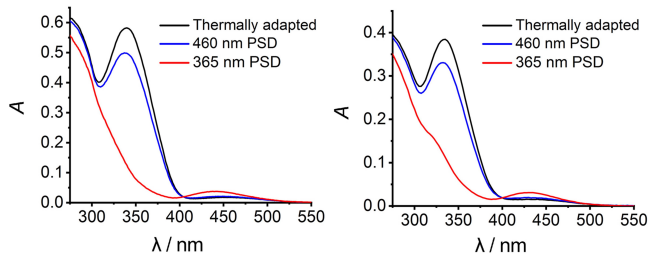

Figure 17. UV-vis absorption spectra of **15** in DMSO (left) and H_2O (right).

Compound **15** has a π→π* absorption maxima at 340 nm in a thermally adapted DMSO solution. Once irradiated by UV 365 nm light, a PSD containing 90% *Z*-isomer was obtained (as determined by ^{1}H-NMR spectroscopy). After additional exposure of this sample to 460 nm light, a PSD with 87% *E*-isomer can be produced. In addition, the thermal stability (half-life) of the *Z*-isomer in DMSO was determined to be $t_{1/2}$ = 208 h (Table 7). The aqueous solution was prepared by dissolving **15·HCl** in H_2O. Both π→π* (*E*-isomer) and n→π* (*Z*-isomer) absorption bands showed a small hypsochromic shift compared to the DMSO solution. The thermal stability of **15** in aqueous solution was determined to be $t_{1/2}$ = 217 h (Table 7). Furthermore, compound **15** showed good fatigue resistance both in DMSO and aqueous solutions, as no significant degradation was observed after 10 cycles of 365 nm and 460 nm irradiation-induced photoswitching (Appendix 7).

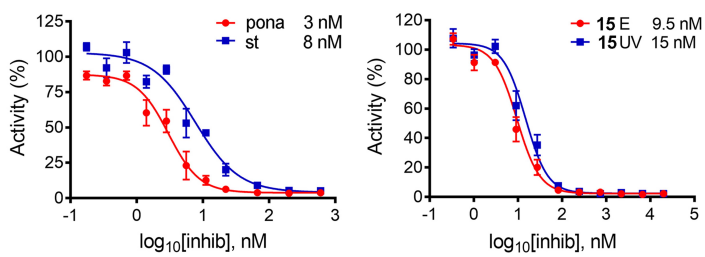

Figure 18. Dose-response curve and IC_{50}: reference compounds (left, pona: ponatinib, st: staurosporine); *E*-isomer and UV-enriched *Z*-isomer of **15** (right).

After assessing the photophysical properties of compound **15**, the kinase inhibition activity was determined by ADP-Glo™ RET kinase assay. In this assay, purified RET kinase was used. With IGF1tide as the substrate, the enzymatic activity was quantified by luminescence which is proportional to the amount of consumed ATP during the kinase reaction.[133] Considering that DFG-out kinase inhibitors tend to be slow binders (low k_{on} and even lower k_{off}),[162] an additional 30 min pre-incubation procedure was executed, based on the

manufacturer's protocol. With the modified procedure, the activities of reference compounds ponatinib and staurosporine were initially tested in this assay, and the IC_{50} values were determined as 3 nM and 8 nM, respectively (see Figure 18). Afterwards, the thermally adapted *E*-isomer and UV-enriched *Z*-isomer of azo compound **15** were analysed in the same assay. However, the IC_{50} value of the *Z*-isomer was only 1.6-fold greater than the *E*-isomer (Figure 18), although both were very potent (low nM range).

We assumed that there are two reasons for the narrow difference of inhibition activity between **15*E*** and UV-enriched **15*Z***: 1) the kinase-binding pocket is so flexible that it can tolerate the binding of **15*Z*** and still demonstrate good inhibition; 2) the PSD after UV enrichment (up to 90%) and thermally reversed isomerisation of the *Z*-isomer resulted in the purity of **15*Z*** being too low during the kinase reaction, causing **15*E*** to dominate the interaction with RET kinase.

5.2.2 Development of stilbene type model inhibitors

The first assumption was identified via computational modelling, performed by docking of **15*E*** and **15*Z*** into the DFG-out RET kinase structure created by homology modelling based on the c-KIT crystal structure (PDB code 4U0I) as a template (Figure 19A).[163] Per our design, **15*E*** adopts a canonical type II binding mode: the quinoline "head" formed an H-bond at the hinge with Ala108, the phenyl azo "linker" traversed the area besides the gatekeeper Val105, and the amide bond formed two H-bonds with Glu76 of the αC-Helix and Asp108 of the DFG motif (out). Furthermore, an additional H-bond formed between the amide and Ser192, which also contributed to the binding affinity of **15*E***. Moreover, the "tail" moiety was located in the hydrophobic pocket adjacent to the catalytic region. However, although the *Z*-isomer of **15** adopted a similar pose to the *E*-isomer, no H-bonds formed with the key amino acids on the hinge, conserved Glu76 and Asp193, while these binding features mainly contributed to the activity of DFG-out RET inhibitors. At this stage, we concluded that the **15*Z*** cannot be fully tolerated by the main drugable pocket of DFG-out RET kinase and should show a greater difference in bioactivity than **15*E***.

Stilbene compounds are reported be more thermally stable and less sensitive to light compared to azo compounds.[164] We investigated the second assumption by developing the corresponding stilbene-type model compounds to mimic the *E/Z*-isomers of azo compound **15**. Development of this pair of stilbene isomers began with molecular docking in the DFG-out RET kinase model (Figure 19B).

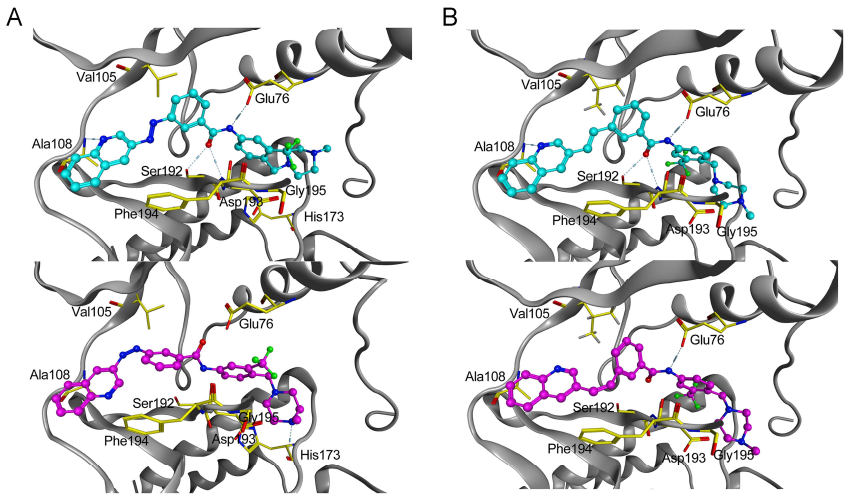

Figure 19. Molecular docking of two isomers of azo compound **15** (A) and corresponding stilbene model compounds (B) with the DFG-out RET kinase. The DFG-out model was obtained by homology modelling, which applied the RET protein sequence (NCBI database GeneID: 547807) on a template of KIT crystal structure (PDB code 4U0I). The dockings were performed by a method of "alpha triangle" placement and "induced fitting" refinement.

The *E*-isomer adopted almost the same binding model with **15*E***, which should show the approximate IC_{50} value in the subsequent biochemical assay. Due to the steric strain, the *Z*-isomer lost H-bonds with the hinge and the DFG motif, and only maintained the bond with Glu76. In this case, the main drugable pocket of DFG-out RET kinase should also not tolerate the binding of the *Z*-isomer of the stilbene model molecule. The synthesis of the stilbene model compounds started from building block **16**, prepared according to reported study and procedure,[165] and then reacted with 3-bromoquinoline to produce the key intermediate **17**. Subsequently, **17** was submitted to two different metal-catalysed stereoselective reduction methods to provide the *E*-isomer (**18*E***) and *Z*-isomer (**18*Z***) of stilbene intermediates.[166,167] They were then hydrolysed with LiOH, and the resulting acids were coupled with "tail" moiety **14** to provide final stilbene compounds **20*E*** and **20*Z*** (Scheme 6). Using the same ADP-Glo^{TM} RET kinase assay used for **15**, the IC_{50} of **20*Z*** was determined to be 900 nM, 115-fold higher than the IC_{50} of **20*E*** (IC_{50} = 7.8 nM). The biochemical assay results for stilbene compounds further supported that *Z*-isomers of stilbene-type inhibitors and azo-type inhibitors cannot be well tolerated by the main drugable pocket of DFG-out RET kinase. Furthermore, the small difference in biological activity between **15*E*** and **15*Z*** likely resulted from the

undesirable photophysical properties (PSD and thermal stability) of the UV-enriched *Z*-isomer.

Scheme 6. Synthesis of stilbene type model inhibitors **20*E*** and **20*Z***.[a]

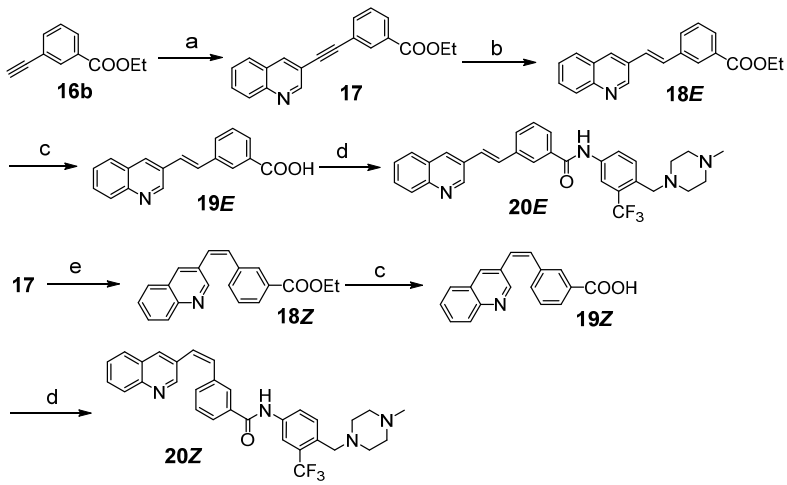

[a]Reagent and conditions: (a) 3-bromoquinoline, $Pd(MeCN)_2Cl_2$, RuPhos, Cs_2CO_3, MeCN, 80 °C, 6 h, 95%; (b) $RuCl_2(PPh_3)_3$, CuI, Zn, H_2O, 1, 4-dioxane,100 °C, 8 h, 21%; (c) LiOH, THF/H_2O/MeOH, 50 °C, 3 h, 72-79%; (d) **14**, EDCI, HOBt, Et_3N, DCM, rt, 36 h, 64-72%; (e) $Pd(OAc)_2$, KOH, DMF, 150 °C, 6 h, 28%.

5.3 Optimization of quinoline "head" based photoswitchable DFG-out RET kinase inhibitor

We could achieve a greater biological activity difference between *E*/*Z*-isomers of photoswitchable RET kinase inhibitors over **15** via three optimization aspects: enlarging the geometric difference between the *E*-isomer and *Z*-isomer, thus weakening the binding affinity of the *Z*-isomer while maintaining the affinity of the *E*-isomer; enhancing the thermal stability of the *Z*-isomer to preserve the purity during the kinase assay and increasing the UV-enriched *Z*-isomer PSD, thus increasing the purity of the *Z*-isomer during kinase assay.

5.3.1 Introducing substituents on the quinoline ring

One way to enlarge the geometric difference is to modify the quinoline ring with substituents. By installing substituents onto the quinoline "head", the activity of the *E*-isomer can be regulated by adjusting the binding affinity of the "head" moiety on the hinge or creating contact between the substituents and amino acid residues in the adenosine binding pocket. More importantly, the bulkier "head" moiety and the increased geometric distortion of the *Z*-isomer

make it more difficult to bind into the adenosine binding pocket compared to the *E*-isomer, thus enlarging the binding affinity difference between them. To evaluate the effect of substituents on the geometric structure and subsequent biological activity of photoswitchable kinase inhibitors, we prepared eight pairs of stilbene-type model compounds with substituents on the C4 and C8 positions of the quinoline "head" (Scheme 7 and 8). Among them, four pairs of stilbene compounds were substituted with alkyls (methyl, ethyl, propyl and isopropyl) in the C8 position of the quinoline ring (**30a-d** and **31a-d**). The other four pairs were substituted with nucleophilic groups (methoxyl, dimethylamine, pyrrolidyl and anilino) in the C4 position of the quinoline ring (**39e-h** and **40e-h**). The substituent that would lead to the largest bioactivity difference should be applied to the azo compound.

Scheme 7. Synthesis of C8 substituted stilbene type model inhibitors.[a]

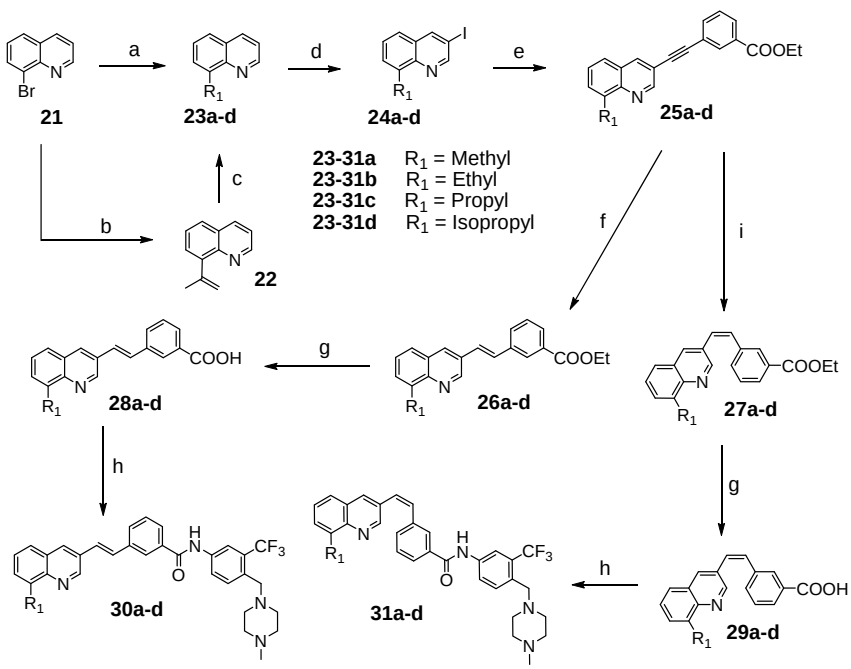

[a]Reagent and conditions: (a) R_1MgBr, $Ni(dppp)Cl_2$, THF, rt, 4 h, 72-76%; (b) Isopropenyl magnesium bromide, $Pd(PPh_3)_4$, THF, 40 °C, 3 h, 78%; (c) 10% Pd/C, H_2, MeOH, rt, 3 h, 45%; (d) NIS, AcOH, 90 °C, 16 h, 33-48%; (e) **16b**, $Pd(MeCN)_2Cl_2$, RuPhos, Cs_2CO_3, MeCN, 80 °C, 6 h, 71-86%; (f) $RuCl_2(PPh_3)_3$, CuI, Zn, H_2O, 1, 4-dioxane, 100 °C, 8 h, 18-28%; (g) LiOH, THF/H_2O/MeOH, 50 °C, 3 h, 63-90%; (h) **14**, EDCI, HOBt, Et_3N, DCM, rt, 36 h, 56-78%; (i) Lindlar cat., H-cube, EtOH, 100 bar, 1.5 mL/min, 80 °C, 43-75%.

The synthesis of C8-substituted stilbene compounds started with a Kumada coupling reaction on 8-bromoquinoline (**21**) to introduce alkyl groups (8-methylquinoline is commercially available).[168] Ethyl and propyl groups were introduced on C8 successfully with decent yields. A mixture of isopropyl and propyl substituted products was obtained when *i*-PrMgBr was used to attempt to install the isopropyl group on the C8 position. In this reaction, the propyl side product resulted from β-H elimination and subsequent olefin insertion after the isopropyl group coordinated on the catalyst complex.[169] Compound **23d** was very difficult to isolate from **23c** since they have almost the same polarity and completely overlapped on TLC plates. An alternate method to prepare **23d** first introduced an isopropenyl group by Kumada coupling then employed hydrogenation to convert isopropenyl to isopropyl.[170] These C8 substituted substrates were then reacted with NIS in AcOH to provide C3 iodinated **24a-d** in low to medium yield.[171] Subsequently, Sonagashira coupling reactions were performed to install the "linker" precursor **16b**,[172] providing the key intermediates **25a-d**. These diarylacetylene intermediates were then treated with two different metal-catalysed stereoselective reduction conditions: a $RuCl_2(PPh_3)_3$/CuI/Zn mixture was used to catalyse the reduction, producing the *E*-isomers of stilbene intermediates **26a-d** in quite low yields.[173] A Lindlar catalyst was applied to generate the *Z*-isomer of stilbene intermediates **27a-d** in medium yields.[174] These stilbene intermediates were then hydrolysed by LiOH, and the resulting acids were coupled with the "tail" moiety to provide target stilbene inhibitors **30a-d** and **31a-d** (Scheme 7).

The synthesis of C4-substituted stilbene compounds started with nucleophilic substitution on commercially available 4-chloro-3-iodoquinoline (**33**) and produced substituted substrates **34e-h**.[175,176] The solvents and heating temperatures used in this reaction depended on different nucleophiles. The following synthesis initially proceeded with the same strategy as C8-substituted stilbene compounds. However, no reaction was observed when the C4-substituted diarylacetylene intermediates were treated with the two previously used metal-catalysed stereoselective reduction conditions. Therefore, we utilised a strategy of initially preparing the *E*-isomer of stilbene intermediates by coupling between **34e-h** and (*E*)-phenyl alkenyl building blocks (**32a-b**) and then converting it to the *Z*-isomer by light-induced isomerisation (Scheme 8). Building blocks **32a-b** were prepared via a benzoic acid-catalysed hydroboration of **16a-b**; the solvent of the reaction mixture was removed and the residue was ready for following use.[177] Subsequently, a Suzuki coupling reaction was run using the crude products of **32a-b** and **34e-h** in high yields to provide **35e-h**, which were then irradiated by 365 nm UV light for 2 h to give a

Scheme 8. Synthesis of C4 substituted stilbene type model inhibitors.[a]

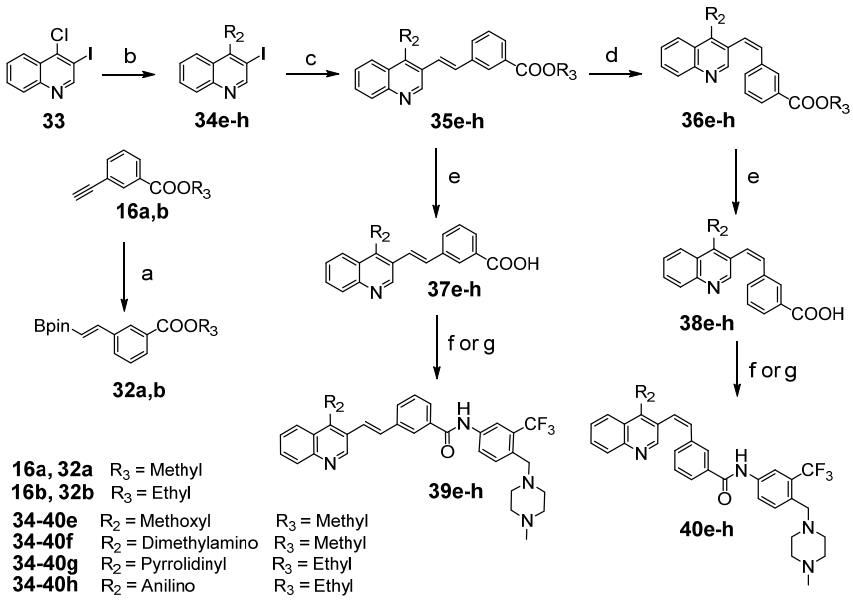

[a]Reagent and conditions: (a) HBpin, benzoic aicd, heptane, 100 °C, 16 h; (b) Nucleophile solution, heating, 88-98%; (c) $Pd(OAc)_2$, RuPhos, H_2O, K_3PO_4, 1,4-dioxane, 80 °C, 16 h; (d) UV 365 nm, MeCN, rt, 2 h, 39-57%; (e) LiOH, THF/H_2O/MeOH, 50 °C, 3 h, 63-90%; (f) **14**, EDCI, HOBt, Et_3N, DCM, rt, 36 h, 56-78%; (g) **14**, HATU or HBTU or TBTU, DIPEA, DMF, rt, 16 h, 32-57%.

mixture of *E*/*Z*-isomers; the *Z*-isomers **36e-h** were isolated by PLC plates. The intermediates **35e-h** and **36e-h** were hydrolysed with LiOH, and the resulting acids formed amide bonds with the "tail" to provide final C4 substituted stilbene compounds **39e-h** and **40e-h**, respectively.

Table 6. IC_{50} of substituted stilbene compounds[a]

Inhibitors	R_1	R_2	IC_{50}	*Z*/*E* (IC_{50}) ratio
30a	methyl	H	257 nM	49
31a	methyl	H	12.6 μM	
30b	ethyl	H	1.9 μM	10.5
31b	ethyl	H	20.0 μM	
30c	propyl	H	5.6 μM	-
31c	propyl	H	> 0.5 mM	
30d	isopropyl	H	9.8 μM	-
31d	isopropyl	H	> 0.5 mM	
39e	H	methoxyl	12.4 nM	142
40e	H	methoxyl	1.8 μM	
39f	H	dimethylamino	98 nM	24.4
40f	H	dimethylamino	2.4 μM	
39g	H	pyrrolidinyl	66 nM	33.4
40g	H	pyrrolidinyl	2.2 μM	
39h	H	anilino	2.3 μM	21.3
40h	H	anilino	49 μM	

[a] IC_{50} values were determined by ADP-Glo™ RET kinase assay. Data represent the mean and standard deviation of three experimental replicates.

The substituted stilbene compounds were evaluated by ADP-Glo™ RET kinase assay to determine their IC_{50} values (listed in Table 6 with the *Z*/*E* IC_{50} ratios). Just as we could conclude from the design, the introduction of alkyl groups on the C8 position largely weakened the activity of the *Z*-isomers, especially for **30c** and **30d**. However, the corresponding *E*-isomers lost more activity (larger IC_{50} value) in all four pairs of C8-substituted compounds since the substituents pushed the nitrogen atom of the quinoline "head" away from the hinge, preventing it from forming the H-bond. Such relative floating of the biological activities led to smaller IC_{50} differences between the *Z*- and *E*-isomers. The results were similar for the C4-substituted compounds, except for methoxyl-substituted **39e** and **40e**. A *Z*/*E* IC_{50} ratio of 142-fold was achieved for this pair

of compounds, while the potency of the *E*-isomer was preserved (IC_{50} = 12.4 nM). The effect of the methoxyl group on the bioactivity of stilbene compounds was also confirmed by molecular docking (Figure 20). Compound **39e** can dock in the DFG-out RET kinase structure by approximately the same pose as **15*E*** or **20*E***. It can also form H-bonds with key amino acid residues, whereas the *Z*-isomer **40e** did not H-bond with the kinase. The successful modification with methoxyl on stilbene compounds encouraged us to develop the corresponding azo compounds with methoxyl substituted on the C4 position of the quinoline ring.

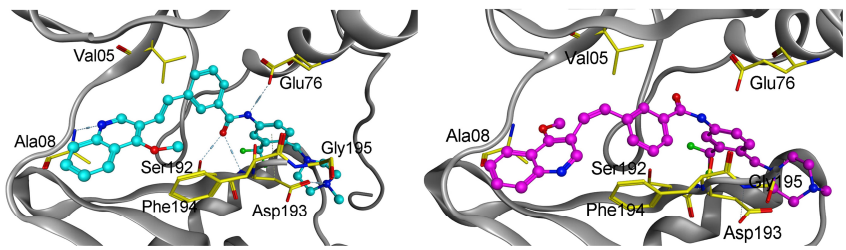

Figure 20. Molecular docking of **39e** (left) and **40e** (right) with the homology model of DFG-out RET kinase.

Using the same strategy as for **15**, the synthesis of this substituted azo compounds started with Buchwald-Hartwig coupling between **10** and **34e** to provide **41** (Scheme 9). Afterwards, this intermediate was submitted to MW heating and subsequent O_2 oxidation to form the azo intermediate **42**, which was then hydrolyzed by LiOH, and the resulting carboxylic acid was coupled with the "tail" to afford the target azo product **44**. This azo compound is susceptible to acid (HCl or AcOH) since the methoxyl group will be hydrolysed and lead to quinolin-4-ol derivative once treated with acid.

Scheme 9. Synthesis of C4 methoxyl substituted azo type inhibitor.[a]

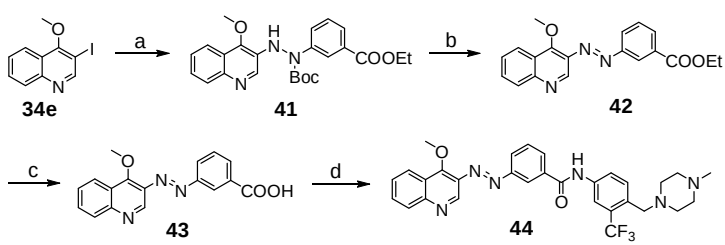

[a]Reagent and conditions: (a) **10**, $Pd(OAc)_2$, Xantphos, Cs_2CO_3, Toluene, MW, 110 °C, 2 h, 63%; (b) DMF, 180 °C, 45 min; then O_2, 100 °C, 2 h, 50%; (c) LiOH, THF/H_2O/MeOH, 50 °C, 3 h, 68%; (d) **14**, EDCI, HOBt, Et_3N, DCM, rt 36 h, 66%.

5.3.2 Introducing the second azo unit

Other than installing substituents on quinoline ring, introducing the second azo unit into the linear structure of azo compound **15** was expected to make more substantial changes in molecular shape, end-to-end distance and dipole moment, thus larger difference in biological activity before and after irradiation.

Scheme 10. Synthesis of diazo type inhibitor.[a]

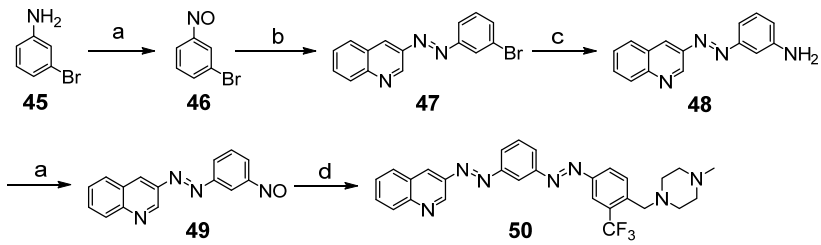

[a]Reagent and conditions: (a) OXONE, DCM/H_2O, rt, 3 h, 42%-63; (b) 3-aminoquinoline, toluene:40% NaOH (1:1), 80 °C, 2 h, 71%; (c) (*N*-methyl)ethanol, CuI, Formamide, 80 °C, 24 h, 53%; (d) **14**, TFA, HOAc/toluene (1:1), rt, 18 h, 25%.

The synthesis started from commercially available 3-bromoaniline (**45**) which was treated with OXONE to provide the nitroso product **46** (Scheme 10). A Mills reaction under alkaline conditions was then conducted with 3-aminoquinoline to construct the first azo bond and afford azo intermediate **47**.[178] The following amination must be performed using anhydride condition to avoid degradation of azo bond. In this case, an (*N*-methyl)ethanol/Formamide mixture,[179] instead of an NH_4OH solution, was used to provide NH_3 and give **48**. This newly formed amino group was further oxidized by OXONE to prepare the nitroso group which subsequently reacted with **14** under acidic Mills reaction conditions to give the target diazo compound **50**.[180] The salt form **50·HCl** was prepared by the same way as **15·HCl**.

5.3.3 Introducing fluorine atoms on phenyl ortho positions of azo bond

Inspired by the work of the Hecht group,[180,181] the third strategy to optimise **15** was to introduce two fluoride atoms onto *ortho*-positions of the "linker" phenyl ring of **15**. By this introduction, we expected to achieve higher *Z*-isomer thermal stability, thus maintaining the purity of the *Z*-isomer during biological assays. An additional benefit of this strategy could be that the introduction of strong electron-withdrawing groups, e.g. fluorine, can separate the n→π* bands of *E/Z*-isomers, allowing their use to trigger forward and reverse isomerisations with visible light.[181]

Scheme 11. Synthesis of *ortho*-difluoride azo type inhibitor.[a]

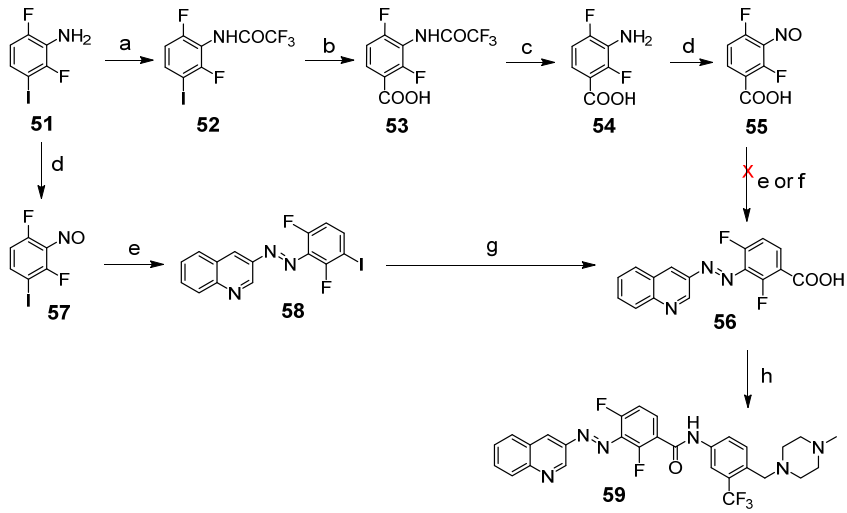

[a]Reagent and conditions: (a) $(CF_3CO)_2O$, DCM, rt, 3 h, 90%; (b) NaH, THF, 0 °C, 15 min, then n-BuLi, -78 °C, 10 min, then CO_2, -78 °C, 15 min, 35%; (c) 5 N NaOH, 100 °C, 4 h, 81%; (d) OXONE, H_2O/DCM, rt, 16 h; (e) 3-aminoquinoline, toluene:40% NaOH (1:1), 80 °C, 2 h; (f) 3-aminoquinoline, TFA, HOAc/toluene (1:1), rt, 18 h; (g) $Pd(OAc)_2$, Xantphos, Ac_2O, HCOOH, Propanol, Et_3N, Toluene, 80 °C, 12 h, 50%; (h) **14**, EDCI, HOBt, Et_3N, DCM, rt, 36 h.

A Mills reaction conducted between the aromatic amino moiety and nitroso compound would construct the azo bond of azoheteroarene. No nitroso product was detected when the 3-aminoquinoline was treated with commonly used oxidants, such as OXONE or m-CPBA. Therefore, we prepared the nitroso group on the phenyl and then ran the Mills reaction with 3-aminoquinoline. The starting material **51** was prepared following a reported study.[182] The synthesis focused on how to synthesize the key intermediate **56** (Scheme 11), while the challenge was to determine the appropriate stage to construct the azo bond. To form the azo bond after carboxylation, the synthesis was initiated by introducing the protection group on the amino of compound **51** with TFAA. The protected product **52** was then treated by lithiation and CO_2 to provide the carboxylation product **53**.[183] After removing the TFA protection group, the resulting aniline derivative was converted to nitroso product **55** by OXONE oxidation. Next, a Mills reaction was conducted using 3-aminoquinoline to try to obtain **56**; however, no target product was detected under either acidic or alkaline conditions. As an alternative strategy, compound **51** was first oxidised to nitroso product **57**, which was then reacted with 3-aminoquinoline in an alkaline Mills reaction to provide **58**. Subsequently, we attempted the

carboxylation condition based on lithiation and CO_2; however, only a dehalogenated product was detected. Instead, a palladium-catalysed carboxylation was conducted with Ac_2O/HCOOH (CO produced *in situ*) to prepare the key intermediate **56**.[184] This intermediate was then coupled with the "tail" moiety **14** to provide the final product **59**. The salt form **59·HCl** was prepared by the same way as **15·HCl**.

5.3.4 Replacing the quinoline "head" with 7-azaindole

7-Azaindole is another aromatic heterocycle frequently used as a hinge binder in kinase inhibitors, e.g. vemurafenib and pemigatinib.[185] We showed in the study of azoheteroarenes in the previous chapter that 7-azaindole-based azoheteroarene could achieve a PSD with 96% *Z*-isomer upon UV irradiation. In contrast, only 4% of the *Z*-isomer switched back after the sample was held in the dark at rt for 24 h. Therefore, replacing the quinoline "head" of **15** with a 7-azaindole ring is an appropriate way to promote the photophysical properties of an azo type inhibitor in terms of light-induced *Z*-isomer enrichment and its thermal stability. Furthermore, molecular docking of this 7-azaindole-based photoswitchable inhibitor with the DFG-out RET homology model was performed (Figure 21). The 7-azaindole moiety formed one more H-bond than the quinoline head with Ala108 in the hinge, which could increase the binding affinity of the *E*-isomer, thus enlarging the biological activity difference between the two isomers.

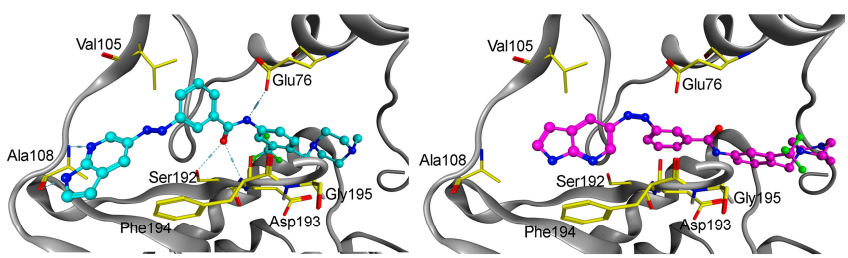

Figure 21. Molecular docking of **63*E*** (left) and **63*Z*** (right) with the homology model of DFG-out RET kinase.

The 7-azaindole-derived inhibitor was synthesised using the same strategy as **15** and **44** (Scheme 12). Compound **1f** reacted with **10** under Buchwald-Hartwig coupling conditions to produce **60**, followed by a "one-pot, two-step" dehydrogenation reaction to form the key azo intermediate **61**. A 5 N NaOH solution was used to hydrolyse the ethyl ester and deprotect the tosyl group,[186] and the resulting acid **62** was then coupled with **14** to provide the target azo compound **63**. The salt form **63·HCl** was prepared by the same way as **15·HCl**.

Scheme 12. Synthesis of 7-azaindole based azo type inhibitor.[a]

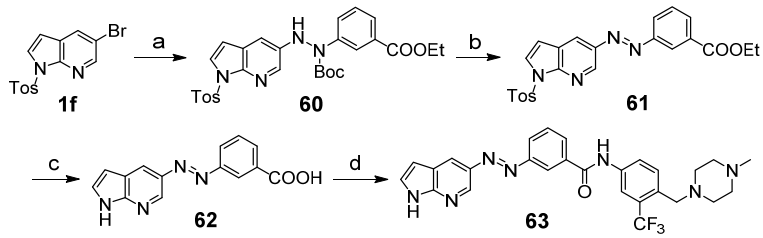

[a]Reagents and conditions: (a) **10**, $Pd(OAc)_2$, Xantphos, Cs_2CO_3, Toluene, MW, 110 °C, 2 h, 86%; (b) DMF, 180 °C, 45 min; then oxigen, 100 °C, 2 h, 56%; (c) NaOH, EtOH/H_2O, 90 °C, 5 h, 92%; (d) **14**, EDCI, HOBt, Et_3N, DCM, rt, 36 h, 78%.

5.3.5 Photophysical properties of the four new azo compounds

Photophysical properties of the newly developed four azo-type RET kinase inhibitors were then characterised based on UV-vis absorption spectra (Figure 22), and the main parameters are listed in Table 7. They were measured both in DMSO and aqueous solutions, respectively. The aqueous solutions were prepared by dissolving their salts in water (**50**, **59** and **63**) or dissolving azo compounds in 20% DMSO/H_2O mixed solvent (**44**). From the UV-vis spectra in Figure 22, we can see that all azo compounds showed a hypsochromic shift by approximately 10 nm from the DMSO to aqueous solutions. The introduction of the methoxyl group on the quinoline ring not only enlarged the bioactivity difference of the *E*/*Z*-isomers but also improved their photophysical properties. Compounds **44** and **63** showed higher *Z*-isomer enrichment (93% and 97%, respectively) than the original azo compound **15** after UV (365 nm) irradiation. They also demonstrated better thermal stability in DMSO and aqueous solutions, e.g. the half-life of **63*Z*** in H_2O was almost 3-fold longer than that of **15*Z***. However, for *ortho*-difluoro azo compound **59**, the results were out of our design. The ratio of *Z*-isomer was only 86% in the UV-induced (365 nm) PSD. In addition, the thermal stability of **59*Z*** in DMSO was much higher than that of **15**, yet its half-life in aqueous solution was only 38 h, indicating that **59*Z*** would lose purity quickly during biological assays. Moreover, the introduction of fluorine atoms on the *ortho* positions indeed separate the n→π* absorption band. However, this advantage is not large enough to enrich the *Z*-isomer PSD by visible light 503 nm comparing to the PSD enriched by UV 365 nm (Appendix 6). Notably, these three azo compounds showed good fatigue resistance in DMSO and aqueous solutions after ten cycles of 365 nm and 460 nm irradiation-induced photoswitching (Appendix 7). The photophysical properties of **50** were more complicated than

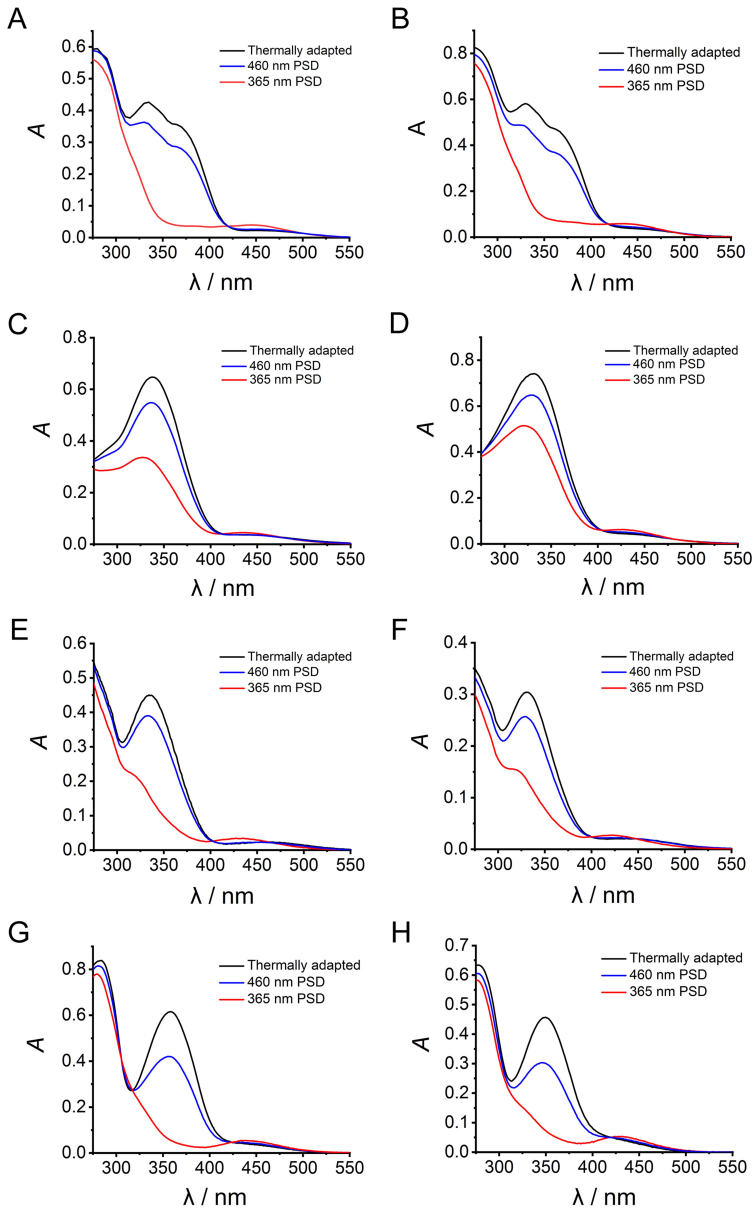

Figure 22. UV-vis isomerization absorption spectra: (A) **44** in DMSO; (B) **44** in 20% DMSO/H_2O; (C) **50** in DMSO; (D) **50·HCl** in H_2O; (E) **59** in DMSO; (F) **59·HCl** in H_2O; (G) **63** in DMSO; (F) **63·HCl** in H_2O.

Table 7. Comparison of photophysical properties of azo type inhibitors

Compound	Ratio of *cis* at PSD[a]	Thermal stability in DMSO	Thermal stability in H_2O
15	90%	$t_{1/2}$ = 208 h	$t_{1/2}$ = 217 h
44	93%	$t_{1/2}$ = 302 h	$t_{1/2}$ = 402 h
59	86%	$t_{1/2}$ = 779 h	$t_{1/2}$ = 38 h
63	97%	$t_{1/2}$ = 377 h	$t_{1/2}$ = 629 h

[a] The PSD were determined by ^{1}H-NMR spectrum in DMSO-*d6*.

other azo compounds since four isomers appeared upon irradiation. The UV-enriched PSD of **50** was determined to be 66% *Z*-isomers (including three isomers) by LC-MS in aqueous solution. Such low enrichment was meaningless for subsequent biological assays; thus, no additional thermal stability data were collected.

5.3.6 DTT/GSH reduction assay

After revealing their photophysical properties, we evaluated the azo-modified compounds biological activity in biochemical and cell assays. DTT was used in ADP-Glo™ kinase assay to maintain the proteins in a reduced state according to the manufacturer's protocol. Although GSH is a natural antioxidant in mammalian cells, DTT and GSH have been reported to be potential reducing factors for azo compounds in biological assays.[187] We excluded the factor of DTT/GSH reduction on the biological assay results by testing the four azo compounds (**15**, **44**, **59**, **63**) in DTT/GSH assays and monitoring the reactions by LC-MS to determine if reduction products were generated (Appendix 8). Azo compounds **15**, **59** and **63** were stable during the incubation with 2 mM DTT or 10 mM GSH for 20 h, as no reduction products were detected by LC-MS. However, reduction products were observed when **44** was treated with 2 mM or 10 mM GSH, but no reduction products when treated with 50 μM DTT (the concentration of DTT used in biochemical assays) (Appendix 8). An additional UV-vis cyclic isomerisation experiment of **44** in aqueous solution containing 1 mM GSH also showed degradation after 2.5 h incubation. The absorption intensity of **44** declined slightly (Figure 23), but no degradation was observed in the assays with **63**.

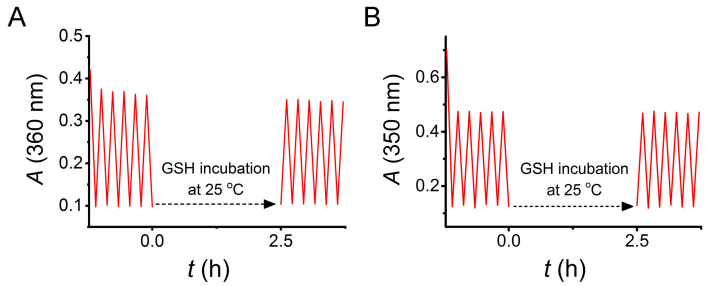

Figure 23. UV-vis cyclic isomerization and incubation of **44** (A) in 33% DMSO/PBS and **63·HCl** (B) in H_2O containing 1 mM GSH.

5.3.7 ADP-Glo™ RET kinase assay for new azo compounds

Before the ADP-Glo™ kinase assay, the azo compounds were thermally adapted to *E*-isomers (nearly 100%), accomplished by heating the stock solution for 30 min at 60 °C. The *Z*-isomer samples were prepared by irradiating the serially diluted *E*-isomer samples on 96-well plates with a 365-nm LED array (12.0 V, 15 min).[188] Using the same protocol as used for **15**, the IC_{50} of **44*E*** was determined to be 24 nM, and UV-enriched **44*Z*** showed a 15-fold decrease in activity with an IC_{50} of 363 nM (Figure 24A). With 7-azaindole as the hinge binder, the activity of compound **63*E*** was IC_{50} 3 nM,

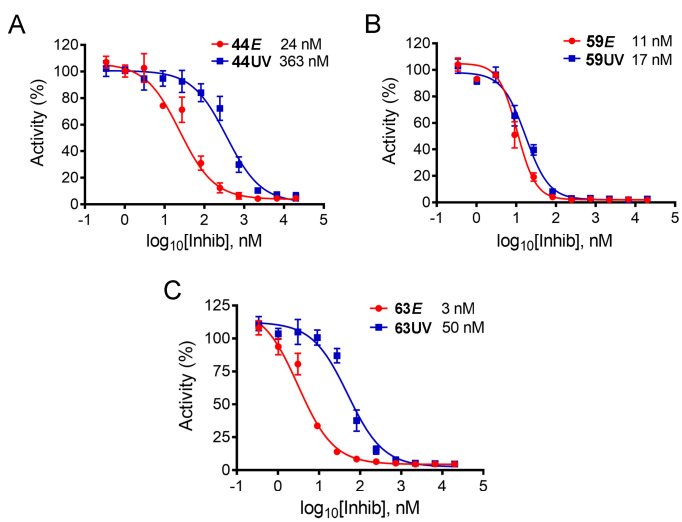

Figure 24. (A) Dose-response curves and IC_{50} for **44*E*** and its UV-enriched *Z*-isomer from ADP-Glo™ RET kinase assay; (B) Dose-response curves and IC_{50} for **59*E*** and its UV-enriched *Z*-isomer from ADP-Glo™ RET kinase assay; (C) Dose-response curves and IC_{50} for **63*E*** and its UV-enriched *Z*-isomer from ADP-Glo™ RET kinase assay.

which is 17-fold more potent than the UV-enriched sample of **63** (Figure 24C). However, the assay with *ortho*-difluoride compound **59** showed only a 1.5-fold difference in activity between the *E*-isomer and UV-enriched *Z*-isomer. Both isomers were potent with IC_{50} values of 11 nM and 17 nM, respectively (Figure 24B). The narrow activity difference could be attributed to the low enrichment of **59*Z*** after UV irradiation and subsequent fast thermal switching in aqueous solution; as a result, the activity of *E*-isomer of **59** dominated in the assay.

5.4 NanoBRET^{TM} TE intracellular RET kinase assay

Based on the largely improved biological activity difference between *E*/*Z*-isomers determined by the biochemical assay, compounds **44** and **63** were tested using the NanoBRET^{TM} intracellular RET kinase assay. Prior to the assay, the thermal switching kinetics of the *Z*-isomers of **44** and **63** were measured at 37 ^{o}C in the assay buffer. After incubation for 90 min, obvious thermal isomerization was observed. Therefore, the incubation time (after the *Z*-isomers were added) at 37 ^{o}C should be as brief as possible to reduce the influence of such thermal switching when quantifying the binding affinity of the *Z*-isomers. However, type II kinase inhibitors require longer incubation times to achieve the best inhibition effects due to their slow binding kinetics. The incubation time was initially screened to balance the risk of thermal switching of the *Z*-isomer and slow binding kinetics of type II inhibitors (Appendix 9A, B, C). To achieve this, we first conducted three parallel experiments with **63** using different incubation times (30 min, 60 min, 90 min) at 37 ^{o}C. However, all incubation times led to less than a 2-fold IC_{50} difference between the *E*/*Z*-isomers. Furthermore, with the incubation time reduced, the IC_{50} value increased significantly. The experiment was repeated with three shorter incubation times at 37 ^{o}C (10 min, 20 min, and 30 min) and a subsequent incubation at 25 ^{o}C for 1 h. Under these conditions, the IC_{50} difference between the two isomers was still only 2–3 fold, even with the shortest incubation time at 37 ^{o}C (Appendix 9D, E, F). Based on the above screening and results, reducing the incubation time was not enough to completely avoid the influence of thermal switching of the *Z*-isomer. However, the bright side is that the *E*-isomer of **63** can achieve full inhibition by incubation for 90 min, or when incubated at 25 ^{o}C in the final 60 min (Appendix 9F). Therefore, the reference compound ponatinib was initially tested by incubation at 37 ^{o}C for 90 min and showed an IC_{50} of 13 nM (Figure 25C). Under the same conditions, the IC_{50} values of **44*E*** and **63*E*** were 0.92 μM and 25 nM, respectively (Figure 25D and 25F).

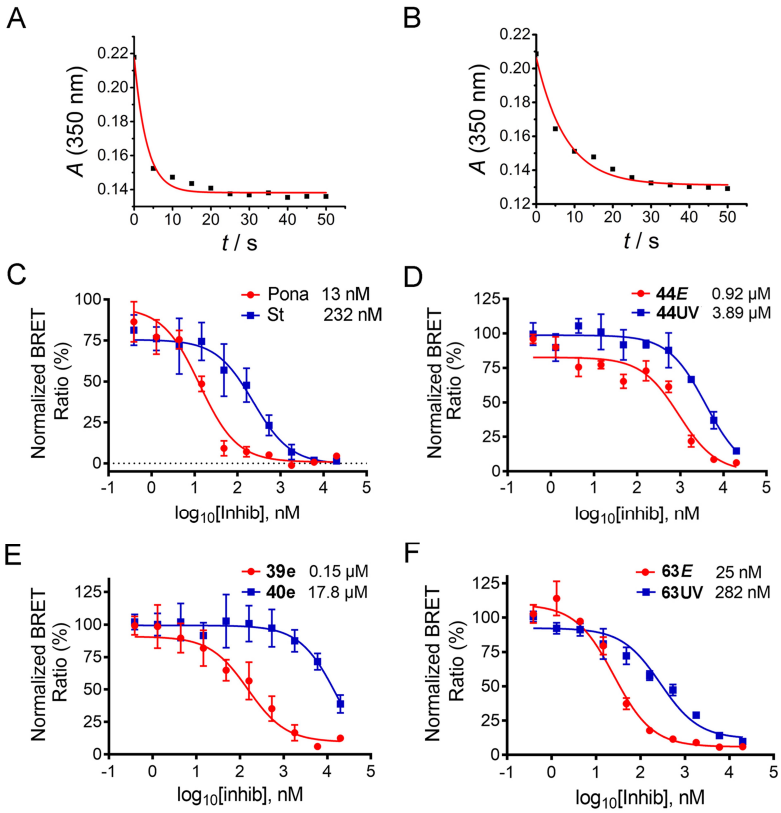

Figure 25. (A) UV-induced switching kinetic of **44** in assay buffer; (B) UV-induced switching kinetic of **63** in assay buffer; (C) Dose-response curves and IC_{50} for reference compounds from NanoBRET™ TE intracellular RET kinase assay; (D) Dose-response curves and IC_{50} for **44*E*** and its UV-enriched *Z*-isomer from NanoBRET™ TE intracellular RET kinase assay. Dose-response curves and IC_{50}; (E) Dose-response curves and IC_{50} for **39e** and **40e** from NanoBRET™ TE intracellular RET kinase assay; (F) Dose-response curves and IC_{50} for **63*E*** and its UV-enriched *Z*-isomer from NanoBRET™ TE intracellular RET kinase assay.

We also evaluated the cellular activity of the *Z*-isomers by stepwise *in situ* irradiation. The *E*-isomer was initially incubated then gradually irradiated during the assay to maximise the UV-induced PSD of the *Z*-isomer throughout the incubation. We employed such a strategy after considering the relatively long residence time of the *E*-isomer bound in the kinase pocket,[189] as it is generally assumed that photoswitching of azo-type inhibitor only occurs when the ligand is not bound to its target.[92] In addition, UV-induced isomerisation kinetics in cell assay medium showed that 35 s of UV exposure was sufficient to achieve the *Z*-isomer PSD (Figure 25A and B). Therefore, a total of 35 s of

UV light was delivered to the cells in three steps: 1) after incubation of **44*E*** or **63*E*** at 37 ^{o}C for 80 min, the cells were irradiated for 15 s using a 365 nm LED array (12.0 V); 2) after an additional 10 min incubation, the cells were irradiated for another 10 s; 3) after equilibrium was achieved at rt, the cells were irradiated for 10 s then incubated at ambient conditions for 10 min before reading the luminescence signals. The IC_{50} of UV-enriched **63*Z*** was determined to be 282 nM (Figure 25F), a factor of 11-fold higher than that observed for the pure *E*-isomer. However, there was only a 4-fold IC_{50} difference between the UV-enriched **44*Z*** and **44*E*** (Figure 25D). The corresponding stilbene compounds **39e** and **40e** were analysed by the NanoBRET RET kinase assay. Their IC_{50} values were 0.15 μM and 17.2 μM, respectively (Figure 25E), resulting in a *Z/E* (IC_{50}) ratio consistent with that measured in the biochemical assay. We rationalized the relative high potency of UV-enriched **44*Z*** and decreased *Z/E* (IC_{50}) ratio in the cellular assay occurred via the GSH reduction of the azo bond because the resulting hydrazine products were reported to be more potent than the original azo compound.[128]

5.5 Summary

In this chapter, we designed and developed the original photoswitchable DFG-out RET kinase inhibitor with quinoline based azoheteroarene, depending on the binding mode of general DFG-out kinase inhibitors. This inhibitor was attempted to optimize in four different ways: installing substituents on the quinoline ring; introducing second azo unit in the structure; introducing fluorine atoms in the *ortho*-positions of the azoheteroarene phenyl ring; and changing the heterocyclic head. Among all the modified azo compounds, the 7-azaindole "head" based photoswitchable DFG-out RET inhibitor **63** showed good photophysical properties, in terms of fatigue resistance over cyclic photoisomerization under GSH reduction stress, light enriched Z-isomer PSD, and the subsequent thermal stability. Compound **63** also exhibited about 17-fold enzymatic inhibition activity difference between *E*-isomer and UV-enriched *Z*-isomer. More importantly, it allowed regulation of the activity of **63** in living cells by irradiation with light during the cell assay which resulted in an 11-fold difference of binding affinity before and after light exposure.

6 Concluding remarks and outlook

This thesis describes the synthesis and characterisation of novel azoheteroarenes photoswitches and their use in the development on photoswitchable kinase inhibitors. The studies show that some azoheteroarenes have favourable photophysical properties that make them promising candidates for future application in photopharmacology, e.g. photoswitchable kinase inhibitors. Furthermore, the 7-azaindole derived photoswitchable DFG-out RET kinase inhibitor makes it possible to photocontrol the RET activity in a live cell. The successful *in vitro* application paves the way for further *in vivo* applications, e.g. in zebrafish. Furthermore, a significant fraction of the kinome is likely targetable by type II inhibitors and this work pave the way for developing photoswitchable DFG-out inhibitors targeting other kinases.

Additional aspects to explore within the subprojects described in this thesis are outlined below.

- In order to achieve distinct OFF/ON switching of kinase activity, the difference in the affinity for the target between the active and inactive form should be significant (>100-fold). Tuning the photophysical properties via structural modifications of the azoheteroarenes could make the switching more efficient. Furthermore, the modification of this molecule can be done by introducing four fluorine atoms on the *ortho* positions both on the phenyl ring and the heterocyclic ring to further separate the n→π* absorption band. Therefore, visible light can be used to enrich the *Z*-isomer in a higher PSD comparing to the *ortho*-difluoride azo compounds since visible light will be more friendly to biological assay, especially *in vivo*, when conducting *in situ* irradiation to switch the azo compound. In addition, the tetrafluoride azo compounds tend to be more thermally stable of the *Z*-isomer compared to the difluoride azo compounds.
- The field of photopharmacology is still comparatively young, and true *in vivo* applications of photoswitchable kinase inhibitors are lacking. A logical next step would be to use the photoswitchable DFG-out RET kinase inhibitor to study the dynamic signalling or RET in model systems like zebrafish, nematodes or mice. These inhibitors will make it possible to turn the kinase “on” or “off” in a tissue or even cell specific way at pre-determined time points. This is not possible with conventional small molecules/drugs. Knowledge from the development and validation of the probes, together with the biological readouts, will break new ground in the understanding of the role of RET signalling.

7 References

1. G. Manning, G. D. Plowman, T. Hunter, S. Sudarsanam, Evolution of protein kinase signalingfrom yeast to man, *Trends Biochem. Sci.* **2002**, *27*, 514-520.
2. G. Manning, D. B. Whyte, R. Martinez, T. Hunter, S. Sudarsanam, The Protein Kinase Complement of the Human Genome, *Science*. **2002**, *298*, 1912-1934.
3. E. G. Krebs, The phosphorylation of proteins: a major mechanism for biological regulation, *Biochem Soc Trans* **1985**, *13*, 813-820.
4. S. S. Taylor, D. R. Knighton, J. Zheng, L. F. T. Eyck, J. M. Sowadski, Structural Framework for the Protein Kinase Family, *Annu. Rev. Cell Bioi.* **1992**, *8*, 429-462.
5. S. G. Buchanan, J. Hendle, P. S. Lee, C. R. Smith, P.-Y. Bounaud, K. A. Jessen, C. M. Tang, N. H. Huser, J. D. Felce, K. J. Froning, *et al*. SGX523 is an exquisitely selective, ATP-competitive inhibitor of the MET receptor tyrosine kinase with antitumor activity in vivo, *Mol Cancer Ther* **2009**, *8*, 3181-3190.
6. Z. Wang, P. A. Cole, Chapter One - Catalytic Mechanisms and Regulation of Protein Kinases, *Methods Enzymol.* **2014**, *548*, 1-21.
7. D. L. Gibbons, S. Pricl, H. Kantarjian, J. Cortes, A. Quinta´s-Cardama, The Rise and Fall of Gatekeeper Mutations? The BCR-ABL1 T315I Paradigm, *Cancer* **2012**, *118*, 293-299.
8. S. Kobayashi, T. J. Boggon, T. Dayaram, P. A. Jänne, O. Kocher, M. Meyerson, B. E. Johnson, M. J. Eck, D. G. Tenen, B. Halmos, EGFR mutation and resistance of non-small-cell lung cancer to gefitinib, *N. Engl. J. Med.* **2005**, *352*, 786-792.
9. B. Nagar, W. G. Bornmann, P. Pellicena, T. Schindler, D. R. Veach, W. T. Miller, B. Clarkson, J. Kuriyan, Crystal Structures of the Kinase Domain of c-Abl in Complex with the Small Molecule Inhibitors PD173955 and Imatinib (STI-571), *Cancer Res*. **2002**, *62*, 4236-4243.
10. L. Zhang, J. Wang, L. Hou, P. Cao, L. Wu, Q. Zhang, H Yang, Y Zang, J Ding, J. Li, Functional Role of Histidine in the Conserved His-x-Asp Motif in the Catalytic Core of Protein Kinases, *Sci Rep* **2015**, *5*, 10115.
11. T. C. Strong, G. Kaur, J. H. Thomas, Mutations in the Catalytic Loop HRD Motif Alter the Activity and Function of Drosophila Src64, *PLoS ONE* **2011**, *6*, e28100.
12. A. C. Carrera, K. Alexandrov, T. M. Roberts, The conserved lysine of the catalytic domain of protein kinases is actively involved in the phosphotransfer reaction and not required for anchoring ATP, *Proc. Natl. Acad. Sci. USA.* **1993**, *90*, 442-446.
13. A. P. Kornev, N. M. Hastet, S. S. Taylort, L. F. Ten Eyck, Surface comparison of active and inactive protein kinases identifies a conserved activation mechanism, *Proc. Natl. Acad. Sci. USA.* **2006**, *103*, 17783-17788.
14. C. R. W. Guimarães, B. K. Rai, M. J. Munchhof, S. Liu, J. Wang, S. K. Bhattacharya, L. Buckbinder, Understanding the Impact of the P-loop Conformation on Kinase Selectivity, *J. Chem. Inf. Model.* **2011**, *51*, 1199-1204.
15. O. A. Karpov, G. W. Fearnley, G. A. Smith, J. Kankanala, M. J. McPherson, D. C. Tomlinson, M. A. Harrison, S. Ponnambalam. Receptor tyrosine kinase structure and function in health and disease. AIMS Biophys, **2015**, *2*, 476-502.

16. P. Saraon, S. Pathmanathan, J. Snider, A.Lyakisheva, V. Wong, I. Stagljar, Receptor tyrosine kinases and cancer: oncogenic mechanisms and therapeutic approaches, *Oncogene* **2021**, *40*, 4079-4093.
17. Z. Du, C. M. Lovly, Mechanisms of receptor tyrosine kinase activation in cancer, *Mol. Cancer* **2018**, *17*, 58.
18. M. Katoh, Fibroblast growth factor receptors as treatment targets in clinical oncology. *Nat. Rev. Clin. Oncol.* **2019**, *16*, 105-122.
19. P. Lahiry, A. Torkamani, N. J. Schork, R. A. Hegele, Kinase mutations in human disease: interpreting genotype-phenotype relationships. *Nat. Rev. Genet.* **2010**, *11*, 60-74.
20. N. Stransky, E. Cerami, S. Schalm, J. L. Kim, C. Lengauer, The landscape of kinase fusions in cancer. *Nat. Commun.* **2014**, *5*, 4846.
21. C. Choudhary, J. V. Olsen, C. Brandts, J. Cox, P. N. G. Reddy, F. D. Böhmer, V. Gerke, D.-E. Schmidt-Arras, W. E. Berdel, C. Müller-Tidow, M. Mann, H. Serve, Mislocalized activation of oncogenic RTKs switches downstream signaling outcomes. *Mol. Cell* **2009**, *36*, 326-339.
22. J.H. Walsh, W.E. Karnes, F. Cuttitta, A. Walker, Autocrine growth factors and solid tumor malignancy. *West J. Med.* **1991**, *155*, 152-163.
23. C. J Tape, S. Ling, M. Dimitriadi, K. M. McMahon, J. D. Worboys, H. S. Leong, I. C. Norrie, C. J. Miller, G. Poulogiannis, D. A. Lauffenburger, C. Jørgensen, Oncogenic KRAS regulates tumor cell signaling via stromal reciprocation. *Cell* **2016**, *165*, 910-920.
24. M. J. Hubbard, P. Cohen, On target with a new mechanism for the regulation of protein phosphorylation, *Trends Biochem. Sci*. **1993**, *18*, 172-177.
25. P. Cohen, The role of protein phosphorylation in human health and disease, *Eur. J. Biochem.* **2001**, *268*, 5001-5010.
26. M. K. Paul, A, K. Mukhopadhyay, Tyrosine kinase - Role and significance in Cancer, *Int. J. Med. Sci.* **2004**, *1*, 101-115.
27. E. Lengyel, K. Sawada, R. Salgia, Tyrosine Kinase Mutations in Human Cancer, *Curr. Mol. Med.* **2007**, *7*, 77-84.
28. A. Torkamani, G. Verkhivker, Nicholas J. Schorka, Cancer driver mutations in protein kinase genes, *Cancer Lett.* **2009**, *281*, 117-127.
29. N. Song, Y. Huang, H. Shi, S. Yuan, Y. Ding, X. Song, Y. Fu, Y. Luo, Overexpression of Platelet-Derived Growth Factor-BB Increases Tumor Pericyte Content via Stromal-Derived Factor-1α/CXCR4 Axis, *Cancer Res.* **2009**, *69*, 6057-6064.
30. T. Zhao, Y. Bao, X. Lu, Y. He, X. Gan, J. Wang, B. Liu, L. Wang, Pyk2 promotes tumor progression in renal cell carcinoma, *Oncol. Lett.* **2018**, *16*, 5953-5959.
31. M. K. Wendt, B. J. Schiemann, J. G. Parvani, Y. Lee, Y. Kang, W. P. Schiemann, TGF-β stimulates Pyk2 expression as part of an epithelial-mesenchymal transition program required for metastatic outgrowth of breast cancer. *Oncogene* **2013**, *32*, 2005-2015.
32. E. Lauretti, O. Dincer, D. Praticò, Glycogen synthase kinase-3 signaling in Alzheimer's disease, *Biochim. Biophys. Acta, Mol. Cell Res.* **2020**, *1867*, 118664.

33. E. J. Henriksen, B. B. Dokken, Role of glycogen synthase kinase-3 in insulin resistance and type 2 diabetes, *Curr. Drug Targets* **2006**, *7*, 1435-1441.
34. R. Roskoski Jr., A historical overview of protein kinases and their targeted small molecule inhibitors, *Pharmacol. Res.* **2015**, *100*, 1-23.
35. P. Cohen, Protein kinases - the major drug targets of the twenty-first century? *Nat. Rev. Drug Discov.* **2002**, *1*, 309-315.
36. R. Roskoski Jr, Properties of FDA-approved small molecule protein kinase inhibitors: A 2021 update, *Pharmacol. Res.* **2021**, *165*, 105463.
37. P. Cohen, D. Cross, P. A. Jänne, Kinase drug discovery 20 years after imatinib: progress and future directions. *Nat. Rev. Drug. Discov.* **2021**, *20*, 551–569.
38. S. A. Rosenzweig, Acquired Resistance to Drugs Targeting Tyrosine Kinases, *Adv. Cancer Res.* **2018**, *138*, 71-98.
39. C. M. Lovly, A. T. Shaw, Molecular Pathways: Resistance to Kinase Inhibitors and Implications for Therapeutic Strategies, *Clin. Cancer Res.* **2014**, *20*, 2249-2256.
40. Y. Gong, W. Pao, EGFR mutant lung cancer, *Curr. Top. Microbiol. Immunol.* **2012**, *355*, 59-81.
41. L. A. Smyth, I. Collins, Measuring and interpreting the selectivity of protein kinase inhibitors. *J. Chem. Biol.* **2009**, *2*, 131-151.
42. C. V. Miduturu , X. Deng, N. Kwiatkowski, W. Yang, L. Brault, P. Filippakopoulos, E. Chung, Q. Yang, J. Schwaller, S. Knapp, R. W King, J.-D. Lee, S. Herrgard, P. Zarrinkar, N. S. Gray, High-Throughput Kinase Profiling: A More Efficient Approach towards the Discovery of New Kinase Inhibitors, *Chem. Biol.* **2011**, *18*, 868-879.
43. A. Lai, C. Crews, Induced protein degradation: an emerging drug discovery paradigm, *Nat. Rev. Drug Discov.* **2017**, *16*, 101-114.
44. I. M. Serafimova, M. A. Pufall, S. Krishnan, K. Duda, M. S. Cohen, R. L. Maglathlin, J. M. McFarland, R. M. Miller, M. Frödin, J. Taunton, Reversible targeting of noncatalytic cysteines with chemically tuned electrophiles, *Nat. Chem. Biol.* **2012**, *8*, 471-476.
45. J. M. Bradshaw, J. M. McFarland, V. O. Paavilainen, A. Bisconte, D. Tam, V. T. Phan, S. Romanov, D. Finkle, J. Shu, V. Patel, T. Ton, *et al.* Prolonged and tunable residence time using reversible covalent kinase inhibitors, *Nat. Chem. Biol.* **2015**, *11*, 525-531.
46. Z. Zhao, Q. Liu, S. Bliven, L. Xie, P. E. Bourne, Determining Cysteines Available for Covalent Inhibition Across the Human Kinome, *J. Med. Chem.* **2017**, *60*, 2879-2889.
47. S. Muller, A. Chaikuad, N. S. Gray, S. Knapp, The *ins* and *outs* of selective kinase inhibitor development. *Nat. Chem. Biol.* **2015**, *11*, 818-821.
48. D. K. Nomura, M. M. Dix, B. F. Cravatt, Activitybased protein profiling for biochemical pathway discovery in cancer, *Nat. Rev. Cancer* **2010**, *10*, 630-638.
49. J. D. Vasta, C. R. Corona, J. Wilkinson, C. A. Zimprich, J. R Hartnett, M. R. Ingold, K. Zimmerman , T. Machleidt, T. A. Kirkland, K. G. Huwiler, *et al*. Quantitative, wide-spectrum kinase profiling in live cells for assessing the effect of cellular ATP on target engagement. *Cell Chem. Biol.* **2018**, *25*, 206-214.

50. D. M. Goldstein, N. S. Gray, P. P. Zarrinkar, High throughput kinase profiling as a platform for drug discovery, *Nat. Rev. Drug Discov.* **2008**, *7*, 391-397.
51. R. Roskoski Jr, Classification of small molecule protein kinase inhibitors based upon the structures of their drug-enzyme complexes, *Pharmacol. Res.* **2016**, *103*, 26-48.
52. O. P. J. van Linden, A. J. Kooistra, R. Leurs, I. J. P. de Esch, C. de Graaf, KLIFS: A Knowledge-Based Structural Database to Navigate Kinase-Ligand Interaction Space, *J. Med. Chem.* **2014**, *57*, 249-277.
53. Z. Zhao, H. Wu, L. Wang, Y. Liu, S. Knapp, Q. Liu, N. S. Gray, Exploration of Type II Binding Mode: A Privileged Approach for Kinase Inhibitor Focused Drug Discovery? *ACS Chem. Biol.* **2014**, *9*, 1230-1241.
54. Z. Zhao, L. Xie, P. E. Bourne, Insights into the binding mode of MEK type-III inhibitors. A step towards discovering and designing allosteric kinase inhibitors across the human kinome, *PLoS One* **2017**, *12*, e0179936.
55. K. J. Cox, C. D. Shomin, I. Ghosh, Tinkering outside the kinase ATP box: allosteric (type IV) and bivalent (type V) inhibitors of protein kinases, *Future Med. Chem*. **2011**, *3*, 29-43.
56. C. M. Gower, M. E. K. Chang, D. J. Maly, Bivalent inhibitors of protein kinases, *Crit. Rev. Biochem. Mol. Biol.* **2014**, *49*, 102-115.
57. S. Lee, J. Kim, J. Jo, J. W. Chang. J. Sim, H. Yun, Recent advances in development of hetero-bivalent kinase inhibitors, *Eur. J. Med. Chem.* **2021**, *216*, 113318.
58. M. S. Davids, J. R. Brown, Ibrutinib: a first in class covalent inhibitor of Bruton's tyrosine kinase, *Future Oncol.* **2014**, *10*, 957-967.
59. V. De Falco, F. Carlomagno, H.-Y. Li, M. Santoro, The molecular basis for RET tyrosine-kinase inhibitors in thyroid cancer, *Best Pract. Res. Clin. Endocrinol. Metab.* **2017**, *31*, 307-318.
60. M. Takahashi, J. Ritz, G. M. Cooper. Activation of a novel human transforming gene, RET, by DNA rearrangement. *Cell* **1985**, *42*, 581-588.
61. C. F. Ibáñez, Structure and Physiology of the RET Receptor Tyrosine Kinase, Cold Spring Harb. Perspect Biol. **2013**, *5*, a009134.
62. K. M. Goodman, S. Kjær, F. Beuron, P. P. Knowles, A. Nawrotek, E. M. Burns, A. G. Purkiss, R. George, M. Santoro, E. P. Morris, N. Q. McDonald. RET recognition of GDNF-GFRa1 ligand by a composite binding site promotes membrane-proximal self-association. *Cell Rep.* **2014**, *8*, 1894-1904.
63. X. Wang, Structural studies of GDNF family ligands with their receptors - insights into ligand recognition and activation of receptor tyrosine kinase RET, *Biochim. Biophys. Acta* **2013**, *1834*, 2205-2212.
64. L. M. Mulligan, RET revisited: expanding the oncogenic portfolio, *Nat. Rev. Cancer* **2014**, *14*, 173-186.
65. S. A. Wells Jr, F. Pacini, B. G. Robinson, M. Santoro. Multiple endocrine neoplasia type 2 and familial medullary thyroid carcinoma: an update. *J. Clin. Endocrinol Metab.* **2013**, *98*, 3149-3164.
66. I. Plaza-Menacho, K. Barnouin, K. Goodman, R. J. Martínez-Torres, A. Borg, J. Murray-Rust, S. Mouilleron, P. Knowles, N. Q. McDonald, Oncogenic RET

kinase domain mutations perturb the autophosphorylation trajectory by enhancing substrate presentation in trans. *Mol. Cell.* **2014**, *53*, 738-751.

67. K. Tsuta, T. Kohno, A. Yoshida, Y. Shimada, H. Asamura, K. Furuta, R. Kushima, RET-rearranged non-small-cell lung carcinoma: a clinicopathological and molecular analysis, *Br J Cancer.* **2014**, *110*, 1571-1578.
68. J. A. Fagin, S. A. Wells Jr, Biologic and clinical perspectives on thyroid cancer, *N. Engl. J. Med.* **2016**, *375*, 1054-1067.
69. J. C. Ricarte-Filho, S. Li, M. E. R. Garcia-Rendueles, C. Montero-Conde, F. Voza, J. A. Knauf, A. Heguy, A. Viale, T. Bogdanova, G. A. Thomas, C. E. Mason, J. A. Fagin, Identification of kinase fusion oncogenes in post-chernobyl radiationinduced thyroid cancers, *J. Clin. Investig.* **2013**, *123*, 4935-4944.
70. P. V. Borre, A. B. Schrock, P. M. Anderson, J. C. Morris 3rd, A. M. Heilmann, O. Holmes, K. Wang, A. Johnson, S. G. Waguespack, S.-H. I. Ou, Pediatric, adolescent, and young adult thyroid carcinoma harbors frequent and diverse targetable genomic alterations, including kinase fusions, *Oncologist* **2017**, *22*, 255-263.
71. S. Kato, V. Subbiah, E. Marchlik, S. K. Elkin, J. L. Carter, R. Kurzrock, RET Aberrations in Diverse Cancers: Next-Generation Sequencing of 4,871 Patients, *Clin. Cancer Res.* **2017**, *23*, 1988-1997.
72. P. Griseri, O. Garrone, A. L. Sardo, M. Monteverde, M. Rusmini, F. Tonissi, M. Merlano, P. Bruzzi, C. Lo Nigro, I. Ceccherini,Genetic and epigenetic factors affect RET gene expression in breast cancer cell lines and influence survival in patients. *Oncotarget* **2016**, *7*, 26465-26479.
73. M. Amit, S. Na'ara, L. Leider-Trejo, Y. Binenbaum, N. Kulish, E. Fridman, A. Shabtai-Orbach, R. J. Wong, Z. Gil, Upregulation of RET induces perineurial invasion of pancreatic adenocarcinoma, *Oncogene.* **2017**, *36*, 3232-3239.
74. C. Jia, W. Chen, Z. Feng, Z. Liu, Recent developments of RET protein kinase inhibitors with diverse scaffolds as hinge binders, *Future Med. Chem.* **2021**, *13*, 45-62.
75. A. Bikas, S. Vachhani, K. Jensen, V. Vasko, K. D. Burman, Targeted therapies in thyroid cancer: an extensive review of the literature. *Expert Rev. Clin. Pharmacol.* **2016**, *9*, 1299-1313.
76. R. S. Herbst, J. V. Heymach, M. S. O'Reilly, A. Onn, A. J. Ryan, Vandetanib (ZD6474): an orally available receptor tyrosine kinase inhibitor that selectively targets pathways critical for tumor growth and angiogenesis, *Expert Opin. Investig. Drugs* **2007**, *16*, 239-249.
77. F. M. Yakes, J. Chen, J. Tan, K. Yamaguchi, Y. Shi, P. Yu, F. Qian, F. Chu, F. Bentzien, B. Cancilla, Cabozantinib (XL184), a novel MET and VEGFR2 inhibitor, simultaneously suppresses metastasis, angiogenesis, and tumor growth, *Mol. Cancer Ther.* **2011**, *10*, 2298-2308.
78. K. Okamoto, K. Kodama, K. Takase, N. H. Sugi, Y. Yamamoto, M. Iwata, A. Tsuruoka, Antitumor activities of the targeted multi-tyrosine kinase inhibitor lenvatinib (E7080) against RET gene fusion-driven tumor models, *Cancer Lett.* **2013**, *340*, 97-103.

79. V. De Falco, P. Buonocore, M. Muthu, L. Torregrossa, F. Basolo, M. Billaud, J. M. Gozgit, F. Carlomagno, M. Santoro, Ponatinib (AP24534) is a novel potent inhibitor of oncogenic RET mutants associated with thyroid cancer, *J. Clin. Endocrinol. Metab.* **2013**, *98*, 811-819.
80. D. B. Mendel, A. D. Laird, X. Xin, S. G. Louie, J. G. Christensen, G. Li, R. E. Schreck, T. J. Abrams, T. J. Ngai, L. B. Lee, *et al*. In vivo antitumor activity of SU11248, a novel tyrosine kinase inhibitor targeting vascular endothelial growth factor and platelet-derived growth factor receptors: determination of a pharmacokinetic/pharmacodynamic relationship, *Clin. Cancer Res.* **2003**, *9*, 327-337.
81. F. Carlomagno, S. Anaganti, T. Guida, G. Salvatore, G. Troncone, S. M. Wilhelm, M. Santoro, BAY 43-9006 inhibition of oncogenic RET mutants, *J. Natl. Cancer Inst.* **2006**, *98*, 326-334.
82. I. Plaza-Menacho, L. Mologni, E. Sala, C. Gambacorti-Passerini, A. I. Magee, T. P. Links, R. M. W. Hofstra, D. Barford, C. M. Isacke, Sorafenib functions to potently suppress RET tyrosine kinase activity by direct enzymatic inhibition and promoting RET lysosomal degradation independent of proteasomal targeting, *J. Biol. Chem.* **2007**, *282*, 29230-29240.
83. S. R. Hayman, N. Leung, J. P. Grande, V. D. Garovic, VEGFR inhibition, hypertension, and renal toxicity. *Curr. Oncol. Rep.* **2012**, *14*, 285-294.
84. N. S. Azad, J. B. Aragon-Ching, W. L. Dahut, M. Gutierrez, W. D. Figg, L. Jain, S. M. Steinberg, M. L. Turner, E. C. Kohn, H. H. Kong, Hand-foot skin reaction increases with cumulative sorafenib dose and with combination antivascular endothelial growth factor therapy. *Clin. Cancer Res.* **2009**, *15*, 1411-1416.
85. H. S. Eidam, J. Russell, K. Raha, M. DeMartino, D. Qin, H. A. Guan, Z. Zhang, G. Zhen, H. Yu, C. Wu, *et al.* Discovery of a First-in-Class Gut-Restricted RET Kinase Inhibitor as a Clinical Candidate for the Treatment of IBS, *ACS Med. Chem. Lett.* **2018**, *9*, 623-628.
86. M. Wang, N. Naganna, H. O. Sintim, Identification of nicotinamide aminonaphthyridine compounds as potent RET kinase inhibitors and antitumor activities against RET rearranged lung adenocarcinoma, *Bioorg. Chem.* **2019**, *90*, 103052.
87. M. Han, S. Li, J. Ai, R. Sheng, Y. Hu, Y. Hu, M. Geng, Discovery of 4-chloro-3-(5-(pyridin-3-yl)-1,2,4-oxadiazole-3-yl)benzamides as novel RET kinase inhibitors, *Bioorg. Med. Chem. Lett.* **2016**, *26*, 5679-5684.
88. V. Gattei, A. Celetti, A. Cerrato, M. Degan, A. De Iuliis, F. M. Rossi, G. Chiappetta, C. Consales, S. Improta, Expression of the RET receptor tyrosine kinase and GDNFR-alpha in normal and leukemic human hematopoietic cells and stromal cells of the bone marrow microenvironment, *Blood* **1997**, *89*, 2925-2937.
89. M. Quartu, M. P. Serra, M. Boi, M. T. Ferretti, M. L. Lai, M. D. Fiacco, Tissue distribution of Ret, GFRalpha-1, GFRalpha-2 and GFRalpha-3 receptors in the human brainstem at fetal, neonatal and adult age, *Brain Res.* **2007**, *1173*, 36-52.
90. C. Brieke, F. Rohrbach, A. Gottschalk, G. Mayer, A. Heckel, Light-controlled tools, *Angew. Chem., Int. Ed.* **2012**, *51*, 8446-8476.

91. L. Fenno, O. Yizhar, K. Deisseroth, The Development and Application of Optogenetics, *Annu. Rev. Neurosci.* **2011**, *34*, 389-412.
92. W. A. Velema, W. Szymanski, B. L. Feringa, Photopharmacology: Beyond Proof of Principle, *J. Am. Chem. Soc.* **2014**, *136*, 2178-2191.
93. J. Broichhagen, J. A. Frank, D. Trauner, A Roadmap to Success in Photopharmacology, *Acc. Chem. Res.* **2015**, *48*, 1947-1960.
94. P. Klán, T. Šolomek, C. G. Bochet, A. Blanc, R. Givens, M. Rubina, V. Popik, A. Kostikov, J. Wirz, Photoremovable Protecting Groups in Chemistry and Biology: Reaction Mechanisms and Efficacy, *Chem. Rev.* **2013**, *113*, 119-191.
95. A. Y. Vorobev, A. E. Moskalensky, Long-wavelength photoremovable protecting groups: on the way to in vivo application, *Comput. Struct. Biotechnol. J.* **2020**, *18*, 27-34.
96. M. J. Fuchter, On the Promise of Photopharmacology Using Photoswitches: A Medicinal Chemist's Perspective, *J. Med. Chem.* **2020**, *63*, 11436-11447.
97. W. Szymański, J. M. Beierle, H. A. V. Kistemaker, W. A. Velema, B. L. Feringa, Reversible Photocontrol of Biological Systems by the Incorporation of Molecular Photoswitches, *Chem. Rev.,* **2013**, *113*, 6114-6178.
98. J. D. Harrisa, M. J. Morana, I. Aprahamiana, New molecular switch architectures. *Proc. Natl. Acad. Sci. U. S. A.* **2018**, *115*, 9414-9422.
99. Z. L. Pianowski, Recent Implementations of Molecular Photoswitches into Smart Materials and Biological Systems, *Chem. Eur. J.* **2019**, *25*, 5128-5144.
100. S. Fredrich, R. Göstl, M. Herder, L. Grubert, S. Hecht, Switching Diarylethenes Reliably in Both Directions with Visible Light, *Angew. Chem., Int. Ed.* **2016**, *55*, 1208-1212.
101. J. Griffiths, II. Photochemistry of azobenzene and its derivatives, *Chem. Soc. Rev.,* **1972**, *1*, 481-493.
102. A. A. Beharry, G. A. Woolley, Azobenzene photoswitches for biomolecules, *Chem. Soc. Rev.,* **2011**, *40*, 4422-4437.
103. C. Falenczyk, M. Schiedel, B. Karaman, T. Rumpf, N. Kuzmanovic, M. Grøtli, W. Sippl, M. Jung, B. König, Chromo-pharmacophores: photochromic diarylmaleimide inhibitors for sirtuins, *Chem. Sci.* **2014**, *5*, 4794-4799.
104. S. Herre, T. Schadendorf, I. Ivanov, C. Herrberger, W. Steinle, K. Ruck-Braun, R. Preissner, H. Kuhn, Photoactivation of an Inhibitor of the 12/15-Lipoxygenase Pathway, *ChemBioChem* **2006**, *7*, 1089-1095.
105. D. Lachmann, R. Lahmy, B. König, Fulgimides as Light-Activated Tools in Biological Investigations, *Eur. J. Org. Chem.* **2019**, 5018-5024.
106. C. L. Fleming, M. Grøtli, J. Andreasson, On-Command Regulation of Kinase Activity using Photonic Stimuli, *ChemPhotoChem* **2019**, *3*, 318-326.
107. R. Ferreira, J. R. Nilsson, C. Solano, J. Andréasson, M. Grøtli, Design, Synthesis and Inhibitory Activity of Photoswitchable RET Kinase Inhibitors, *Sci. Rep*. **2015**, *5*, 9769.
108. M. Schehr, C. Ianes, J. Weisner, L. Heintze, M.P. Müller, C. Pichlo, J. Charl, E. Brunstein, J. Ewert, M. Lehr, U. Baumann, D. Rauh, U. Knippschild, C. Peifer, R. Herges, 2-Azo-, 2-diazocine-thiazols and 2-azo-imidazoles as photoswitchable

kinase inhibitors: limitations and pitfalls of the photoswitchable inhibitor approach, *Photochem. Photobiol. Sci.* **2019**, *18*, 1398-1407.

109. M. Hoorens, M. E. Ourailidou, T. Rodat, P. E. Wouden, P. Kobauri, M. Kriegs, C. Peifer, B. L. Feringa, F. J. Dekker, W. Szymanski, Light-controlled inhibition of $BRAF^{V600E}$ kinase, *Eur. J. Med. Chem*, **2019**, *179*, 133-146.
110. D. Kolarski, C. Miró-Vinyals, A. Sugiyama, A. Srivastava, D. Ono, Y. Nagai, M. Iida, K. Itami, F. Tama, W. Szymanski, T. Hirota, B. L. Feringa, Reversible modulation of circadian time with chronophotopharmacology, *Nat. Commun.* **2021**, *12*, 3164.
111. M. Reynders, A. Chaikuad, B.-T. Berger, K. Bauer, P. Koch, S. Laufer, S. Knapp, D. Trauner, Controlling the Covalent Reactivity of a Kinase Inhibitor with Light, *Angew. Chem. Int. Ed.* 10.1002/anie.202103767.
112. K. Hunger, *Industrial Dyes: Chemistry, Properties, Applications,* ed. Wiley-VCH, Weinheim, Germany, 2003.
113. W. J. Sandborn, Rational selection of oral 5-aminosalicylate formulations and prodrugs for the treatment of ulcerative colitis, *Am. J. Gastroenterol.* **2002**, *97*, 2939-2941.
114. S. Hvilsted, C. Sánchezb, R. Alcalá, The volume holographic optical storage potential in azobenzene containing polymers, *J. Mater. Chem.* **2009**, *19*, 6641-6648.
115. B. L. Feringa, R. A. Van Delden, N. Koumura, E. M. Geertsema, Chiroptical Molecular Switches, *Chem. Rev.* **2000**, *100*(5), 1789-1816.
116. E. Merino, Synthesis of azobenzenes: the coloured pieces of molecular materials, *Chem. Soc. Rev.*, **2011**, *40*, 3835-3853.
117. C. Mills, XCIII. -Some new azo-compounds, *J. Chem. Soc. Trans.* **1895**, *67*, 925-933.
118. B. C. Yu, Y. Shirai, J. M. Tour, Syntheses of new functionalized azobenzenes for potential molecular electronic devices, *Tetrahedron*, **2006**, *62*, 10303.
119. K. Haghbeen, E. W. Tan, Facile Synthesis of Catechol Azo Dyes, *J. Org. Chem.* **1998**, *63*, 4503-4505.
120. D. Kolarski, W. Szymanski, B. L. Feringe, Two-Step, One-Pot Synthesis of Visible-Light-Responsive 2, 6‑Azopurines, *Org. Lett.* **2017**, *19*, 5090-5093.
121. Y.-K. Lim, K.-S. Lee, C.-G. Cho, Novel Route to Azobenzenes via Pd-Catalyzed Coupling Reactions of Aryl Hydrazides with Aryl Halides, Followed by Direct Oxidations, *Org. Lett.* **2003**, *5*, 979-982.
122. H.-M. Kang, J.-W. Jung, C.-G. Cho, Practical Synthesis of Azobenzenophanes, *J. Org. Chem.* **2007**, *72*, 679-682.
123. K. Orito, T. Hatakeyama, M. Takeo, S. Uchiito, M. Tokuda, H. Suginome, Dimerization of anilines and benzylamines with mercury(II) oxide-iodine reagent, *Tetrahedron*, **1998**, *54*, 8403-8410.
124. G. R. Srinivasa, K. Abiraj, D. C. Gowda, Facile synthesis of azo compounds from aromatic nitro compounds using magnesium and triethylammonium formate, *Aust. J. Chem.* **2004**, *57*, 609-610.
125. D. Bléger, S. Hecht, Visible-light-activated molecular switches. *Angew. Chem. Int. Ed.* **2015**, *54*, 11338-11349.

126. M. Dong, A. Babalhavaeji, S. Samanta, A. A. Beharry, G. A. Woolley, Red-shifting azobenzene photoswitches for in vivo use, *Acc. Chem. Res.* **2015**, *48*, 2662-2670.
127. M. Wegener, M. J. Hansen, A. J. M. Driessen, W. Szymanski, B. L. Feringa, Photocontrol of antibacterial activity: shifting from UV to red light activation, *J. Am. Chem. Soc.* **2017**, *139*, 17979-17986.
128. J. Garcia-Amorós, A. Sánchez-Ferrer, W. A. Massad, S. Nonell, D. Velasco, Kinetic study of the fast thermal cis-to-trans isomerisation of para-. *ortho*- and polyhydroxyazobenzenes, *Phys. Chem. Chem. Phys.* **2010**, *12*, 13238-13242.
129. C. Knie, M. Utecht, F. Zhao, H. Kulla, S. Kovalenko, A. M. Brouwer, P. Saalfrank, S. Hecht, D. Bléger, *ortho*-fluoroazobenzenes: visible light switches with very long-lived *Z*-somers. *Chem. Eur. J.* **2014**, *20*, 16492-16501.
130. H. M. Bandara, S. C. Burdette, Photoisomerization in different classes of azobenzene. *Chem. Soc. Rev.* **2012**, *41*, 1809-1825.
131. S. Chen, Y. Zhang, K. Chen, Y. Yin, C. Wang, Insight into a fast-phototuning azobenzene switch for sustainably tailoring the foam stability. *ACS Appl. Mater. Interfaces* **2017**, *9*, 13778-13784.
132. T. Worzella, M. Butzler, J. Hennek, S. Hanson, L. Simdon, S. Goueli, C. Cowan, H. Zegzouti, A Flexible Workflow for Automated Bioluminescent Kinase Selectivity Profiling, *SLAS Technol.* **2017**, *22*, 153-162.
133. H. Zegzouti, M. Zdanovskaia, K. Hsiao, S. A. Goueli, ADP-Glo: A Bioluminescent and Homogeneous ADP Monitoring Assay for Kinases, *Assay Drug Dev. Technol.* **2009**, *7*, 560-572.
134. M. B. Robers, M. L. Dart, C. C. Woodroofe, C. A. Zimprich, T. A. Kirkland, T. Machleidt, K. R. Kupcho, S. Levin, J. R. Hartnett, K. Zimmerman, *et al.* Target engagement and drug residence time can be observed in living cells with BRET, *Nat. Commun.* **2015**, *6*, 10091.
135. J. D. Vasta, C. R. Corona, J. Wilkinson, C. A. Zimprich, J. R. Hartnett, M. R Ingold, K. Zimmerman, T. Machleidt, T. A. Kirkland, K. G. Huwiler, *et al.* Quantitative, wide-spectrum kinase profiling in live cells for assessing the effect of cellular ATP on target engagement. *Cell Chem. Biol.* **2018**, *25*, 206-214.
136. A. Gomtsyan, Heterocycles in drugs and drug discovery, *Chem. Heterocycl Comp*. **2012**, *48*, 7-10.
137. M. Baumann, I. R. Baxendale, S. V. Ley, N. Nikbin, An overview of the key routes to the best-selling 5-membered ring heterocyclic pharmaceuticals, *Beilstein J. Org. Chem.* **2011,** *7,* 442-495.
138. N. Kerru, L. Gummidi, S. Maddila, K. K. Gangu , S. B. Jonnalagadda, A Review on Recent Advances in Nitrogen-Containing Molecules and Their Biological Applications, *Molecules* **2020**, *25*, 1909.
139. V. Sharma, R. Kamal, V. Kumar, Heterocyclic Analogues as Kinase Inhibitors: A Focus Review, *Curr. Top. Med. Chem.* **2017**, *17*, 2482-2494.
140. T. Wendler, C. Schütt, C. Näther, R. Herges, Photoswitchable azoheterocycles via coupling of lithiated imidazoles with benzenediazonium salts, *J. Org. Chem.* **2012**, *77*, 3284-3287.

141. C. E. Weston, R. D. Richardson, P. R. Haycock, A. J. P. White, M. J. Fuchter, Arylazopyrazoles: azoheteroarene photoswitches offering quantitative isomerization and long thermal half-lives, *J. Am. Chem. Soc.* **2014**, *136*, 11878-11181.
142. C. E. Weston, R. D. Richardsona, M. J. Fuchter, Photoswitchable basicity through the use of azoheteroarenes, *Chem. Commun.* **2016**, *52*, 4521-4524.
143. D. Kolarski, W. Szymanski, B. L. Feringa, Two-Step, One-Pot Synthesis of Visible-Light Responsive 6-Azopurines *Org. Lett.* **2017**, *19*, 5090-5093.
144. J. Otsuki, K. Suwa, K. Narutaki, C. Sinha, I. Yoshikawa, K. Araki, Photochromism of 2-(Phenylazo)imidazoles, *J. Phys. Chem. A*, **2005**, *109*, 8064-8069.
145. J. Calbo, C. E. Weston, A. J. P. White, H. S. Rzepa, J. Contreras-García, M. J. Fuchter, Tuning Azoheteroarene Photoswitch Performance through Heteroaryl Design, *J. Am. Chem. Soc.* **2017**, *139*, 1261-1274.
146. T. T. Yin, Z. -X. Zhao, H. X. Zhang, A theoretical study on the thermal cis-trans isomerization of azoheteroarene photoswitches, *New J. Chem.* **2017**, *41*, 1659.
147. N. A. Simeth, S. Crespi, M. Fagnoni, B. König, Tuning the Thermal Isomerization of Phenylazoindole Photoswitches from Days to Nanoseconds, *J. Am. Chem. Soc.* **2018**, *140*, 2940-2946.
148. L. Stricker, E.-C. Fritz, M. Peterlechner, N. L. Doltsinis, B. J. Ravoo, Arylazopyrazoles as Light-Responsive Molecular Switches in Cyclodextrin-Based Supramolecular Systems, *J. Am. Chem. Soc.* **2016**, *138*, 4547-4554.
149. Y.-K. Lim, K.-S. Lee, C.-G. Cho, Novel Route to Azobenzenes via Pd-Catalyzed Coupling Reactions of Aryl Hydrazides with Aryl Halides, Followed by Direct Oxidations, *Org. Lett.* **2003**, *5*, 979-982.
150. X. Lu, Control of the β-hydride elimination making palladium-catalyzed coupling reactions more diversified, *Top. Catal.* **2005**, *35*, 73-86.
151. A. S.Shawali, synthesis and tautomerism of aryl- and hetaryl-azoderivatives of bi- and tri-heterocycles, *J. Adv. Res.* **2010**, *1*, 255-290.
152. L. Coyne, R. Mariner, A. Rice, Air-oxidation of hydrazine. 1. Reaction kinetics on natural kaolinites, halloysites, and model substituent layers with varying iron and titanium oxide and oxygen(1-) center contents, *Langmuir* **1991**, *7*, 1660-1674.
153. V. H. Rawal, M. P. Cava, Thermolytic Removal of tbutyloxycarbonyl (BOC) Protecting Group on Indoles and Pyrroles, *Tetrahedron Lett.* **1985**, *26*, 6141- 6142.
154. P. S. Baran, R. A. Shenv, Total Synthesis of (±)-Chartelline C, *J. Am. Chem. Soc.* **2006**, *128*, 14028-14029.
155. S. Sharma, S. Mehndiratta, S. Kumar, J. Singh, P. M S Bedi, K. Nepali, Purine Analogues as Kinase Inhibitors: A Review, *Recent Pat. Anticancer Drug Discov.* **2015**, *10*, 308-341.
156. J.-L. Haesslein, N. Jullian, Recent advances in cyclin-dependent kinase inhibition. Purine-based derivatives as anti-cancer agents. Roles and perspectives for the future, *Curr. Top. Med. Chem.* **2002**, *2*, 1037-1050.
157. M. T. Conconi, G. Marzaro, L. Urbani, I. Zanusso, R. D. Liddo, I. Castagliuolo, P. Brun, F. Tonus, A. Ferrarese, A. Guiotto, A. Chilin, Quinazoline-based multi-

tyrosine kinase inhibitors: synthesis, modeling, antitumor and antiangiogenic properties, *Eur. J. Med. Chem.* **2013**, *67*, 373-383.
158. J. A. Tucker, T. Klein, J. Breed, A. L. Breeze, R. Overman, C. Phillips, R. A. Norman, Structural Insights into FGFR Kinase Isoform Selectivity: Diverse Binding Modes of AZD4547 and Ponatinib in Complex with FGFR1 and FGFR4, *Structure* **2014**, *22*, 1764-1774.
159. R. Elisei, M. J. Schlumberger, S. P. Müller, P. Schöffski, M. S. Brose, M. H. Shah, L. Licitra, B. Jarzab, V. Medvedev, M. C. Kreissl, *et al*, Cabozantinib in progressive medullary thyroid cancer, *J. Clin. Oncol.* **2013**, *31*, 3639-3646.
160. A. Martorana, G. L. Monica, A. Lauria, Quinoline-Based Molecules Targeting c-Met, EGF, and VEGF Receptors and the Proteins Involved in Related Carcinogenic Pathways, *Molecules* **2020**, *25*, 4279.
161. W. Shen, M. S. Tremblay, V. A. Deshmukh, W. Wang, C. M. Filippi, G. Harb, Y.-q. Zhang, A. Kamireddy, J. E. Baaten, Q. Jin, *et al*. Small-molecule inducer of β cell proliferation identified by high-throughput screening. *J. Am. Chem. Soc.* **2013**, *135*, 1669-1672.
162. J. Regan, C. A. Pargellis, P. F. Cirillo, T. Gilmore, E. R. Hickey, G. W. Peet, A. Proto, A. Swinamera, N. Moss, The Kinetics of Binding to p38 MAP Kinase by Analogues of BIRB 796, *Bioorg. Med. Chem. Lett*. **2003**, *133*, 3101-3104.
163. A. P. Garner, J. M. Gozgit, R. Anjum, S. Vodala, A. Schrock, T. Zhou, C. Serrano, G. Eilers, M. Zhu, J. Ketzer, *et al*, Ponatinib Inhibits Polyclonal Drug-Resistant KIT Oncoproteins and Shows Therapeutic Potential in Heavily Pretreated Gastrointestinal Stromal Tumor (GIST) Patients. *Clin Cancer Res* **2014**, *20*, 5745-5755.
164. Waldeck, D. H. Photoisomerization dynamics of stilbenes, *Chem. Rev.* **1991**, *91*, 415-436.
165. T. Iijima, Y. Endo, M. Tsuji, E. Kawachi, H. Kagechika, K. Shudo, Dicarba-closo-dodecaboranes as a pharmacophore. Retinoidal antagonists and potential agonists, *Chem. Pharm. Bull.* **1999**, *47*, 398-404.
166. T. Schabel, C. Belger, B. A. Plietker, Mild Chemoselective Ru-Catalyzed Reduction of Alkynes, Ketones, and Nitro Compounds, *Org. Lett.* **2013**, *15*, 2858-2861.
167. J. Li, R. Hua, T. Liu, Highly Chemo- and Stereoselective Palladium-Catalyzed Transfer Semihydrogenation of Internal Alkynes Affording *cis*-Alkenes, *J. Org. Chem.* **2010**, *75*, 2966-2970.
168. A. Piontek, W. Ochędzan-Siodłak, E. Bisz, M. Szostak, Nickel-Catalyzed C(sp^2)-C(sp^3) Kumada Cross-Coupling of Aryl Tosylates with Alkyl Grignard Reagents, *Chembiochem* **2019**, *361*, 2329-2336.
169. M. Kumada, Phosphine-Nickel Complexes as Catalysts for Cross-Coupling Reaction of Grignard Reagents with Vinylic, Aromatic and Heteroaromatic Halides. In *Organotransition-Metal Chemistry*. Ishii, Y. (Ed.); Springer, **1975**, 211-222.
170. Y. Xu, Z. Yin, X. Lin, Z. Gan, Y. He, L. Gao, Z. Song, 1,4-Hydroiodination of Dienyl Alcohols with TMSI To Form Homoallylic Alcohols Containing a

Multisubstituted Z-Alkene and Application to Prins Cyclization, *Org. Lett.* **2015**, *17*, 1846-1849.

171. R. A. Day, J. A. Blake, C. E. Stephens, Convenient and improved halogenation of 3, 5- diarylisoxazoles using N-halosuccinimides, *Synthesis* **2003**, *10*, 1586- 1590.
172. T. Iijima, Y. Endo, M. Tsuji, E. Kawachi, H. Kagechika, K. Shudo, Dicarba-closo-dodecaboranes as a pharmacophore. Retinoidal antagonists and potential agonists, *Chem. Pharm. Bull*. **1999**, *47*, 398-404.
173. T. Schabel, C. Belger, B. A. Plietker, Mild Chemoselective Ru-Catalyzed Reduction of Alkynes, Ketones, and Nitro Compounds, *Org. Lett.* **2013**, *15*, 2858-2861.
174. C. Moreno-Marrodan, F. Liguori, P. Barbaro, Continuous-flow processes for the catalytic partial hydrogenation reaction of alkynes, *Beilstein J. Org. Chem.* **2017**, *13*, 734-754.
175. M. Zurro, S. Asmus, S. Beckendorf, C. Mück-Lichtenfeld, O. G. Mancheño, Chiral Helical Oligotriazoles: New Class of Anion-Binding Catalysts for the Asymmetric Dearomatization of Electron-Deficient N-Heteroarenes, *J. Am. Chem. Soc.* **2014**, *136*, 13999-14002.
176. R. Saari, J.-C. Törmä, T. Nevalainen, Microwave-assisted synthesis of quinoline, isoquinoline, quinoxaline and quinazoline derivatives as CB2 receptor agonists, *Bioorg. Med. Chem.* **2011**, *19*, 939-950.
177. H. E. Ho, N. Asao, Y. Yamamoto, T. Jin, Carboxylic Acid-Catalyzed Highly Efficient and Selective Hydroboration of Alkynes with Pinacolborane, *Org. Lett.* **2014**, *16*, 4670-4673.
178. A. Jankowiak, E. Obijalska, P. Kaszynski, Cyclization of substitued 2-(2-fluorophenylazo)azines to azino[1,2-*c*]benzo[*d*][1,2,4]triazinium derivatives, *Beilstein J. Org. Chem.* **2013**, *9*, 1873-1880.
179. A. Aillerie, S. Pellegrini, T. Bousquet, L. Pelinski, In situ generation of ammonia for the copper-catalyzed synthesis of primary aminoquinolines, *New J. Chem.* **2014**, *38*, 1389-1391.
180. C. Knie, M. Utecht, F. Zhao, H. Kulla, S. Kovalenko, A. M. Brouwer, P. Saalfrank, S. Hecht, D. Bleger, *ortho*-Fluoroazobenzenes: Visible Light Switches with Very LongLived *Z* Isomers, *Chem. Eur. J.* **2014**, *20*, 16492-16501.
181. D. Bleger, J. Schwarz, A. M. Brouwer, S. Hecht, *o*‐Fluoroazobenzenes as Readily Synthesized Photoswitches Offering Nearly Quantitative Two-Way Isomerization with Visible Light, *J. Am. Chem. Soc.* **2012**, *134*, 20597-20600.
182. T. Arif, C. Cazorla, N. Bogliotti, N. Saleh, F. Blanchard, V. Gandon, R. Métivier, J. Xie, A. Voituriez, A. Marinetti, Bimetallic goldIJI) complexes of photoswitchable phosphines: synthesis and uses in cooperative catalysis, *Catal. Sci. Technol.* **2018**, *8*, 710-715.
183. T. Koźlecki, L. Syper, K. A. Wilk, 4-Lithio-4'-alkylazobenzenes as Convenient Intermediates for the Preparation of Azobenzene Derivatives, *Synthesis* **1997**, *6*, 681-684.
184. C.-L. Li, X. Qi, X.-F. Wu, Palladium-Catalyzed Hydroxycarbonylation of Aryl Halides with the in-situ Generation of CO and H_2O, *ChemistrySelect* **2016**, *1*, 1702-1704.

185. B. Daydé-Cazals, B. Fauvel, M. Singer, C. Feneyrolles, B. Bestgen, F. Gassiot, A. Spenlinhauer, P. Warnault, N. V. Hijfte, N. Borjini, G. Chevé, A. Yasri, Rational Design, Synthesis, and Biological Evaluation of 7-Azaindole Derivatives as Potent Focused Multi-Targeted Kinase Inhibitors, *J. Med. Chem.* **2016**, *59*, 3886-3905.
186. J.-Y. Mérour, F. Buron, K. Plé, P. Bonnet, S. Routier, The Azaindole Framework in the Design of Kinase Inhibitors, *Molecules* **2014**, *19*, 19935-19979.
187. C. Boulegue, M. Loeweneck, C. Renner, L. Moroder, Redox Potential of Azobenzene as an Amino Acid Residue in Peptides, *Chem. Bio. Chem.* **2007**, *8*, 591-594.
188. A. M. Amitrano, B. J. Berry, K. Lim, K.-D. Kim, R. E. Waugh, A. P. Wojtovich, M. Kim, Optical Control of $CD8^+$ T Cell Metabolism and Effector Functions, *Front. Immunol*. **2021**, *12*, 666231.
189. J. Regan, C. A. Pargellis, P. F. Cirillo, T. Gilmore, E. R. Hickey, G. W. Peet, A. Proto, A. Swinamera, N. Moss, The Kinetics of Binding to p38 MAP Kinase by Analogues of BIRB 796, *Bioorg. Med. Chem. Lett*. **2003**, *133*, 3101-3104.

8 Acknowledgements

Five years passed, and I have finally reached the end of my PhD journey. It was exciting and growing journey, but also challenging and tough journey. There were so many wonderful and memorable moments occurred during these years. I can image these moments would just like some sweet dreams years later when I retrospect at the other end of the continent. Herein, I would like to appreciate all the people helped me during my PhD journey.

First of all, I would like to express my sincere gratitude to my supervisor, Prof. Morten Grøtli, thank you so much for giving me the opportunity to study and work in your group. Your all-round supports leave me able to fully focus on study new knowledge and promote my PhD project. Thank you for your patience and dedication to discuss with me, give me helpful advices, and encourage me when I was struggling with my projects. Particularly, your recognition and trust to my working ability, as well as giving me so much freedom to explore the ideas I was interested in, make me more confident to overcome all challenges. Additionally, thank you for your home-made delicious food every semester, you are great chef.

My co-supervisor, Prof. Joakim Andréasson. Thank you for your discussion and teaching over these years. Your profound knowledge, passion to scientific research, humour and cheerful attitude to life really inspired me so much. It's a great honor to have you in my project.

My examiner, Prof. Kristina Luthman. Thank you for your guidance and cares for my study and life in Sweden.

All co-authors and collaborates. Dr. Chunxia Gao, thank you for your contribution to molecular modelling of azo inhibitors and the quantum calculation of azoheteroarenes, as well as your tips on my CADD study. Dr. Thomas Lundbäck, thank you for teaching and discussion of the biological assay. Dr. Liliana Håversen, thank you for preparing the cells and the following discussion of the cell assay, you are very good collaborator. Dr. Simon Moussaud, thank you for your effort on biochemical assay anyway. Måns Andreasson, thank you for synthesizing the two pairs of stilbene compounds.

All past and current MedChem group colleagues (time order): Tanja, Marta, Cassandra, Tina, Marcus, Chunxia, Umberto, Fadi, Måns, Shno, Leticia, Josipa, Anders, Amalyn, Alexandra, Diego, Eric, Julia, Malin, Oscar, Sara, Anna, David, Abdu, Muhammad. You are nice and helpful people, thank you for your support and patience in the labs and office, these are memorable years working

with you guys. Mattias and Mariell, much thanks for borrowing some urgent reagents from Astrazeneca and dealing with my samples in the system.

Special appreciation to Morten, Joakim, Kristina, Amalyn and Diego, thank you so much for taking the time to proofread my thesis or/and manuscripts. Your inputs are extremely valuable for me!

Bijan Nekousihahraki and Patrik Jarvoll, thank you for training and helps with running NMR. Hanna Thomsen and Monika Malak, thank you for all your helps in the cell lab.

Our climbing group: David, Alex, Jurgen, Clara, August, Alica, Diego, Amalyn, Sara, Karan, Anna, that's a great time with you guys in the climbing gym. And my hiking companions: Jürgen, Yufang, Aifang, Wang Chi, Diego, Amalyn, and Alesia's family and group, I enjoyed the time of exploring Scandinavian forest and mountains with you.

Living and studying in foreign country is exciting that we have the opportunity to experience different culture, but sometimes it is lonely and homesick. Thanks to my Chinese friends (time order): Hao Wang, Chaoyi Gu, Xin Liu, Yong Lu, Naren Gaowa, Yuan Wang, Yao Zhou, Ying Ye, Aifang Chen, Mingshu Xie, Xiaojing Chen, Yihao Tian, Gang Li, Xin Wen, Yufang Ye, Yarong Tian, Zhicheng Hu, Yi Yu, Yaqin Li, Guoqiang Zhang, Guojiang Xie, and Jie Yang. Cooking Chinese food or had hotpot/BBQ with you during weekends, or especially festivals, gave a sense of home. All you are big cheves.

Yangyang, my love, your encouragement and consolation are my power for groping in the dark and looking into the future.

Finally, I would like to express my greatest thanks to my parents; you raise me up, and always support my further studying and other decisions.

9 Appendixes

Appendix 1: UV-vis absorption spectra of azoheteroarenes.

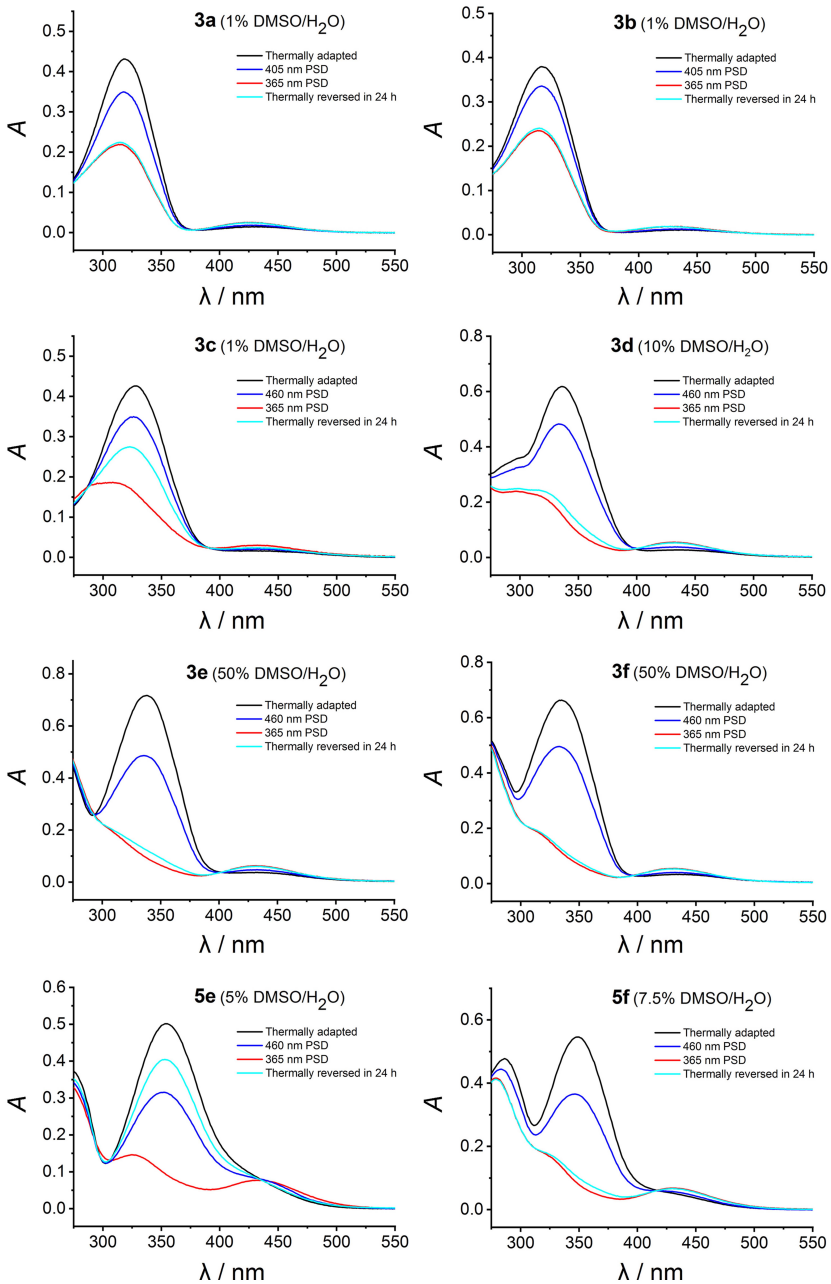

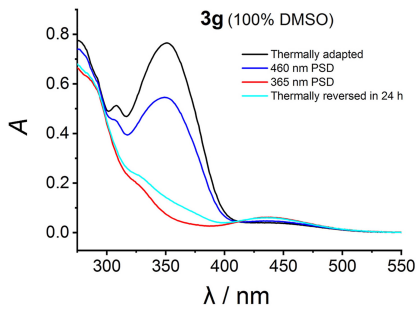
3g (100% DMSO)
Thermally adapted
460 nm PSD
365 nm PSD
Thermally reversed in 24 h
A
λ / nm

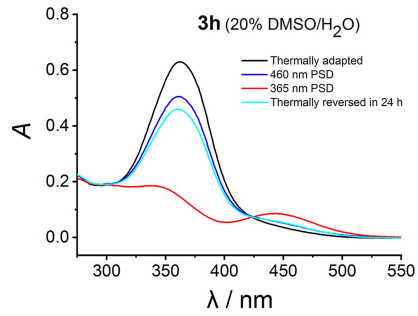
3h (20% DMSO/H2O)
Thermally adapted
460 nm PSD
365 nm PSD
Thermally reversed in 24 h
A
λ / nm

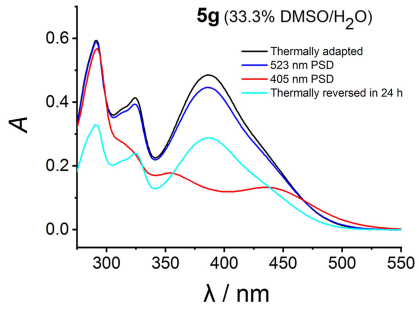
5g (33.3% DMSO/H2O)
Thermally adapted
523 nm PSD
405 nm PSD
Thermally reversed in 24 h
A
λ / nm

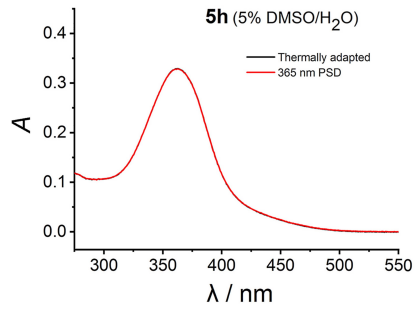
5h (5% DMSO/H2O)
Thermally adapted
365 nm PSD
A
λ / nm

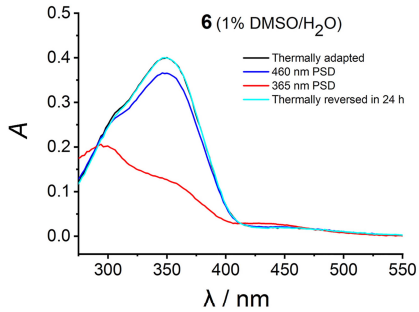
6 (1% DMSO/H2O)
Thermally adapted
460 nm PSD
365 nm PSD
Thermally reversed in 24 h
A
λ / nm

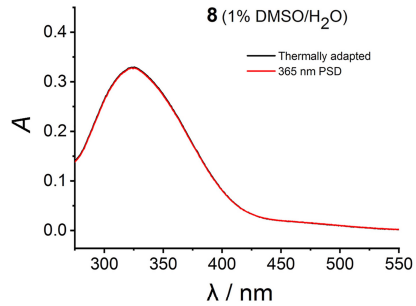
8 (1% DMSO/H2O)
Thermally adapted
365 nm PSD
A
λ / nm

Appendix 2: Fatigue resistance of azoheteroarenes over cyclic isomerization induced by irradiation of two different wavelengths.

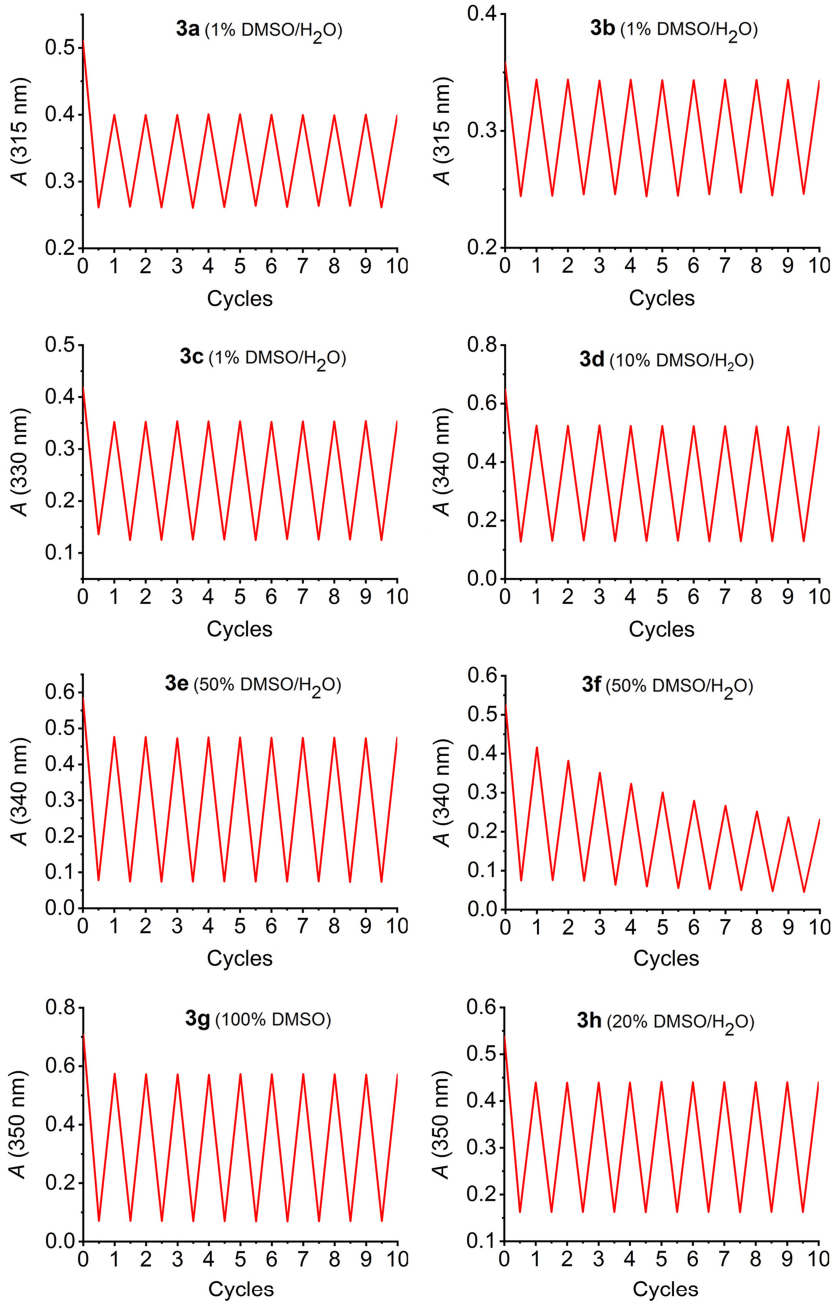

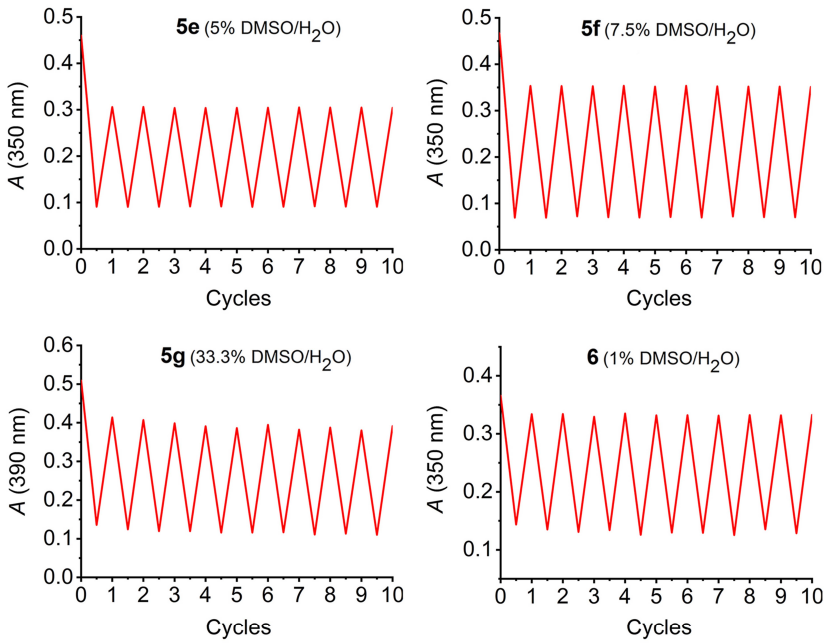
5e (5% DMSO/H2O)
A (350 nm)
Cycles
5f (7.5% DMSO/H2O)
A (350 nm)
Cycles
5g (33.3% DMSO/H2O)
A (390 nm)
Cycles
6 (1% DMSO/H2O)
A (350 nm)
Cycles

Appendix 3: Determination of half-life of azoheteroarenes.

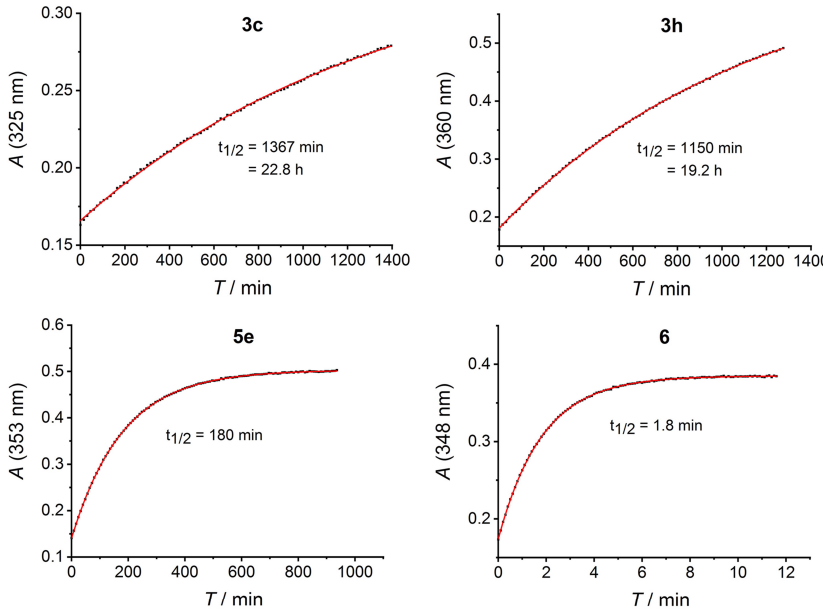

Appendix 4. Activation energies for the thermal *Z*→*E* isomerization through inversion.

Compounds	$\Delta G‡_{TS1}$ (kcal/mol)	$\Delta G‡_{TS2}$ (kcal/mol)	$\Delta G‡_{TS3}$ (kcal/mol)	$\Delta G‡_{TS4}$ (kcal/mol)
3a	-26,1	-34,45	-26,92	-30,06
3b	-27,92	-29,81		
3c	-24,79	-35,45	-27,17	-28,43
3d	-26,23	-31,88	-26,42	-28,93
3e	-29,87	-36,14	-29,93	-42,48
3f	-36,27	-29,99	-48,94	-36,39
3g	-25,1	-37,65	-24,85	-37,4
3h	-25,03	-41,98	-26,42	-30,81
5e	-24,16	-33,57	-24,22	-33,63
5f	-25,16	-33,32	-25,04	-32,57
5g	-24,66	-33,45	-24,03	-33,45
6	-31,31	-37,59	-30,37	-34,76
5h	-27,85	-32,13	-27,3	-36,08
8	-35,39	-31,63	-39,47	-37,59

Appendix 5: The dihedral angle X-C_3-N_1=N_2. Please note that the dihedral angle is defined such that atom "X" is always positioned above N_2, atom X is changed in going from conformer I to conformer II so that the dihedral angle is always > 90°.

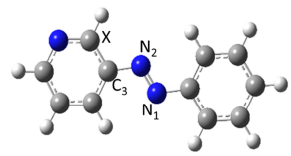

Compound	*E*(C_5-C_3-N_1=N_2)(°)	*Z*(C_5-C_3-N_1=N_2)(°)
3a-I	179,5	137,9
3a-II	165,3	135,5
3b	166,4	136,3
3c-I	179,6	124,2
3c-II	172	141,3
3d-I	179,9	140,3
3d-II	180	141,1
3e-I	180	143,2
3e-II	179,2	143,8
3f-I	179,8	144,5
3f-II	179,5	141,6
3g-I	179,8	142,1
3g-II	179,1	143,8
3h-I	179,9	139,4
3h-II	179,2	160,9
5e-I	180	145,2
5e-II	180	146,6
5f-I	180	147,5
5f-II	180	143,6
5g-I	180	147,9
5g-II	180	147,7
6-I	149,2	119,8
6-II	179,9	129,2
5h-I	180	141,6
5h-II	179,9	156,8
8-I	139,6	134,1
8-II	151,3	104,4

Appendix 6: PSD of compound **59** achieved by different light irradiation with Xenon lamp and specific filters.

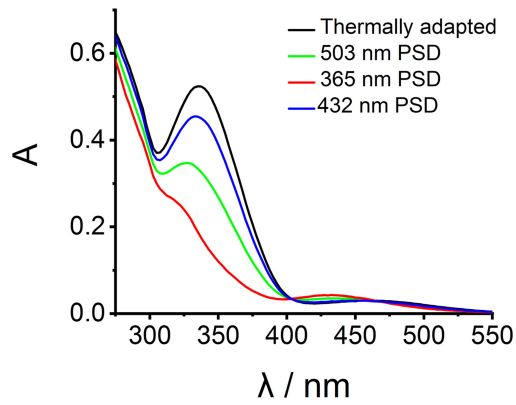

Appendix 7: Fatigue resistance of azo type DFG-out RET inhibitors over cyclic isomerization induced by irradiation of 365 nm and 460 nm light.

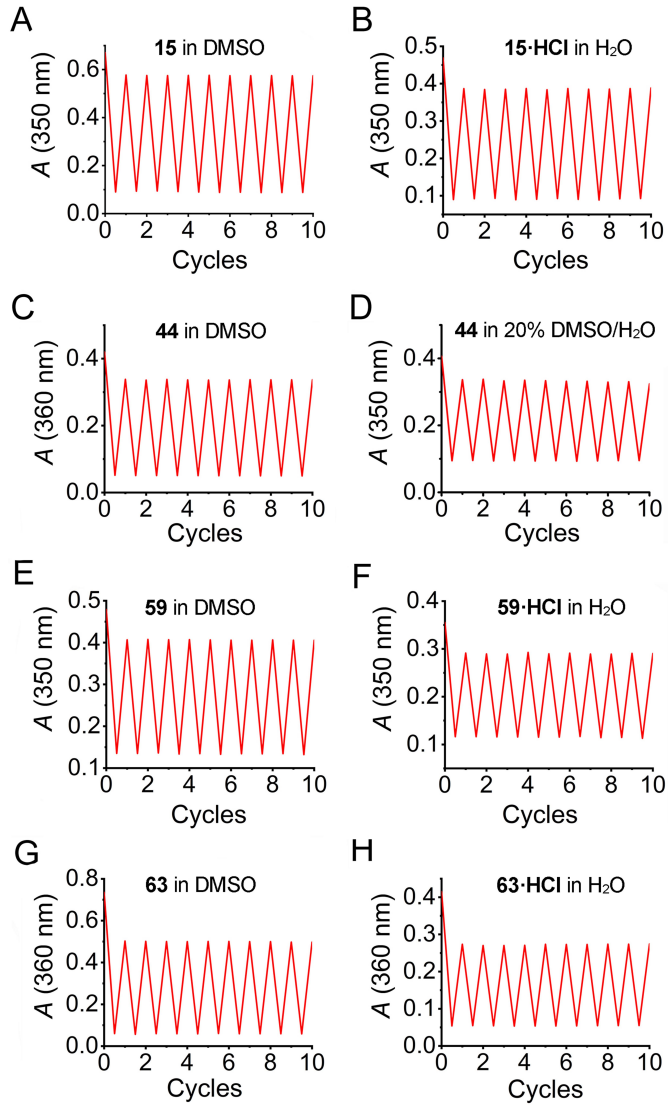

Appendix 8: The results of DTT/GSH assays of azo type inhibitors, displayed below as UV spectra of LC-MS.

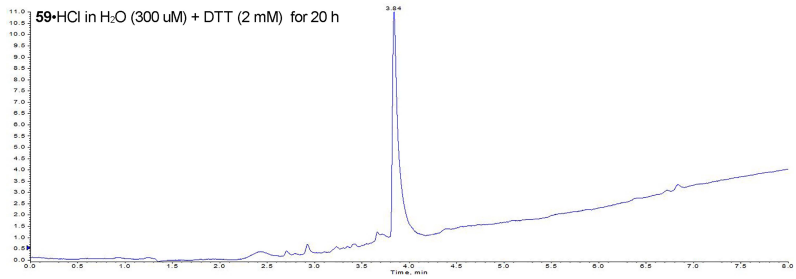

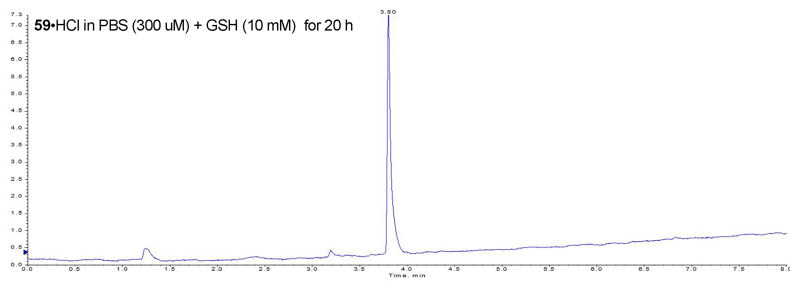

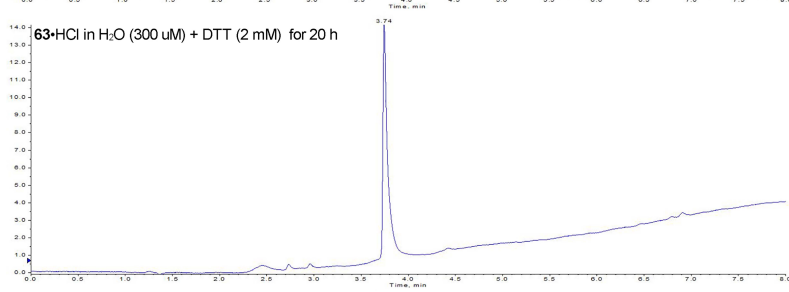

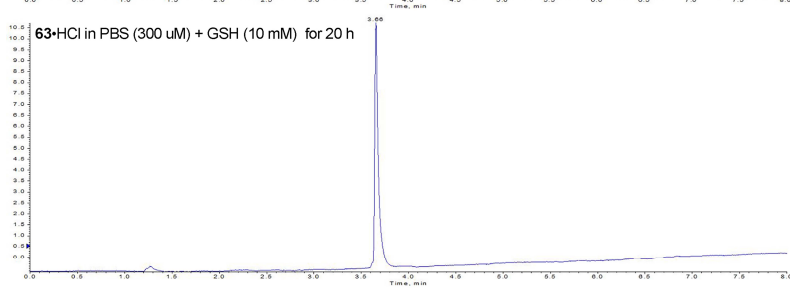

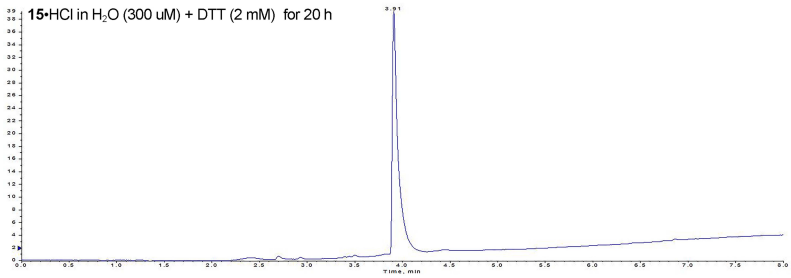
15•HCl in H2O (300 uM) + DTT (2 mM) for 20 h
3.91
Time, min

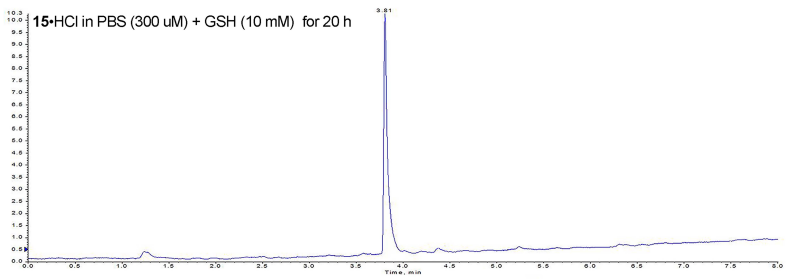
15•HCl in PBS (300 uM) + GSH (10 mM) for 20 h
3.81
Time, min

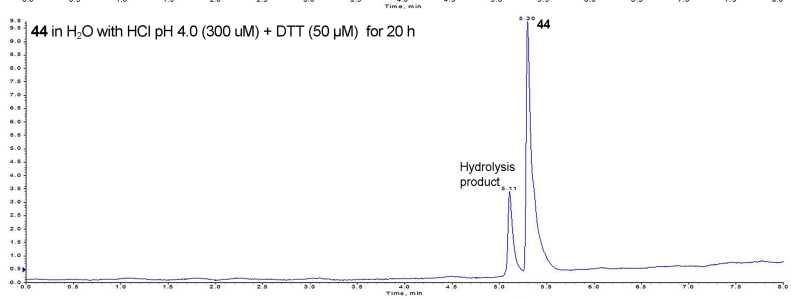
44 in H2O with HCl pH 4.0 (300 uM) + DTT (50 µM) for 20 h
5.30
44
Hydrolysis product
5.11
Time, min

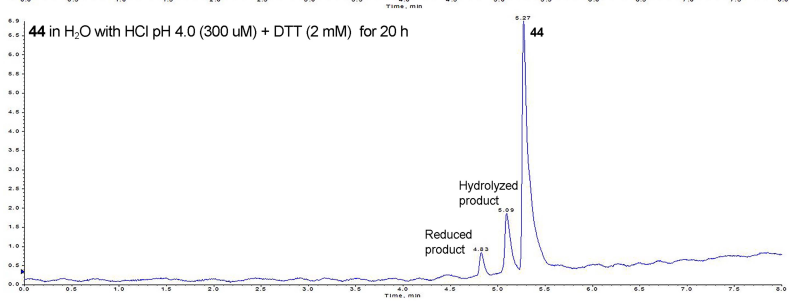
44 in H2O with HCl pH 4.0 (300 uM) + DTT (2 mM) for 20 h
5.27
44
Hydrolyzed product
5.09
Reduced product
4.83
Time, min

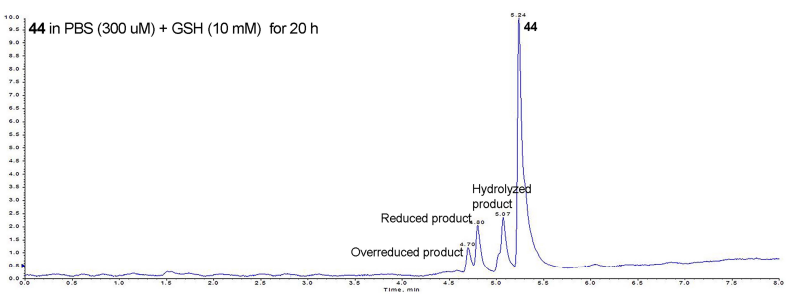
44 in PBS (300 uM) + GSH (10 mM) for 20 h
5.24
44
Hydrolyzed product
5.07
Reduced product
4.80
Overreduced product
4.70
Time, min

Appendix 9: Incubation time and temperature screening for NanoBRET™ TE intracellular RET kinase[a]

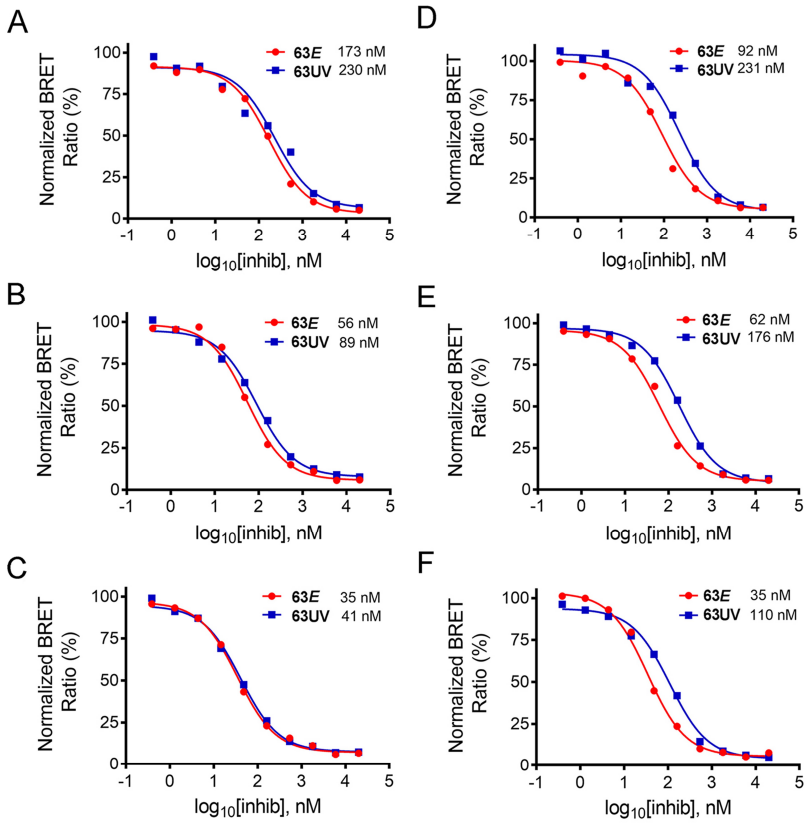

[a] (A) 30 min at 37 °C; (B) 60 min at 37 °C; (C) 90 min at 37 °C; (D) 10 min at 37 °C, then 60 min at 25 °C; (E) 20 min at 37 °C, then 60 min at 25 °C; (F) 30 min at 37 °C, then 60 min at 25 °C.